Experimental investigation of $Ca(OH)_2$ as thermochemical energy storage at process relevant boundary conditions

A thesis accepted by the Faculty of Energy-, Process- and Bio-Engineering of the University of Stuttgart to fulfil the requirements for the degree of Doctor of Engineering Sciences (Dr.-Ing.)

by
Matthias Schmidt
born in Mainz

Main referee: Prof. Dr. rer. nat. habil. André Thess

Co-referee: Prof. Dr.-Ing. Bernhard Hoffschmidt

Date of oral exam: 17.10.2017

Institute of Energy Storage - University of Stuttgart - 2017

Kurzfassung

Die Reaktion von Calciumhydroxid zu Calciumoxid und Wasserdampf eignet sich aufgrund der bereits demonstrierten Reversibilität besonders gut zur Speicherung thermischer Energie. Zudem ist das Material kostengünstig, auf der ganzen Welt in großen Mengen verfügbar und bietet potentiell eine hohe erreichbare Speicherdichte. Da der Reaktionspartner Wasserdampf jedoch ca. 40 % der Energie des Speicherprozesses enthält, ist es für einen effizienten Speicherbetrieb zwingend notwendig den energetischen Aufwand für die Bereitstellung in den Anwendungsprozess zu integrieren. Dies führt wiederum dazu, dass das Reaktionssystem in einem sehr weiten Druck- und Temperaturbereich betrieben werden muss. Da bisher kaum experimentelle Erkenntnisse zum Betrieb unter solchen realen Prozessbedingungen vorhanden sind, werden diese Betriebsweisen im Rahmen der vorliegenden Arbeit untersucht.

Dazu wurde ein Reaktionsbett für eine repräsentative Masse (2.4 kg) an Speichermaterial und einer generischen Geometrie entwickelt. Mit diesem experimentellen Aufbau im Labormaßstab wurde durch systematische Parametervariation erstmalig die thermische Leistungsfähigkeit des Reaktionssystems im gesamten prozessrelevanten Betriebsbereich untersucht.

Als ein wesentliches Ergebnis der experimentellen Untersuchung konnten im gesamten Druckbereich technisch relevante thermische Be- und Entladeleistungen demonstriert werden. Jedoch zeigte sich auch, dass bei geringen Wasserdampfdrücken (1.4 – 50 kPa), die langsame Reaktionsgeschwindigkeit des Rohmaterials die erzielbaren Be- und Entladetemperaturen, teilweise einschränkt.

Auf Basis der experimentellen Erkenntnisse wurde der Einsatz des Speichers in einem bestehenden thermischen Solarkraftwerk konzeptionell untersucht. Dabei zeigte sich, dass insbesondere dann eine hohe Speichereffizienz erzielt werden kann, wenn die für die Speicherentladung notwendige Wasserdampfbereitstellung thermisch in den stromerzeugenden Kraftwerksprozess integriert wird. Insgesamt eröffnen die in dieser Arbeit demonstrierten Betriebsweisen den effizienten Einsatz des Speichersystems für unterschiedlichste Anwendungen.

Abstract

The reaction of calcium hydroxide to calcium oxide and water vapour is, due to the demonstrated reversibility, particularly suitable for the storage of thermal energy. In addition the material is available in enormous quantities, at low cost all over the world and offers a high achievable energy storage density. However the reaction partner water vapour contains approximately 40 % of the energy of the storage process. For an efficient operation of the storage system it is therefore necessary to integrate the required energy for the vapour supply into the process application. This in turn demands the operation of the storage system in a wide pressure and temperature range. Since up to now experimental data on the operation at such real process relevant conditions rarely exist, these operation modes are investigated in this work.

For this purpose a reaction bed of a generic geometry and for a representative mass (2.4 kg) of storage material was developed. By means of this experimental set up in laboratory scale and a systematic parameter variation the thermal capability of the reaction system was investigated for the first time in the entire process relevant operating range.

One fundamental result of the experiments was the demonstration of technically relevant thermal charge and discharge powers in the complete pressure range. However, the experiments also revealed, that at low vapour pressures (1.4 – 50 kPa), the slow reaction rate of the basic raw material partially limits the achievable charging and discharging temperatures.

Based on the experimental results the application of the storage system in an existing solar thermal power plant was conceptually analysed. It could be shown, that a high storage efficiency can be achieved, especially if the required energy for evaporation during the discharge procedure is thermally integrated in the steam power cycle of the plant. Overall the demonstrated operation modes allow for an efficient use of the storage system in various process applications.

Publications

Parts of this work have been published in:

Scientific Journals:

Schmidt M, Linder M. Power generation based on the $Ca(OH)_2$/ CaO thermochemical storage system – experimental investigation of discharge operation modes in lab scale and corresponding conceptual process design. Appl Energy 2017;203:594-607. doi:10.1016/j.apenergy.2017.06.063

Schmidt M, Gutierrez A, Linder M. Thermochemical energy storage with CaO/Ca(OH)2 – Experimental investigation of the thermal capability at low vapor pressures in a lab scale reactor. Appl Energy 2017;188:672–81. doi:10.1016/j.apenergy.2016.11.023.

Roßkopf C, Afflerbach S, Schmidt M, Görtz B, Kowald T, Linder M, et al. Investigations of nano coated calcium hydroxide cycled in a thermochemical heat storage. Energy Convers Manag 2015; 97:94–102. doi:10.1016/j.enconman.2015.03.034.

Linder M, Roßkopf C, Schmidt M, Wörner A. Thermochemical Energy Storage in kW-scale based on CaO/Ca(OH)2. Energy Procedia 2014;49:888–97. doi:10.1016/j.egypro.2014.03.096.

Schmidt M, Szczukowski C, Roßkopf C, Linder M, Wörner A. Experimental results of a 10 kW high temperature thermochemical storage reactor based on calcium hydroxide. Appl Therm Eng 2014; 62:553–9. doi:10.1016/j.applthermaleng.2013.09.020.

International Conferences:

Schmidt M, Gollsch M, Giger F, Grün M, Linder M. Development of a moving bed pilot plant for thermochemical energy storage with CaO/Ca(OH)2. SOLARPACES 2015 Int. Conf. Conc. Sol. Power Chem. Energy Syst., vol. 1734, AIP Publishing; 2016, p. 50041. doi:10.1063/1.4949139.

Schmidt M, Linder M. Operation Modes of a High Temperature Thermochemical Energy Storage System based on Calcium Hydroxide. Proc. Greenstock Conf., Beijing: 2015

Schmidt M, Roßkopf C, Linder M, Wörner A. Operation modes and process integration of a thermochemical heat storage system based on CaO/Ca(OH)2. Proc. Eurotherm Semin. No 99, Lleida, Spain: 2014.

Schmidt M, Linder M. Operation Modes and Process Integration of a High Temperature Thermochemical Heat Storage System. Proc. Gd. Renew. Energy, 2014.

Schmidt M, Roßkopf C, Linder M, Wörner A. High Temperature Thermochemical Heat Storage: Operation Modes of a 10kW Pilot Reactor Based on $CaO/Ca(OH)_2$. Presentation. IRES, Berlin, Germany: 2013.

Schmidt M, Roßkopf C, Linder M, Wörner A. High Temperature Thermochemical Heat Storage: Experimental Results of a Pilot Reactor Based on CaO/ Ca(OH)2. Presentation. IRES, Berlin, Germany: 2012.

Table of Contents

Kurzfassung I

Abstract III

Publications V

Table of Contents VII

List of Figures IX

List of Tables X

Nomenclature XI

1 Introduction 1

2 State of technology 4
2.1 High temperature thermal energy storage 4
2.2 The reaction system calcium hydroxide 8
2.2.1 Material characterisation 10
2.2.2 Experimental research in lab and pilot scale 14
2.2.3 Process integration 22
2.3 Aim of this work 28

3 Experimental set up 29
3.1 Lab-scale reactor 29
3.2 Test bench 32
3.3 Material 34
3.4 Experimental procedure 35
3.5 Thermogravimetric analysis 36

4 Experimental results 37
4.1 Set in operation 37
4.2 Thermal charging 39
4.2.1 Dehydration at 10 kPa 40
4.2.2 Dehydration at pressures 1.4 – 100 kPa 47
4.3 Thermal discharging 52
4.3.1 Hydration at 200 - 470 kPa 52
4.3.2 Hydration at 8.7 kPa 58
4.3.3 Hydration at 4-50 kPa 63
4.4 Changes of the reaction bed 65
4.5 Summary and discussion of experimental results 67

5. Process integration based on molten salt CSP 71
5.1 Integration concept for CSP plant 71

5.2 Power generation driven by the storage system 73
5.3 Solar charging 82
5.4 Results and discussion 83

6. Summary and outlook 85

References 88

Appendix 95
A Technical drawings 95
B Calibration of filling level meter 98
C Insulation of the reactor 98
D Measurement uncertainty 100

List of Figures

Figure 1 De- and rehydration of calcium hydroxide 10
Figure 2 Reported thermodynamic equilibrium lines of the CaO/ $Ca(OH)_2$ 11
Figure 3 Directly operated fixed bed [73] 15
Figure 4 Fluidized bed reactor [75] 16
Figure 5 Reactor coupled to evaporator presented by Ogura [77] 17
Figure 6 Scheme of the test bench [78] 18
Figure 7 Indirectly heated reaction bed for 20 kg $Ca(OH)_2$ [81] 19
Figure 8 left: Heat exchanger for moving particles and air [87] 21
Figure 9 Pilot plant for moving bed reactor [87] 22
Figure 10 Moving bed pilot plant for 100 kWh and 10 kW at DLR [87] 22
Figure 11 T, h diagram for the charging procedure 24
Figure 12 T, h diagram for proposed discharge procedure 25
Figure 13 Exemplary charging and discharging conditions 26
Figure 14 Top: heat exchanger plate used as reactor 30
Figure 15 Left: pressure resistant casing pipe 31
Figure 16 Schematic view of the reaction bed in the casing pipe 31
Figure 17 Schematic layout of the test bench 32
Figure 18 Photography of the complete experimental set up 34
Figure 19 Hydration experiment at 100 kPa 38
Figure 20 Dehydration experiment at 10 kPa 41
Figure 21 Dehydration experiments at 10 kPa at different heat loads 43
Figure 22 Dehydration at 500 °C induced through sudden pressure drop 45
Figure 23 Effect of the temperature on the dehydration reaction of Ca(OH) 46
Figure 24 Dehydration at 4.3 kPa and a dehydration temperature of 480 °C ... 48
Figure 25 Dehydration experiments at 1.4, 10 and 20 kPa 49
Figure 26 Dehydration at 100 kPa and an air inlet temperature of 560 °C 51
Figure 27 Hydration experiment at 470 kPa 53
Figure 28 Hydration at 470 kPa under different cooling loads 55
Figure 29 Hydration experiment at 200, 270 and 470 kPa 57
Figure 30 Hydration experiment at 8.7 kPa 59
Figure 31 Hydration experiments at 8.7 kPa under different cooling loads 61
Figure 32 Effect of the temperature on the hydration reaction of CaO 62
Figure 33 Hydration at 4 kPa and a starting temperature of 280 °C 64
Figure 34 Hydration at 4, 10, 20 and 50 kPa and comparable cooling loads ... 65
Figure 35 right: reaction bed after 35 cycles 66
Figure 36 Summary of the operating conditionsl 70
Figure 37 Conceptual process design in a CSP plant configuration 73
Figure 38 Flow sheet of power block operation 75
Figure 39 Storage efficiency 80

Figure 40 Amount of stored thermal energy 83
Figure 41 Technical drawing of pressure resistant casing pipe 95
Figure 42 Technical drawing of heat exchanger plate 96
Figure 43 Technical drawing of filter plate 97
Figure 44 Filling level height in the condenser and volume of water 98
Figure 45 left: heating cables attached to the firs insulation layer 99

List of Tables

Table 1 Selected chemical reaction systems..... 7
Table 2 Parameters of dehydration experiments presented in chapter 5.2 39
Table 3 Conditions for all discharge experiments presented in chapter 5.3 52
Table 4 Nominal values for power block cycle..... 73
Table 5 General values for the calculations..... 76
Table 6 Calculated thermal Power 79

Nomenclature

Abbreviations:

B	Reaction bed
CSP	Concentrated solar power
cp	Specific heat capacity
d_{50}	Median diameter of the particle size distribution
el	Electric
EV	Evaporator
EXP	Extraction point
F	Filling level / mm
G	Gaseous
H	Enthalpy
HEX	Heat exchanger
HP	High pressure
HTF	Heat transfer fluid
LP	Low pressure
M	Molar mass
P	Electrical power output
p	Pressure
PB	Power Block
PH	Preheater
p_{H2O}	Partial pressure of water vapour
R	Universal gas constant
S	Solid
T	Temperature / K
t	Time
Tc	Thermocouple
TCS	Thermochemical system
TGA	Thermogravimetric analysis
V	Valve
X_{tot}	Conversion

Symbols:

$\dot{V}$	Volume flow rate
$\dot{n}$	Molar rate of reaction
$\dot{m}$	Mass flow rate
η	Efficiency
ΔH	Change in enthalpy
ΔS	Change in entropy
$\dot{Q}$	Thermal power
ϑ	Temperature measurement point, thermocouple
λ	Thermal conductivity
%w	Weight percentage

1 Introduction

195 nations worldwide committed, within the frame of the climate protection agreement from 2015 in Paris, to reduce their net greenhouse gas emissions to zero by the mid of this century [1]. It is clear that this goal can only be achieved by massive implementation of renewable energy sources all over the world. But due to their inherent intermittence such an increase in renewable energy production requires the installation of large storage capacities at the same time. In this context thermal energy storage systems are considered as one key technology to balance the fluctuations between supply and demand. One distinguished advantage of thermal storage technologies is that they are in general based on cheap, environmental friendly and abundantly available materials.

Concentrated solar power (CSP) plants with large thermal energy storage systems already offer a solution for a year round dispatchable and clean electricity generation. The application of thermal storage systems can increase the energy efficiency in industrial processes by the reintegration of waste heat or enhance the flexibility of conventional power plants to quickly response to fluctuations in the grid. They also play an important role for the development of isentropic energy storage systems (power to heat to power concepts) which have the potential to facilitate the integration of renewable energy sources all over the world [2]. Accordingly, all future energy scenarios foresee the necessity of a cross linked energy infrastructure where the energy sectors, electricity, heat and cold generation as well as transport are linked by efficient storage technologies. The development of innovative cost and energy efficient storage technologies is therefore of distinguished importance for the transformation of the energy system.

Among all thermal energy storage technologies thermochemical systems offer in theory a very promising potential. Some of the reaction systems have high energy densities, the storage principal itself is free of losses and especially the temperature at which the heat is released can be adjusted within a certain range.

In particular the reversible reaction of calcium hydroxide to calcium oxide and water vapour:

$$CaO + H_2O \leftrightharpoons Ca(OH)_2 + 104\ (kJ/mol) \quad (1)$$

is discussed for the use as energy storage material due to several advantages. First of all, the material is very cheap and abundantly available in industrial scale. Combined with the high enthalpy of reaction, the material offers in principle a very cheap storage capacity. Secondly theoretical discharge temperatures of 600 °C or more allow operating thermodynamic cycles with high Carnot efficiencies. Thirdly, the gaseous reactant, water vapour, can safely be handled and stored volume efficient as liquid water.

Despite these advantages the technology is still in an early research state. Even though intensive work has been carried out to characterize fundamental properties of the reaction system like the thermodynamic equilibrium and the kinetics of the reaction, the development of storage systems for real applications remains challenging. On the one hand the predictive value of developed simulations tools is limited because the complex interaction of heat and mass transfer in a reactive bulk is not completely understood. On the other hand experimental data on the operation of reactors with a larger mass of storage material is also almost non-existent. Furthermore for the calcium hydroxide system it is of particular importance to consider the handling of the reaction gas since the condensation and evaporation of water vapour contains approximately 40 % of the storable energy. Only if the reaction gas handling is thermally integrated into the process application a reasonable storage efficiency can be achieved. This in turn demands an operation of the storage system in a wide pressure and temperature range depending on the specific process boundary conditions.

The aim of this work was therefore to develop a reactor with a representative mass of storage material in a generic reaction bed geometry. By means of this experimental set up it is for the first time possible to investigate the reaction system under process relevant operating conditions. This in particular means the determination of the operating characteristics of the basic raw material across the whole required temperature and pressure range. The obtained experimental data will enhance the understanding of the operation of the storage system and

thus support future reactor developments. It will serve for the validation of simulation models and allows for more realistic process simulations and integration strategies.

2 State of technology

2.1 High temperature thermal energy storage

High temperature thermal energy storage systems are one key technology on the pathway to a complete renewable energy supply. The performance and applicability of thermal energy storage systems highly depend on the thermophysical properties of the storage material itself. It is clear that there is not one thermal storage solution but different technologies have to be developed to fit to the requirements of the variety of potential applications. In general the technologies are categorized by its storage principal into sensible, latent and thermochemical storage systems. This chapter provides a brief introduction to each storage method, identifies main differences and hereby indicates preferred application scenarios.

Sensible storage systems

Sensible storage mediums are in general solid or liquid and do not change their state during the charging or discharging process. The amount of stored thermal energy is proportional to the induced temperature difference. The probably most popular sensible storage technology is the hot water tank for domestic households. At higher temperatures, molten salt stored directly in two tanks is the state of the art and commercially available storage system for today's concentrated solar power plants. However in a typical configuration the salt itself accounts for around 50 % of the cost of the storage system [3]. In order to reduce the costs researchers investigate alternative thermal storage solutions. In the thermocline concept for example the expensive salt is partly replaced with inexpensive filler materials and only one storage tank is used [4]. Due to their low cost concrete and castable ceramics are studied as solid state heat storage mediums [5]. So called regenerator storages where a gaseous heat transfer fluid flows through a packed bed of for example basalt or ceramic honeycombs are another option for the application in concentrated solar or conventional power plants [6]. An innovative concept to overcome the direct attachment of capacity and heat exchanger with storage material is the recently presented CellFlux concept [7]. In this concept an intermediate closed air loop to transfer

energy between the heat transfer fluid and the solid storage medium (bricks or stones) is used [8]. The concept allows on one hand a cost efficient design of the heat exchanger according to the power level and on the other hand also an independent modular scale up of the storage capacity. In general sensible thermal energy storage is a mature technology. Due to the storage principle the systems are most suitable for applications where the heat transfer fluid undergoes a large temperature difference.

Latent storage systems

In latent heat storage systems the storage medium changes it´s state, for example from liquid to vapour or - more common - solid to liquid and vice versa during the charging and discharging process. Thus an additional proportion of thermal energy, the enthalpy of the phase change, can be exploited to achieve higher energy storage densities. Another distinctive feature is that in contrast to sensible storage mediums, the thermal energy is taken up or released at a constant temperature (the respective temperature of the phase change). Typical phase change materials are paraffin's, salts or low melting metals. One proposed application for low temperatures is the integration of phase change materials in building envelops to reduce the energy demand of the building [9]. High temperature latent storage systems have yet a relatively low market penetration. Some systems are investigated for the application in direct steam generation concentrated solar power plants or the assistance of conventional steam accumulators [10]. One actual research line focuses on the detachment of the heat exchanger from the storage material for example by the use of a screw heat exchanger [11] or in the recently reported PCM Flux concept where the storage material is mechanically separated by an intermediate fluid layer from the heat transfer surface [12]. Another area of research is the microencapsulation of the storage material in order to enhance their thermal conductivity and prevent interactions with the surrounding [13]. More proposed storage materials and their state of maturity can be found in the review of Kenisarin [14]. Latent storage systems offer in general a high energy density at a small temperature difference. Therefore the technology in particular suites to applications where the heat transfer fluid also changes it´s state during the charging (e. g. condensation) or discharging (e. g. evaporation) process.

Thermochemical storage

The term thermochemical storage in general refers to the use of either sorption processes or reversible chemical reactions to store thermal energy. The difference is that in chemical reactions a real conversion of the chemical substance takes place while sorption processes are generally defined through the adhesion or solution of gases on a solid surface or in a liquid. In general a reversible gas solid reaction is described by the following equation:

$$AB_{(s)} + \Delta H_{reaction} \rightleftharpoons A_{(s)} + B_{(g)} \quad (2)$$

In the, so called, charging step, the solid substance AB is decomposed in its two components A (solid) and B (gaseous) by suppling the required enthalpy of reaction. The two components A and B are then separated from each other, which is easy for the particular case if one component is solid and the other one is gaseous. The two components are then stored separately from each other. In order to reduce the required storage volume it might be beneficial to condense or compress the gaseous component during the storage period. The inherent advantage of the thermochemical systems compared to all other storage methods is that during the storage phase the components can be stocked, for an unlimited period of time without losing their chemical potential. Once the component A and B are brought together again the exothermal back reaction takes place and the released thermal energy can be exploited. The back reaction refers to the so called discharging step. The achievable energy densities of thermochemical systems depend mostly on the enthalpy of reaction in conjunction with the material density and are for most reactions much higher (100 – 700 kWh/m³) compared to latent (50 – 100 kWh/m³) or sensible (25 – 150 kWh/m³) storage materials [15]. Another important characteristic of thermochemical reactions is the distinct correlation between the pressure of the gaseous reactant and the temperature at the equilibrium state, which is generally described by the equation [16]:

$$\ln(p_{equilibrium}) = \frac{\Delta H_{reaction}}{R\,T} + \frac{\Delta S}{R} \quad (3)$$

Based on this equation, the so called Van´t Hoff plot, a graphical representation for the temperature and pressure range of the reaction, can be derived. The plot is widely used in order to assess the suitability of a reaction system for a certain

application and will be introduced for the calcium hydroxide reaction system later. Besides the temperature range also the effective speed of the reaction and the reversibility play an important role for the choice as storage material. In addition more generic criteria's like the availability, the price and the toxicity of the material need to be taken into account. Despite their great potential thermochemical systems are still in a fundamental research state. For most systems, elementary questions like the determination of the thermodynamic equilibrium, the reaction kinetics and the reversibility still need to be solved. While for some reactions, which are already better characterized on the material level, also small reactors in lab scale are presented.

Table 1 summarizes exemplarily some of the reactions suggested for thermochemical energy storage and their temperature range. It becomes obvious that with thermochemical systems a wide range of temperatures and thus also a variety of potential applications can be covered. A detailed overview on more reactions which are discussed for thermochemical storage and their state of maturity is given in several recently published reviews [15,17–22].

Table 1 Selected chemical reaction systems investigated for thermal energy storage

Classification	Reaction	Temperature range / °C
Salthydrates	$CaCl_2 \cdot h\ H_2O \rightleftharpoons CaCl_2 + h\ H_2O$	80 – 180 [23]
	$MgSO_4 + 7\ H_2O(G) \rightleftharpoons MgSO_4 \cdot 7\ H_2O(s)$	25 – 265 [24]
Metallhydroxides	$Mg(OH)_2 \rightleftharpoons MgO + H_2O$	250 – 400 [25–27]
	$Ca(OH)_2 \rightleftharpoons CaO + H_2O$	280 – 600 [28]
Metalloxides	$Co_3O_4 \rightleftharpoons 3\ CoO + 0.5\ O_2$	800 – 1000 [29]
	$6Mn_2O_3 \rightleftharpoons 4Mn_3O_4 + O_2$	700 - 1000 [30]

Richter et al. recently demonstrated the feasibility of the working pair of $CaCl_2$/ H_2O for the upgrade of industrial waste heat from 100 °C to 165 °C in a reactor for 700 g of material [31,32]. The dehydration of magnesium hydroxide is investigated for the use as chemical heat pump in industrial processes for temperatures between 250 – 400 °C. The principal has already been demonstrated in a small packed bed reactor (10 g) [33] and intensive research on the improvement of the material is still ongoing [34]. The redox reaction of manganese ox-

ide takes place at temperatures between 700 – 1000 °C and is therefore proposed as a thermal storage system for future concentrated solar power plants with volumetric air or direct particle receivers. The system has been demonstrated in a reactor for 1.8 kg corresponding to a thermal storage capacity of 100 Wh [35]. In general thermochemical storage systems offer adaptable charge and discharge temperatures. The operation principle can thus be classified as a compromise between the sensible (large temperature difference required) and the latent (constant temperature) storage principle. One underlying motivation of this work is therefore to evaluate the suitability and the benefits of this operation principle for the process application.

2.2 The reaction system calcium hydroxide

2.2.1 Basic properties

Karst landscapes cover large belts over America, Europe and Asia. In total 15 % of the earths land mass persists of this type of bedrock [36]. Karst is defined in the geology as bedrock which contains a high yield of calcium carbonate ($CaCo_3$). Calcium carbonate, also known as limestone, in turn is the basic raw material for the production of calcium hydroxide $Ca(OH)_2$. In the first step the limestone, extracted from mines, is calcinated at temperatures of more than 900 °C according to the reaction [37]:

$$CaCO_3 + 182.1\ (kJ/mol) \rightarrow CaO + CO_2 \tag{4}$$

The CO_2 is in general released to the ambient and calcium oxide (CaO) also known as quicklime, is obtained. By the hydration of the calcium oxide with water according to the reaction:

$$CaO + H_2O \leftrightharpoons Ca(OH)_2 + 104\ (kJ/mol) \tag{5}$$

calcium hydroxide, also known as hydrated lime or slaked lime is obtained. If calcium hydroxide is exposed to the ambient it will take up carbon dioxide from the air and the, at ambient conditions, very slow carbonisation reaction takes place:

$$Ca(OH)_2 + CO_2 \rightarrow CaCO_3 + H_2O \tag{6}$$

Consequently the, so called, technical lime cycle is closed, and the initially extracted natural product calcium carbonate as most stable phase is reached again.

Until today the lime production is among the biggest chemical industries in the world. In the year 2011 330 million tons of lime were produced worldwide [38] for various applications. The building industry for example is one of the largest consumers of quicklime which is still one of the most important components for concrete [39,40]. Another 30 % of the quicklime production supplies the steel industry since for the production of 1 ton of steel approximately 70 kg of lime is required [41]. The material is also used as fertilizer in the agricultural sector [42] or as acidity regulator in the food industry. The carbonization reaction in particular is used in environmental protection technologies to capture CO_2 for example from exhaust gases in conventional power plants. Due to the abundant worldwide resources of the raw material and the installed industrial scale production capacities the material is very cheap. In December 2016 the price for 1 ton of calcium hydroxide was around 70 $.

Application as thermal energy storage system

Due to its good availability, the low cost and environmental friendliness of the material the de- and rehydration of $Ca(OH)_2$ has been proposed for thermal energy storage already decades ago [43]. Figure 1 illustrates the generic principle of thermal energy storage with the material. The dehydration of calcium hydroxide by means of high temperature heat, is called the charging step. During the procedure the solid $Ca(OH)_2$ is decomposed into CaO and water vapour. The water vapour must be separated from the CaO, preferably through condensation while the calcium oxide is stored in solid state. Once the reactants CaO and water are brought together again the exothermal back reaction takes place and heat is released which can be incorporated into the process application. Depending on the application, the hydration reaction can either be performed with liquid water or with water vapour which allows for higher reaction temperatures.

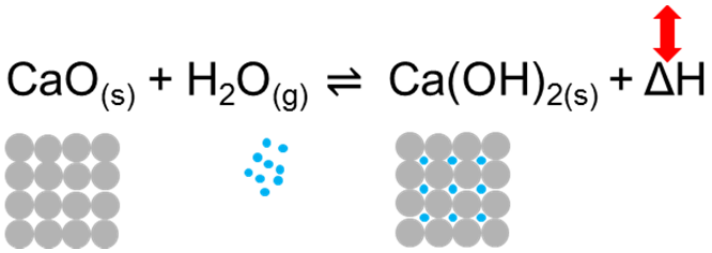

Figure 1 De- and rehydration of calcium hydroxide

Consequently the applicability of the system is discussed for various processes: ranging from preheating of car engines [44,45] to power generation on the moon [46]. The most intensively discussed applications are related to the storage of solar thermal energy in concentrated solar power plants [19,28,47–49] and the development of chemical heat pumps based on calcium hydroxide [17,50,51].

2.2.1 Material characterisation

Due to the above positive aspect of the reaction system and it´s wide range of potential applications, intensive work has already been carried out in order to characterize important thermodynamic and kinetic properties of the material.

Thermodynamic Equilibrium

The thermodynamic equilibrium of the chemical reaction describes the distinct correlation between temperature, pressure and the amount of reactants. In an equilibrium state no further change in the concentration of the reactants will occur because the forward and the backward reaction proceed at an equal reaction rate. In order to proceed with the reaction in one direction either a temperature (heating or cooling) or a pressure (change in concentration of the gaseous reactant) change is required. Especially if the reaction system is exploited as thermal energy storage system the knowledge of this relation is essential. Therefore the thermodynamic equilibrium of the reaction system has been investigated in many works. The nowadays most commonly used method to determine the reaction equilibrium is to perform a systematic measurement series in a thermogravimetric device. In this method a small sample mass (few milligrams) is placed on a high precision weight and brought in contact with a tem-

pered stream of nitrogen and water vapour. The temperature of the material is then increased or decreased with a constant but slow heating rate until a mass change is detected which indicates that the reaction sets in and thus the equilibrium temperature is exceeded. Figure 2 summarizes the determined thermodynamic equilibrium lines of several authors.

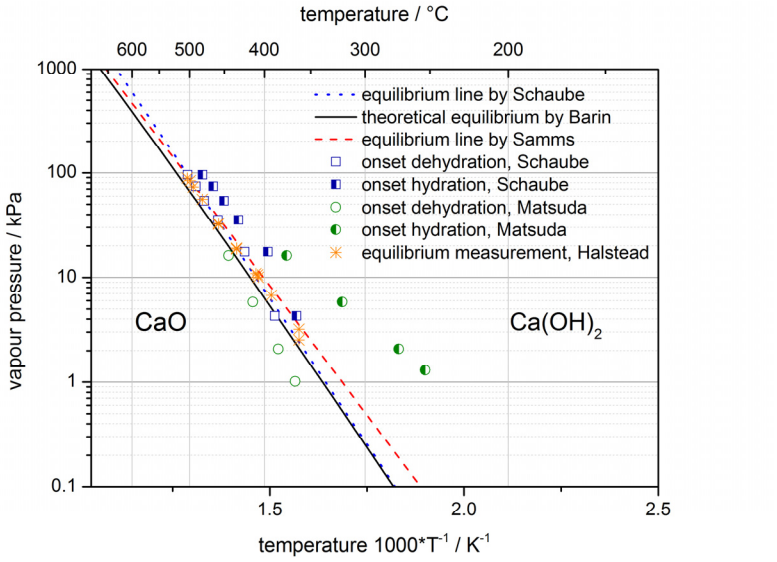

Figure 2 Reported thermodynamic equilibrium lines of the CaO/ $Ca(OH)_2$ reaction system and measurement points from several authors

Schaube measured onset temperatures for the de- and rehydration at 4.3, 17.6, 35.5 and 95.6 kPa (blue squares in Figure 2) and derived an equation for the equilibrium line (blue dotted line) based on the measured values [52]. Matsuda et al. measured the onset temperatures in a pressure range from 1.2 to 16 kPa. (green circles) [53]. Samms and Evans determined the equilibrium temperature between 100 and 5000 kPa. However, instead of TGA measurements they used a self-developed experimental set up. The main difference to the TGA measurement is that the sample is not exposed to a gas stream. In their set up they suddenly increase the vapour pressure in the vessel with a CaO sample and measure the induced temperature peak due to the formation of $Ca(OH)_2$. Based on the respective temperature values they derived the equation for the thermodynamic equilibrium (red dotted line) [54]. Halstead and Moore placed $Ca(OH)_2$ in an evacuated tube, adjusted a certain temperature and measured the pressure which was reached. Depending on the conditions it took several hours or

days until the system balanced [43]. Their measurements ranged from 2.5 to 90 kPa and are illustrated in Figure 2 (orange stars). The black line presents the thermodynamic equilibrium calculated by tabulated values of the Gibbs free enthalpy provided in the textbook of Barin [55]. In general the experimentally determined equilibriums lines of Schaube and Samms as well as the theoretically calculated one are in an adequate accordance. However it is obvious that especially at low vapor pressures the experiments are scarce and the results vary significantly. This indicates that the reaction might be very sensitive to changes of the local reaction conditions in this pressure range as well as the raw material itself might have an influence. The enthalpy of reaction determined by several authors vary between 94.6 kJ/mol [54] and 106.8 kJ/mol. [52]. For all calculations of the equilibrium temperature in this work the equation presented by Samms and Evans is used [54]:

$$\ln\left(p_{H_2O} * 10^{-5}\ Pa\right) = \frac{-11375\ K}{T_{equilibrium}} + 14.574 \tag{7}$$

Cycle stability

Long term cycle stability is another important material aspect which must be evaluated especially if the use of the material is considered in storage technologies with a desired lifetime of 20 years or more. Already in 1979 Rosemary and his colleagues demonstrated cycle stability of the reaction for 1171 cycles [47]. Schaube confirmed these findings in 2012 with a demonstration of 100 cycles in the thermal analysis [52]. However in technical reactors depending on the operation principle and conditions either agglomeration of the material or side reaction due to the presence of other gases or materials can occur which might affect the reactivity during long operational times. In general it can be stated that if the reaction is performed under defined conditions and impurities due to the presence of e.g. CO_2 is avoided the reaction is completely reversible and no degradation will occur.

Reaction kinetics

Numerous works deal with the determination of kinetic equations for the reaction system in general also obtained by measurement series performed in the TGA. The dehydration was experimentally examined in various works under vacuum or in a nitrogen or air atmosphere [56–60]. Other groups also investi-

gate the dehydration at low steam partial pressures [53,61] while more recent works from Schaube and Criado focused on the de- and rehydration at vapour pressures between 17.6 and 100 kPa [52,62]. Lin and Wang reported hydration kinetics performed in a high pressure thermogravimetric analysis between 670 and 3800 kPa [63,64]. Even though so much data is available on this topic no common understanding is achieved in the interpretation of the results. The authors propose entirely different reaction mechanism, the physical interpretations of the effects differ and the determined activation energies vary widely from 34 – 190 kJ/mol [52]. Therefore, the hypotheses arises that the kinetics of the reaction is highly sensitive to the experimental procedure, the pressure and temperature range as well as the nature of the sample material. This in turn leads to the conclusion that the predictive value of known kinetic equations for the behaviour of the reaction system in a real technical application at various operating conditions is severely limited.

Thermal conductivity and heat capacity

The heat capacity of materials can be determined by differential scanning calorimetry (DSC) and a standardized methodology. Schaube measured the heat capacity of CaO and $Ca(OH)_2$ in the temperature range between 20 and 500 °C via the DSC method. The values range from 0.75 kJ/kgK to 0.8 kJ/kgK for CaO and 1.1 kJ/kgK to 1.5 kJ/kgK for $Ca(OH)_2$ [65] at the respective temperatures and are in very good accordance with the tabulated values from textbooks [55,66] and Lander [67].

The thermal conductivity of a bulk of the storage material was also investigated by Schaube with three different devices: the thermal conductivity tester, the hot disk and the laser flash device. For temperatures below 200 °C the thermal conductivity was around 0.1 W/mK while at higher bulk densities and higher temperatures increased values of 0.38 to 0.55 W/mK were measured [65]. Since even the higher obtained thermal conductivity of the bulk is still very low, this property is a major challenge for the design of efficient reactors. However these values account for a non-reacting stationary bulk of the particles thus their predictive value for a reactive bulk is limited. The volume expansion due to an ongoing reaction as well as the presence of the reacting water vapour in the bulk might significantly influence the thermal conductivity. Therefore the meas-

urement of the actual thermal conductivity in reactive bulks is a currently addressed question. Reliable results are still pending due to the complexity of the required measurements.

Material modifications

Besides the investigation of pure $Ca(OH)_2$ the modification of the storage material with small amounts of additives in order adapt the reaction temperature and enhance the rate of reaction is also addressed by several groups. If it would be possible to tailor these parameters, storage materials could be designed to meet the requirements of the particular application and thus reach higher storage efficiencies. The group of Kato et al. where the first who demonstrated that the doping of magnesium hydroxide with inorganic salts lead to an enhancement of the reaction rate and a reduced dehydration temperature by 40 K. They granted that the effect was contributed to the hygroscopic property of the salts which improve the penetration of the water vapour into the reacting particle [68]. Shaktulov et al. picked up the idea of his colleagues and doped $Ca(OH)_2$ with potassium nitrate (KNO3). They reported that the dynamics of the dehydration was improved but the reduction of the reaction temperature was limited to only 5 – 10 K [69]. Kariya et al. impregnated the storage material with vermiculite and Yan et al. investigated the effect of Li and Mg doping. Both reported an increased reaction speed for the dehydration [70,71]. The so far reported results in this field are promising. A faster reaction rate and a lower dehydration temperature will in principle allow more compact reactor designs and enhance applications possibilities. However further research is required in order to understand the underlying effects and to achieve larger improvements. Material modifications also might oppose the advantage of using a cheap natural raw material.

2.2.2 Experimental research in lab and pilot scale

The investigations on the material level are important to improve the fundamental understanding of the reaction system. But as already pointed out, the predictive value of the determined characteristics in mg scale for larger systems is still very limited. Therefore, additional experimental research in larger reactors and under process relevant boundary conditions is essential in order to gain the

necessary knowledge and experience for the design of real thermochemical storage systems. Currently two different types of reactor concepts are adressed in lab and pilot scale.

Directly heated reactor concepts

In the so called directly heated concept the heat transfer fluid is in direct contact with the reacting particles. Consequently only a gaseous heat transfer fluid can be used. The heat transfer fluid is a mixture of the reaction gas water vapour and another inert gas, in general nitrogen or surplus steam, which takes up or delivers the heat of reaction. Due to the carbonization reaction of $Ca(OH)_2$ with CO_2 ambient air cannot be used as the heat transfer fluid. Clearly advantageous in this concept is that the direct contact between the particles and the gas allows for both: a high heat transfer rate as well as a large heat exchange surface (the particles). Disadvantageous is that the pressure drop over the bulk of storage material can be significant and needs to be compensated with higher pump powers. Also in order to keep a low water vapour partial pressure in the gas stream a large volume flow of the additional inert gas is required. This in turn limits the achievable temperature increase of the heat transfer fluid.

A first reactor directly heated by air was presented by Fuji[72]. Schaube et al. demonstrated the operation of a fixed bed reactor where the material (60 g) is in direct contact with a gas mixture of nitrogen and water vapour (shown in Figure 3).

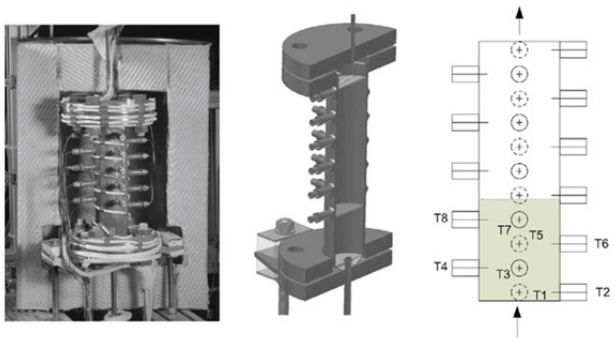

Figure 3 Directly operated fixed bed for 60 g material presented by Schaube [73]

The de- and rehydration, in total 25 cycles, was performed for different steam partial pressures: 17.6, 35.5, 74.1 and 95.6 kPa [73]. Based on these experi-

ments a kinetic model determined at the same pressures in the TGA was validated. After some cycles severe agglomeration of the particles exposed to the hot gas stream lead to inhomogeneous gas distribution in the bulk. Thus current efforts are related to the coating of the material in order to improve the powder bed properties [74].

Pardo et al. carried out the reaction in a fluidized bed reactor (shown in Figure 4) using a mixture of $Ca(OH)_2$ and 70 wt% inert easy to fluidize particles [75]. The dehydration was performed by an electrical heating of the reactor wall and the thermal energy released during hydration could not be recovered by the heat transfer fluid. Very recently the group of Rougé proofed the concept experimentally in a newly constructed lab scale set up [76].

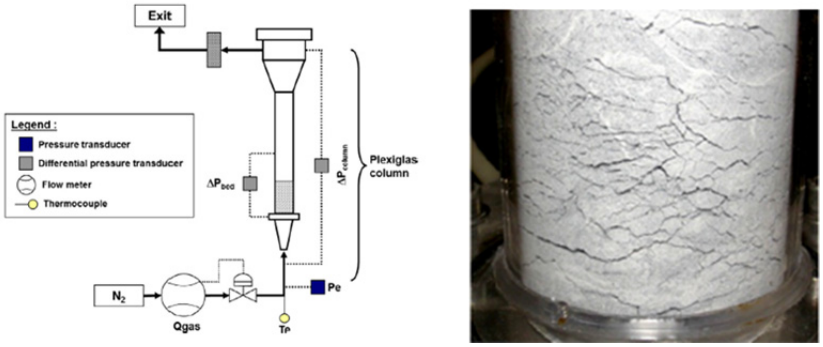

Figure 4 Fluidized bed reactor and test bench presented from Pardo [75]

In general it seems difficult to achieve a homogenous reaction due to the bulk properties.

Indirectly heated reactor concepts

The different concepts have their specific advantages and are worth investigating since at the current state of development an optimal reactor design is not available. However, some process applications require an indirectly heated concept. For example, if the heat transfer fluid of the process is liquid or a direct contact of the flue gas and the storage material could cause impurities. In both cases thermal energy has to be transferred via a heat exchanging surface that separates the reaction from the heat transfer fluid – a so called indirect concept. An additional advantage of this concept is that the reaction temperature can be adapted independently from the power output. This in conclusion leads to more

flexible operating modes and thus could extend process integration possibilities. Disadvantageous in this concept is that the low thermal conductivity of the bulk enforces complex reaction bed designs to achieve sufficient power densities. Also the mass transport of the reaction gas is challenging due to the low permeability of the bulk.

Experimental data on the operation of indirectly heated reactors is rather scarce. Ogura et al. presented a reactor using a double pipe heat exchanger (shown in Figure 5). The inner pipe is filled with a 200 mm high particle bed (400 g material) and connected to an evaporator. The heat released by the exothermal reaction was transferred to an air flow at ambient temperature in the shell pipe. They investigated the discharge procedure at an evaporation temperature of 17 °C and reached a maximum temperature of around 210 °C in the reaction bed with this vapour pressure. The temperature of the air increased by the released thermal energy from 20 to 55 °C [77].

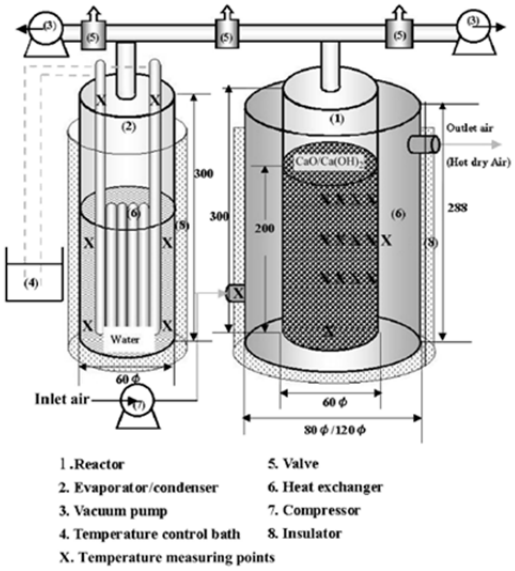

Figure 5 Reactor coupled to evaporator presented by Ogura [77]

Yan et al. reported experiments with 400 g of material in a fixed bed. Figure 6 shows a scheme of their test bench and a photography of the reactor. They analyzed the hydration reaction at different vapor pressures from 180 to 320 kPa but the reactor concept did not allow the recovery and the measurement of the released heat. Furthermore the dehydration reaction was driven by an electrical heating jacket [78].

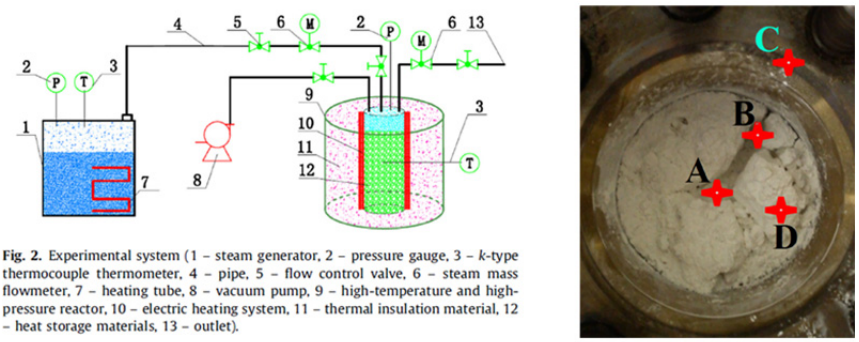

Fig. 2. Experimental system (1 – steam generator, 2 – pressure gauge, 3 – *k*-type thermocouple thermometer, 4 – pipe, 5 – flow control valve, 6 – steam mass flowmeter, 7 – heating tube, 8 – vacuum pump, 9 – high-temperature and high-pressure reactor, 10 – electric heating system, 11 – thermal insulation material, 12 – heat storage materials, 13 – outlet).

Figure 6 Scheme of the test bench and picture of the reactor presented by Yan [78]

In conclusion the data base for the operation of lab scale reactors is not only very limited but also the experiments do not sufficiently represent the required operation modes of an indirectly heated storage system in the real application. In most of the real applications the endo- and exothermal reaction will be thermally driven by the heat transfer fluid and the reaction system has to be operated in a wide pressure and temperature range which depends on the boundary conditions of the process.

Some of the recent works at DLR therefore focus on the operation of indirectly heated reactors in technically relevant scale. For this purpose a multifunctional pilot plant for thermochemical storage reactors up to a power of 10 kW was developed and set into operation [79]. Our group also presented the first concept in which not only the discharging but also the charging step was driven by an indirect coupling of the reaction bed with the heat transfer fluid [79,80]. Figure 7 shows a drawing of the reactor based on a plate heat exchanger concept. Air, serving as the heat transfer fluid, flows inside the ten spot-welded thermoshelves. The storage material is placed between the heat exchanger plates in 20 mm wide channels. Along the length of the reactor the air takes up or releases heat to or from the powder bed and leaves the reactor at the opposite site. The water vapor enters or leaves the reaction chamber through an inlet pipe placed in the center of the cover plate.

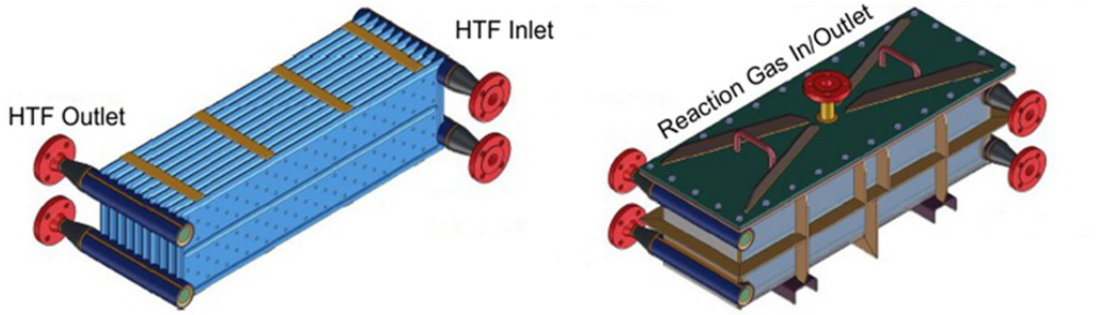

Figure 7 Indirectly heated reaction bed for 20 kg $Ca(OH)_2$ left: plate heat exchanger with channels for the storage material; right: closed reactor with connection for water vapour on top [81]

With the developed reactor the thermal charging and discharging at powers up to 8 kW was firstly demonstrated and the storage capacity of 10 kWh corresponding to 20 kg of material represents a technically relevant scale. Especially the discharge at reaction gas pressures of 100 and 200 kPa showed good performance and a temperature increase of the heat transfer fluid from 350 to 485 °C was observed. Also the demonstration of different operation modes adjusted through the variation of the water vapour pressure hereby controlling the power output independently from the volume flow of the heat transfer fluid was achieved. Additionally the simulation model used for the design of the reactor could be validated for the discharge pressures of 100 and 200 kPa with the experimental data [82].

On the other hand the design of the reaction bed limited the operating range of the reactor. Particularly at low vapor pressures the performance during charging and discharging was significantly limited. We mainly contributed this limitation to the mass transfer of the reaction gas due to the low permeable reaction bed and its height of 200 mm. The discharge pressure was additionally limited to 200 kPa due to the rectangular design of the reactor. Nevertheless, as soon as energy efficient process integration is considered, the operation of the storage system at low vapor pressures and pressures of more than 200 kPa is of high technical relevance.

Development of a moving bed pilot plant

Yet, due to the low thermal conductivity of the reacting material large storage capacities operated in an indirectly heated fixed bed also require large heat transfer surfaces. In other words the fixed bed concept somehow opposes one

of the main advantages of $Ca(OH)_2$, its low material costs. One approach to overcome this issue is to detach the costly reactor including the heat exchanger (power) from the inexpensive storage material (capacity). Besides the already mentioned fluidized bed concept [75,83,84] a moving bed concept was identified from Rosskopf et al. as alternative possibility [85]. To realize such a concept it is necessary to move the material through the reactor. $Ca(OH)_2$ is a fine, cohesive powder (d_{50} = 5 µm), hence its flowability is in general very poor. Additionally, the thermal conductivity of the material is low, therefore only a short distance between the particles and the heat exchanger surface can be allowed in order to ensure sufficient heat flux inside the reaction bed. Consequently the design of a heat exchanger for moving $Ca(OH)_2$ particles under reaction conditions is challenging and demands a modification of the material. These topics have been addressed for the first time within the European research project TCS Power [86].

In this context, a recent study [87] investigated the influence of coating calcium hydroxide with SiO_2 nanoparticles on the bulk properties. It was shown that coating with nanoparticles prevents agglomeration of the material due to reduction of cohesive forces between the particles. But besides this positive effect also unfavourable side reactions between the SiO_2 particles and the $Ca(OH)_2$ did occur during cycling. The formed side product is $Ca_5(SiO_4)$ and does not react in the desired operating range of the $Ca(OH)_2$ storage system [87]. As a result the storage capacity of the modified material is clearly reduced.

To overcome this issue mixtures of $Ca(OH)_2$ with different nano-additives have been investigated regarding their influence on the flowability of the bulk and on the reaction. In summary all of the tested nano-additives could improve the flowability but also formed reactive or inertial side products during cycling. Even though the activities are still ongoing an Al_2O_3 based nano particle product was chosen as an additive for investigations in larger scale. The mixture with Al_2O_3 seems to be stable during cycling and shows a higher conversion compared to a mixture of $Ca(OH)_2$ and SiO_2 nano particles even though the amount of additive needed to improve the flowability is significantly higher [88].

Figure 8 shows the basic design of the heat exchanger developed for the Al_2O_3 modified material. The storage material flows in 158 tubes with an inner

diamter of 28 mm. On the shell side of the heat exchnager the heat transfer fluid air flows in counter-current direction. It enters the reactor at the connection at the right side and flows around the tubes directed by six baffle plates. The heat transfer fluid leaves the reactor at the opposite side. With an overall heat transfer area of 5 m² the heat exchanger is designed to transfer a power of 10 kW at a nominal airflow of 160 Nm³/h and a temperature difference between air in- and outlet of 200 K [88].

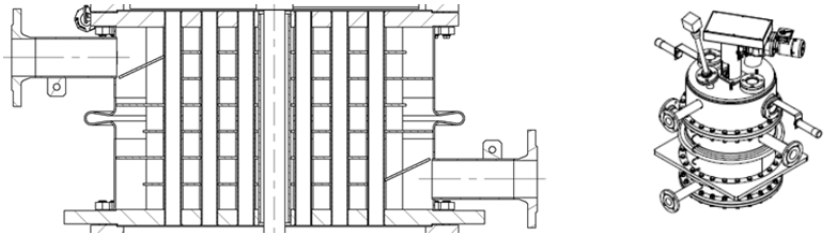

Figure 8 left: Heat exchanger for moving particles and air; right: moving bed reactor [88]

Figure 9 shows the design of the complete moving bed pilot plant including transport and storage facilities for the material. In each storage container approximately 270 kg of $Ca(OH)_2$ material can be stored. The material is transported via a screw feeder into the gas lock situated above the reactor inlet. In the gas lock the atmosphere between the storage container and the reactor atmosphere can be exchanged. The particles then fall out of the gas lock into the reactor. While the particles move through the tube bundle, thermal energy is delivered by the heat transfer fluid (air) driving the reaction of the material. The reaction gas is supplied into the reactor at the connections at the top and the bottom of the reactor. Once the material has reacted it leaves the reactor and is transported to the outlet gas lock where the atmosphere of the reactor is changed to ambient atmosphere (for storage). The material is then transported into the product container. The two containers can be exchanged to conduct the reverse reaction [88].

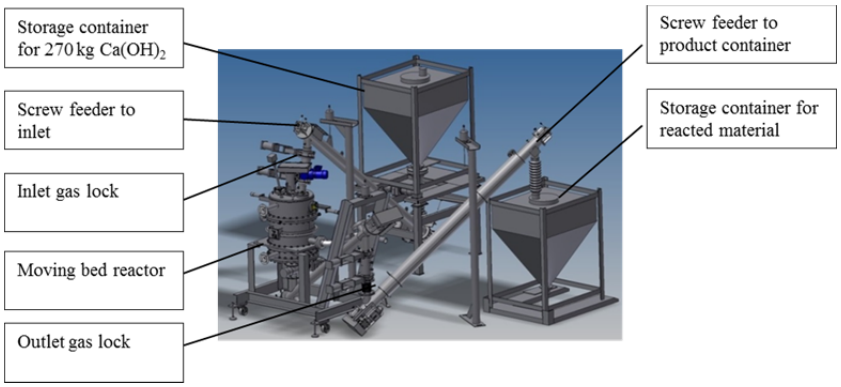

Figure 9 Pilot plant for moving bed reactor [88]

The pilot plant was successfully commissioned and set into operation. Thermal energy could be transferred to and from a constant mass flow of moving particles. However under reaction conditions when water vapour is present in the tubes the gravity assisted flow of the particles was partially hindered. Current research is therefore addressing the optimization of the operation under reacting conditions.

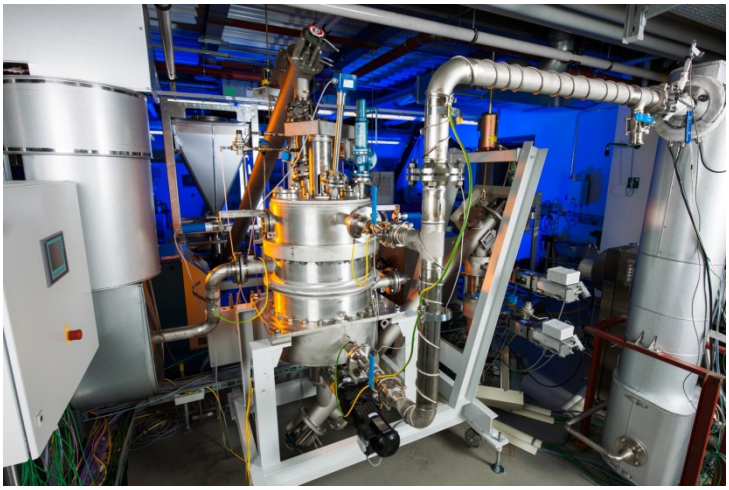

Figure 10 Moving bed pilot plant for 100 kWh and 10 kW at DLR [88]

2.2.3 Process integration

The reaction system $Ca(OH)_2$ can in theory be integrated in various process applications. In general excess thermal energy at high temperatures coming either from an industrial process or a concentrating solar field can be used to drive the charging process. A second possibility is to charge the storage system in times when renewable sources, for example wind or photovoltaic farms, pro-

duce surplus electricity. The charged material is then stored until a time or local shifted energy demand arises. During discharge the storage releases thermal energy which can either directly supply a high temperature processes, drive a Rankine steam cycle or any other consumer (e. g. a household heating system).

Since the storage operation in a CSP plant corresponds to two generic operation modes which are in general relevant for many applications, it is chosen as the exemplarily reference process for this work:

1. The thermal charging of the thermochemical system induced by a sensible heat transfer fluid
2. The generation of electricity with CaO and water via a Rankine steam cycle

In both operation modes technical and thermodynamic challenges arise when the characteristics of the processes and the thermochemical storage are taken into account. Main difference in the operation compared to sensible or latent storage system is that the temperature of the reaction can be adapted and the energetic effort for condensation and evaporation of the reaction gas needs to be integrated into the process.

Thermal charging with a sensible heat transfer fluid

The challenges for the thermal charging procedure are described exemplarily for the reference process of a CSP plant with a molten salt as the heat transfer fluid. Figure 11 shows the charging process of the thermochemical system with the sensible heat transfer fluid in a T, h diagram. The red line represents the cooling line for the molten salt, which operates at an upper temperature of 565 °C and should return to the solar receiver with a minimum temperature of 290 °C. The black lines present possible reaction temperatures of the TCS system at different condensation pressures. Exemplarily the temperature levels for the reaction at 330 °C, 400 °C and 455 °C are illustrated. From the diagram it becomes obvious that the molten salt and the storage system have an opposed characteristic. While for the sensible heat transfer fluid, the amount of transferred thermal energy is proportional to the change in temperature, the thermochemical reaction absorbs the enthalpy of reaction at a constant temperature level. This leads to a pinch point which limits the maximum amount of thermal

energy which can be incorporated into the storage system. From the illustration it can be concluded that an as low as possible reaction temperature should be maintained if the storage is charged with a sensible heat transfer fluid.

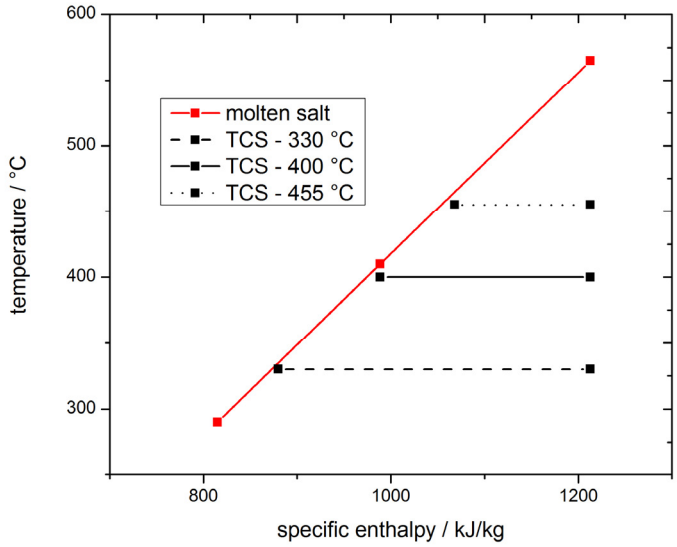

Figure 11 T, h diagram for the charging procedure of molten salt and the reaction system at different reaction temperatures

Thermal discharge to drive a Rankine steam cycle

Figure 12 shows the T, h diagram of a standard Rankine steam cycle configuration. The preheater operates from 250 °C to 330 °C while the major amount of thermal energy is required at the evaporator at a constant temperature level of around 330 °C depending on the live steam pressure. The superheater increases the steam temperature from 330 °C to 560 °C. The red lines present two possible discharge temperatures for the thermochemical storage system. Since a major part of the required thermal energy is at a temperature of 330 °C a reaction temperature of for example 400 °C would be sufficiently to supply the preheater and the evaporator. Only a smaller thermal load needs to be released at a higher reaction temperature of 600 °C to power the superheater.

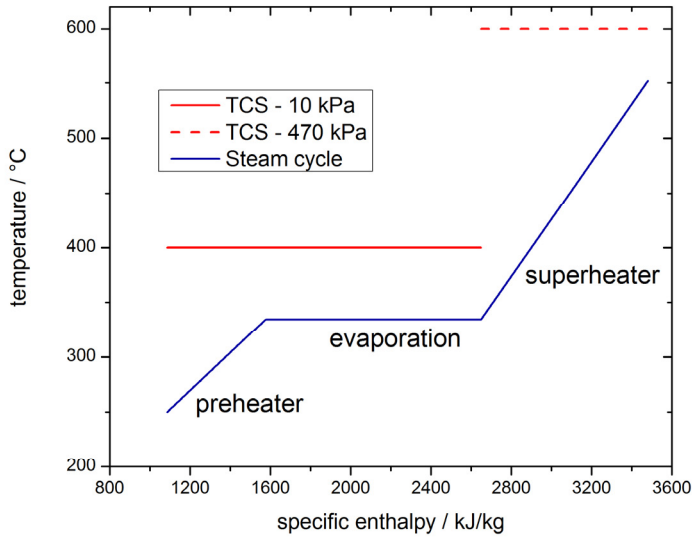

Figure 12 T, h diagram for proposed discharge procedure of the reaction system to drive a Rankine steam cycle

Reaction gas handling

Due to the distinct correlation between the reaction temperature and the gas pressure (explained in 2.2.1) it is indispensable to consider the reaction gas handling for the proposed operation modes. This in general means that the water vapour has to be continuously condensed or evaporated at the respective pressures during the charging and discharging procedure. In order to reach a high storage efficiency ideally no additional cooling power should be required to maintain the condensation pressure during the charging procedure. Consequently the heat sink for condensation can only be air or water cooling at ambient temperature, depending on the availability at the specific location. This in turn causes a dependency of the charging temperature and the ambient conditions of the process.

For the discharge procedure water vapour must be continuously supplied at the respective pressure in order to maintain the required discharge temperature. Again, in this case if an additional heat source is used for the evaporation the storage efficiency decreases drastically. But if the storage system drives a thermodynamic cycle thermal energy at the lower temperature level of the cycle might be available in order to supply the required heat of evaporation. In particular if a Rankine cycle is powered with the storage it seems likely to make

use of the thermal energy which in general needs to be rejected to the ambient. In general the discharge of the storage system at low vapour pressures enhances the possibilities to use low grade thermal energy from the process for the evaporation and is therefore an important operating range of the thermochemical system.

Furthermore a discharge at higher reaction temperatures (e. g. 560 °C for the Rankine cycle) might be required in order to meet the upper temperature level of the thermodynamic cycle. Consequently the discharge of the storage at high vapour pressures is also of high relevance for the technical application.

Figure 13 shows the theoretical equilibrium line of the reaction system and the condensation /evaporation line of saturated steam. Beyond that, the discussed possible operating conditions of the system are marked: the red squares indicate theoretical reaction temperatures for charging and discharging and the blue triangles mark the corresponding condensation /evaporation pressure and temperature.

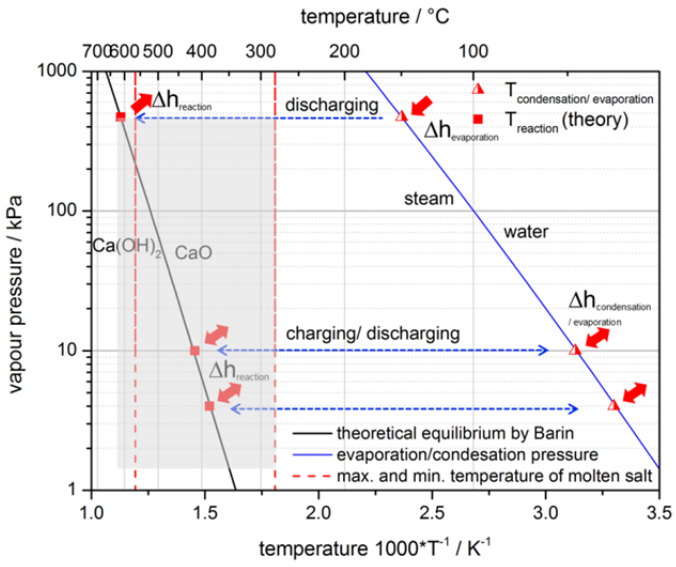

Figure 13 Exemplary charging and discharging conditions at 4, 10 and 470 kPa; complete process relevant operating range marked as grey area

With regard to the reference process, the CSP plant, mostly air cooling systems are used which achieve a minimal condensation temperature of 45 °C [89]. This in turn corresponds to a vapour pressure of 10 kPa thus a theoretical minimal charging temperature of 400 °C (blue dashed line in Figure 13). Simultaneously,

if the Rankine steam cycle operates at the same condensation pressure of 10 kPa a discharge of the storage system at this pressure is relevant.

Clearly, for other locations or wet cooling systems lower condensations pressures might be achievable and are thus also important operating points of the storage system. Exemplarily the charging and discharging at a pressure of 4 kPa are illustrated which corresponds to a condensation / evaporation temperature of 30 °C. In this work a charging pressure of 1.4 kPa corresponding to a condensation temperature of 12 °C is assumed as the lower boundary. Besides the charging and discharging at rather low vapour pressures the discharge at high vapour pressures is essential and has so far not been investigated. Exemplarily the evaporation at 470 kPa and 150 °C is illustrated which corresponds to a theoretical reaction temperature of 600 °C. This temperature level would be high enough to operate standard Rankine cycles at its nominal conditions and is therefore in this work considered as the upper temperature boundary for the discharging process.

The grey area in Figure 13 indicates the relevant operating range for the thermochemical storage with regard to realistic boundary conditions of the reference process. It was identified that the storage system must be operated at pressures between 1.4 kPa and 470 kPa and temperatures between 280 °C and 600 °C.

2.3 Aim of this work

The reversible reaction of calcium hydroxide to calcium oxide and water vapour is intensively discussed as an alternative thermal energy storage solution but the development of the technology is still in an early research state. So far the majority of the research focuses on investigations with small sample masses in a thermogravimetric apparatus where e. g. the cycle stability, the thermodynamic equilibrium or the reaction kinetics are assessed (refer to 2.2.1). These investigations on the material level are important for improving the fundamental understanding of the reaction. However, experimental research in larger reactors is indispensable for the development of thermochemical storage systems. As pointed out in the literature review experimental data on the operation of indirectly heated reactors with a representative amount of storage material are scarcely reported and the experimental conditions in general do not sufficiently represent the operation modes which are relevant for the real application (refer to 2.2.2).

The aim of this work is therefore to experimentally bridge the gap between lab-scale experiments and process integration by characterizing the reaction system in a lab-scale reactor under operating conditions which are relevant for one reference process. This in particular means thermal charging and discharging at vapour pressures between 1.4 kPa and 470 kPa and temperatures of 280 °C to 600 °C (as derived in 2.2.3). A special focus lies on the analysis of the thermal capability of the storage material under different thermal loads induced by the heat transfer fluid. By means of systematic variation of the operating parameters the technically relevant operational limits of the reaction system as well as expectable temperature levels are examined.

Based on the experimental results a first integration of the storage system in a reference solar power plant is conceptually analysed. Especially the thermal integration of the reaction gas supply (evaporation) into the Rankine steam cycle and the effect on the overall storage efficiency are analysed. This method in combination with the experimental results can be transferred to other potential applications of thermochemical energy storage with $Ca(OH)_2$.

3 Experimental set up

3.1 Lab-scale reactor

The aim of the reactor development was to enable the evaluation of the performance of the storage material in a wide operating range. The main limitations that are generally contributed to the reactor (not to the material) are mainly caused by the low permeability and the poor thermal conductivity of the bulk material. Bearing in mind to minimize these limitations without affecting the material properties two important design constraints for the novel reactor were derived. First of all, the reaction gas should only pass through a very thin layer of storage material. Secondly, the furthest distance between a single particle and the heat exchange surface should be short. Both design constrains would in principle lead to a very small mass of reaction material. In contrast, a representative mass of reaction material is mandatory in order to be able to operate the material according to the later application as thermochemical storage and to allow for both: a proper analysis of the thermal capability of the reaction and the analysis of the impact of the indirect heating or cooling. Additionally the geometry of the reaction bed and the position of the measurement sensors should be designed in a way that the experimental set up can serve for model validations.

Taken all design constraints into account it is obvious that the reactor has to offer a reasonable compromise between a reactor for generic investigations and a reactor for thermochemical energy storage. For this purpose, a single heat exchanger plate was chosen as basis for the reaction bed (see Figure 14, top). In this concept, the heat transfer fluid, air, flows inside the plate while the storage material lies on the plate. The plate is on both sides surrounded by a metallic frame of 10 mm height. The inner sides of the frame measure 150 mm in width and 1600 mm in length leading to 0.48 m² heat exchange surface. Consequently the reactor offers a cubic volume of 4.8 l (2.4 l on each side of the plate) for the storage material (see Figure 14, bottom left). A gas permeable metallic filter (pore size is 5 µm) placed over the powder material and screwed to the frame encases the reaction bed (see Figure 14, bottom right). The large

filter area allows for a negligible pressure drop between the powder material and the reaction gas supply.

Figure 14 Top: heat exchanger plate used as reactor; bottom left: storage material filled into the frame; bottom right: filter plate to encase the reaction bed

The heat exchanger plate with the encased bed on both sides is mounted into a pressure resistant casing pipe (shown in Figure 15).The casing pipe has an inner diameter of 200 mm and is made of stainless steel (alloy 1.4571). The shell is 3 mm thick and designed to operate at pressures from 0 – 1000 kPa at a maximum temperature of 550 °C.

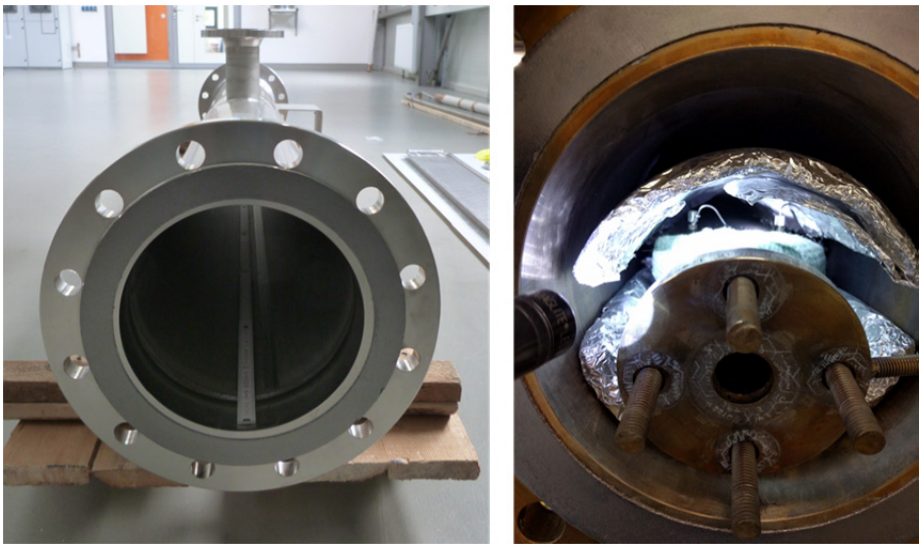

Figure 15 Left: pressure resistant casing pipe; right: heat exchanger plate mounted into the casing pipe with Al-foil as thermal shield

Measurement equipment

Figure 16 shows a schematic view of the whole set up including important dimensions and positions of the measurement instruments.

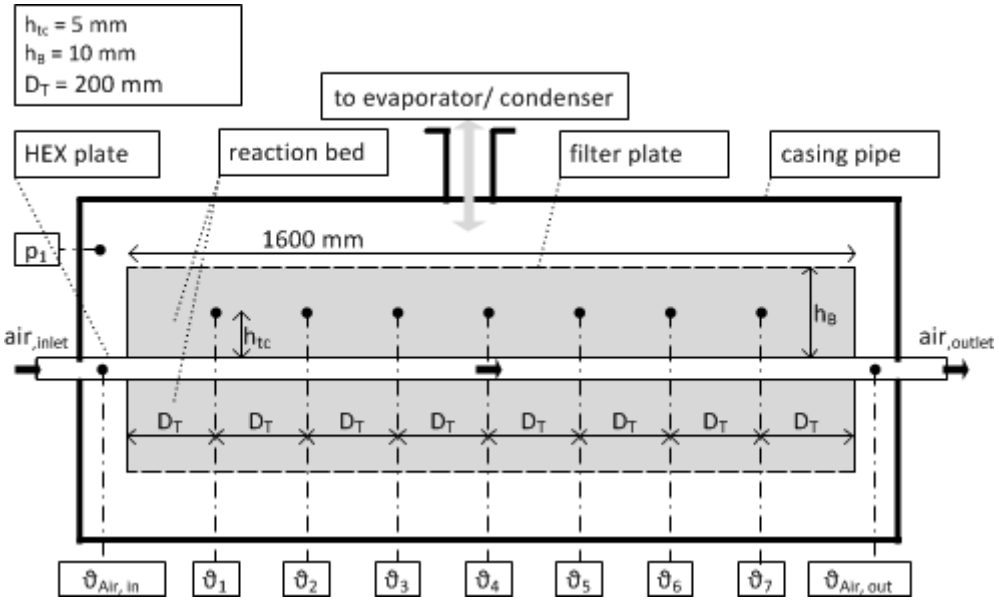

Figure 16 Schematic view of the reaction bed in the casing pipe including important dimension and positions of thermocouples and the pressure sensor (not to scale)

To observe the reaction progress, seven thermocouples $\vartheta_{1\text{-}7}$ (type K, ± 0.4 % ·T) are located in the middle of the beds height (h_{tc}), at a vertical distance of 5 mm to the heat exchange surface. In the horizontal direction of air flow the distance

between each measurement point is 200 mm (D_t) with the first point 200 mm away from the beginning of the reaction bed. Additional thermocouples measure the air temperature directly at the air in- ($\vartheta_{Air,in}$) and outlet ($\vartheta_{Air,out}$) of the plate. Furthermore a pressure sensor p_1 (PPA-35XHTT, Keller Ges. für Druckmesstechnik mbH, ± 0.8 kPa) measures the gas pressure in the reaction chamber

3.2 Test bench

Figure 17 shows the schematic process flow diagram of the test bench. The test bench was designed to operate the reactor under different thermal load conditions and at a wide range of vapor pressures. Therefore, it was most important to be able to adjust the thermal power of the heat transfer fluid and the vapor pressure in the reaction chamber independently of each other.

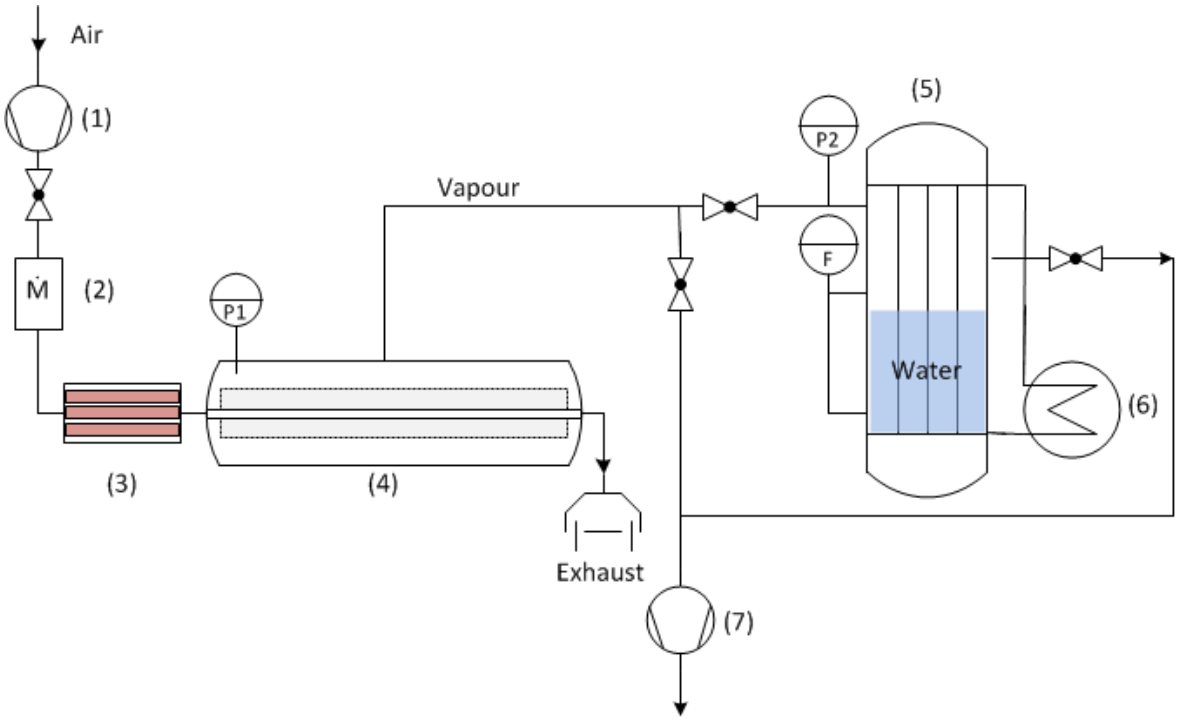

Figure 17 Schematic layout of the test bench

Heat transfer fluid supply

Due to the required temperatures, ambient air is used as heat transfer fluid in the experiments and is supplied by a compressor (1). The air volume flow can be adjusted by a mass flow controller (2) (Bronkhorst, digital flow controller, ±

0.4 %) before it splits up and enters three parallel electrical heating units (3). Each heating unit has an electrical power of 2 kW and preheats the air to a maximum temperature of 600 °C. After these heating units the air flows merge again in a diminishing pipe. This diminishing pipe is equipped with a controllable auxiliary heating to ensure a homogenous air temperature at the reactor inlet.

Reaction gas handling

During an ongoing reaction we must either remove water vapor from or supply it to the reaction bed. To realize this, a tube bundle heat exchanger (5) and a vacuum pump (7) are connected to the reactor. With the vacuum pump inert gases are removed from the system ensuring a pure vapor atmosphere. The tube bundle heat exchanger operates as condenser or evaporator depending on the type of reaction. A thermal oil flows inside the tubes of the bundle. The oils inlet temperature can be tempered between 3-160 °C by a thermostatic bath (6). On the shell side is liquid water (for condensation or evaporation) and the water temperature can be maintained constant during experiments because the thermal oil takes up the heat of condensation or supplies the heat of evaporation. Accordingly the evaporation/condensation pressure in the system can be varied between 0.7 - 618 kPa and be kept constant during an ongoing reaction. A pressure sensor at the outlet flange measures the pressure in the evaporator/condenser and the change of the water level is measured with a filling level meter (Vegaflex 65, ± 2 mm). By means of this value the reaction can be monitored and its conversion calculated.

Figure 18 shows a photography of the complete experimental set up. In the front the insulated casing pipe (4) with reaction bed inside can be seen. The vertical outlet pipe in the center of the reactor connects the reaction chamber with the condenser/ evaporator (5). Next to the condenser is the thermostatic bath located (6).

Figure 18 Photography of the complete experimental set up. Front: reactor; Back: condenser /evaporator (vertical)

3.3 Material

All experiments presented in this work are performed with $Ca(OH)_2$, product type “Sorbacal®H”, supplied by Rheinkalk GmbH/Lhoist group. Based on the products data sheet the purity of the material is approximately 98 %, the specific surface area is 19 m²/g and the d_{50} is 5.5 µm. In total 2.4 kg are filled in the reactor, equally distributed on each side of the heat exchanger plate. The presented experiments are based on two series of measurements. The first measurement series were performed with one batch of material which was cycled 35 times in total. Before the second series of measurements (all experiments with pressures more than 200 kPa) a new batch of material was filled in the reactor and cycled 10 times in total.

3.4 Experimental procedure

Before every experiment the whole set up is evacuated to 0.5 kPa ± 0.3 kPa and afterwards all valves are closed. The reactor is preheated to a set starting temperature with the air volume flow and additional auxiliary heating cables attached to the casing pipe. Simultaneously the vapor pressure for the experiment in the condenser /evaporator was adjusted by the thermostatic bath. As soon as the pressure in the condenser /evaporator and the temperatures in the reaction bed reached a constant level an experiment was initiated. The different operating conditions for all experiments are given in the respective sections. From the equilibrium line for water and saturated steam (blue solid line in Figure 13) the operating temperature of the condenser /evaporator at the required pressure can be determined.

Thermal charging procedure - dehydration

At the beginning of each dehydration the reactor contains $Ca(OH)_2$ and the set up is preheated to a temperature below the equilibrium temperature of the reaction at the adjusted vapor pressure. To start the experiment the valve between condenser and reactor is opened and simultaneously the air inlet temperature is increased to the set dehydration temperature. The induced heat load drives the dehydration reaction. Accordingly water vapor comes out of the reaction bed and condenses in the condenser. As soon as no further increase of the water level is observed the dehydration is finished and the respective valves are closed.

Thermal discharging procedure - hydration

At the beginning of every hydration experiment the reactor contains CaO and the set up is preheated to a set starting temperature below the equilibrium temperature of the adjusted evaporation pressure. To start the experiment the valve between reactor and evaporator is opened. In that moment water vapor streams into the reaction chamber and initiates the exothermic hydration reaction. The air flow takes up the heat of reaction as long as the reaction proceeds. The experiment is finished as soon as the temperature in every region of the reaction bed has reached its initial starting value.

3.5 Thermogravimetric analysis

To compare some results observed in the reactor a small sample mass (10 mg) of the same batch has additionally been analyzed in the thermogravimetric analysis (TGA). For these experiments a NETZSCH simultaneous thermal analysis (STA 449 F3 Jupiter ®) was used, equipped with a molar humidity generator (MHG32). The atmosphere during the measurements was inert using nitrogen, or a mixture of nitrogen and water vapor as purge gas (surrounds the sample) and pure nitrogen as the protective gas. The pressure inside the furnace was ambient pressure at ~97 kPa and a volume flow of 100 ml/min of purge gas was used. The bottom of the furnace was heated to 120 °C and a protection gas volume flow of 20 ml/min nitrogen was supplied, in order to protect the thermo-balance of condensation drops. The furnace design does not allow the mixing between the purge and protective gases, thus the protective gas flow does not affect the concentration of humidity inside of the furnace. The conversion is calculated by the ratio of the measured mass change of each cycle to the measured mass change of the first complete dehydration cycle. With this set up isothermal hydration and dehydration experiments in the TGA at vapor pressures comparable to the conditions in the reactor were performed.

4 Experimental results

4.1 Set in operation

In order to prove the correct function of the reactor and the measurement equipment a hydration experiment at an evaporation pressure of 100 kPa according to the procedure described in chapter 3.4 Experimental procedure was performed. For comparison experimental data for the pressure of 100 kPa is reported by several references including my own measurements with a previously investigated reactor [80].

Figure 19 shows the results of the experiment. The air inlet temperature $\vartheta_{Air,in}$ (red solid line) was kept constant at 450 °C during the experiment. At t = 0 min the valve between evaporator and reactor was opened thus the pressure in the reactor rises to 100 kPa (black dash dotted line). Due to the exothermic reaction the temperatures in the reaction bed ϑ_1 (green solid line) and ϑ_7 (blue solid line) jump up to a maximum of 507 °C. This temperature accords to the theoretical equilibrium temperature (grey dashed line) which was calculated by the measured pressure and the respective correlation given by Samms et al. [54] and equation (11) (compare Figure 2). Also Schaube et al. [52] and Halstead and Moore [43] reported equilibrium temperatures between 505 °C and 510 °C for a vapour pressure of 100 kPa. The slight difference between the equilibrium temperature and the bed temperatures during the first 10 min is related to small pressure differences between the measured pressure in the casing pipe and the local pressure in the reaction bed (compare Figure 16). These differences are only significant during the initial period where highly dynamic changes occur in the system.

We also observe a reaction front along the flow direction of the air. Close to the air inlet the cooling of the reaction bed is maximal due to the largest temperature difference between the bed and the air. Thus the reaction proceeds quickly and 10 min after the initiation the temperature ϑ_1 drops again. This indicates that a major part of the material is already converted in this region and the heat released by the reaction decreases. In contrast, in the rear region of the reactor the temperature between the bed and the air flow is small in the beginning. As a

consequence the reaction proceeds slower indicated by the constant temperature plateau which is hold for 25 min. As more and more material has reacted in this part also the temperature ϑ_7 starts to drop. After 100 min the bed reaches its initial temperature again indicating that no more heat is released. Accordingly, a conversion of 90 % (black cross dots) is measured at this point. The difference before and after the reaction between air inlet temperature and temperatures inside the reaction bed are contributed to radiative heat losses inside the reaction chamber, that have been minimized but cannot be completely removed.

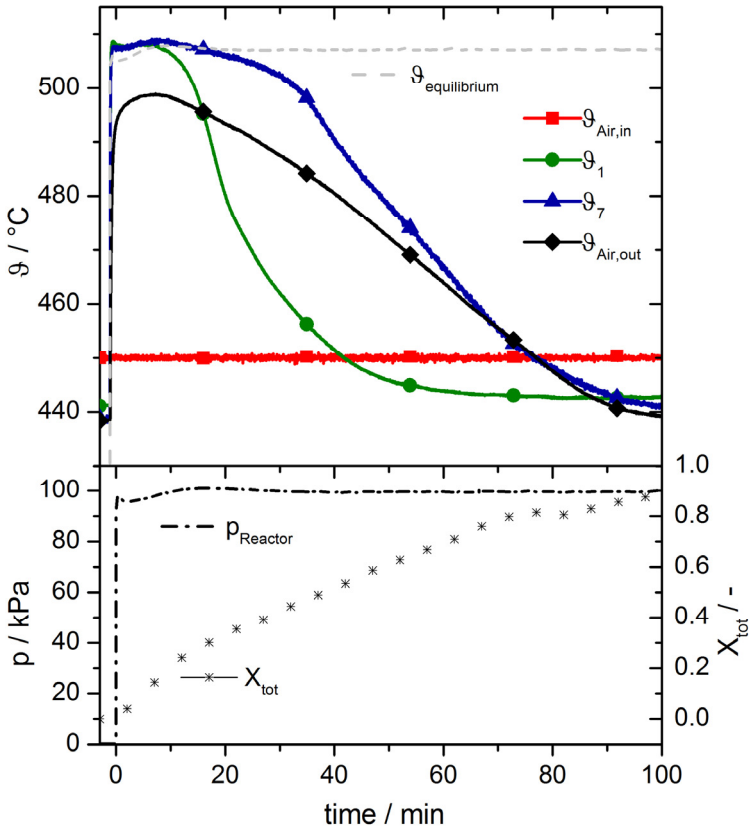

Figure 19 Hydration experiment at 100 kPa and a starting temperature of 450°C

Based on this experiment it could be shown that the temperature and pressure sensors work reliably. Additionally the determined conversion based on the measured filling level meter and the weight of the filled in material is reasonable. A conversion of 95 % was measured after 160 min while the purity of the material is specified with 98 %. The reaction proceeds as expected according to

the theory. It is remarkable that the whole reaction bed reaches the theoretical equilibrium temperature of 505 – 510 °C.

4.2 Thermal charging

In this section the charging characteristic of the reaction system is investigated under various operating conditions which are relevant for various applications. Experiments are performed at different vapour pressures, operation modes and heat loads of the heat transfer fluid. Table 2 summarizes all relevant parameters for each dehydration experiment discussed in the following section. Two different operation modes are applied to initiate the dehydration, the first one is based on a temperature increase and the second one is based on a pressure decrease. The term behind the label of the experiment defines the operation mode of the dehydration experiment: (T+) refers to a temperature increase and (p-) refers to a pressure decrease.

Table 2 Parameters of dehydration experiments presented in chapter 5.2

Experiment (mode)	$T_{air,\ initial}$ / °C	$\dot{V}_{Air}$ / $\frac{\mathbf{Nm^3}}{\boldsymbol{h}}$	$T_{air,dehydration}$ / °C	$p_{condenser}$ / kPa	$T_{condensation}$ / °C
A (T+)	400	20	560	10	45
B (T+)	400	12	560	10	45
C (T+)	400	12	520	10	45
D (T+)	400	12	480	10	45
E (T+)	400	12	560	19.9	60
F (T+)	400	12	560	1.4	12
G (p-)	500	20	500	10	45
H (p-)	500	24	500	10	45
J (p-)	500	28	500	10	45
I (T+)	370	12	480	4.3	30
K (p-)	560	24	560	100	99

4.2.1 Dehydration at 10 kPa

Reference experiment

A reference dehydration experiment has been performed with a preheating temperature of 400 °C and a condensation pressure of 10 kPa (condensation temperature 45 °C). Figure 20 shows the temperature, pressure and conversion trends. At t = 0 min the air inlet temperature starts to rise up to the set dehydration temperature of 560 °C (red solid line). Exemplarily the temperatures ϑ_1 (green solid line) ϑ_3 (blue solid line) and ϑ_7 (orange solid line) positioned in the front, middle, and rear region (compare Figure 16) of the bed are plotted. Within the first 30 min the material temperatures increase to 445 °C due to the incoming heat flux. At a temperature of 445 °C a significant change occurs in the slope of the temperature trend. In particular in the middle (ϑ_3) and rear region (ϑ_7) of the bed a temperature plateau can be observed. The temperature plateau indicates that the heat input from the heat transfer fluid is completely absorbed by the endothermic reaction. Accordingly during this time we also observe that the conversion trend (black cross dots) shows a constant rate indicating the ongoing reaction with a constant thermal charging power. After 120 min almost 80 % of the material is converted thus the heat input in the rear region slowly becomes larger than the amount of heat which is still absorbed by the endothermal reaction. Consequently the material temperatures rise again until after 200 min a conversion of 96 % is reached and all bed temperatures reach their constant maximum. What might seem controversy is that the temperature plateau lies at 445 °C while the equilibrium temperature at the condensation pressure of 10 kPa is 400 °C (grey dash dotted line). This significant distance to the theoretical equilibrium temperature is further analyzed with a variation of thermal power of the heat transfer fluid.

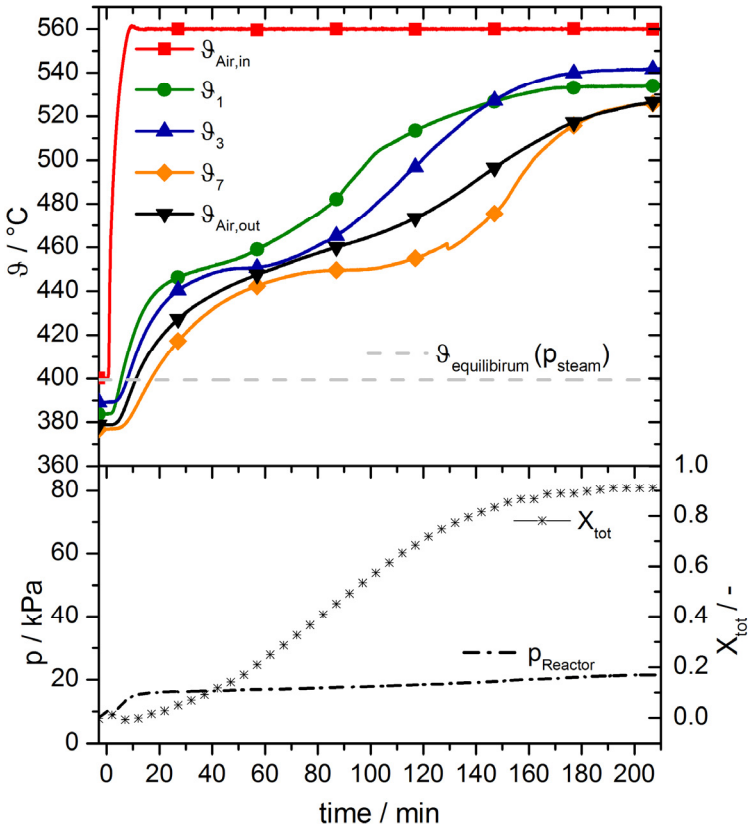

Figure 20 Dehydration experiment at 10 kPa and an air inlet temperature of 560 °C

Variation of thermal power induced by the heat transfer fluid

In order to analyze the influence of the thermal power induced by the heat transfer fluid on the dehydration reaction, we perform the dehydration experiments at a condensation pressure of 10 kPa with 4 different thermal heat fluxes into the reaction bed. The results are shown in Figure 21. Experiment A (red curves) was performed with a 60 % higher volume flow than the reference experiment B (green curves) but with the same air inlet temperature of 560 °C. Experiment C (blue curves) and D (orange curves) run with the nominal volume flow but at reduced air inlet temperatures of 520 °C respectively 480 °C (compare Table 2 for all parameters). The conversion curves show that the influence of the heat flux into the bed directly correlates with the speed of conversion. With the largest heat flux we receive the shortest dehydration time (red squares experiment A), whereas smaller heat fluxes prolong the dehydration times (B to C to D).

Figure 21 also shows the temperature trend of ϑ_7 for every experiment. We can see that independently from the heat flux into the bed, the material temperatures increase within the first 30 min. This indicates that initially the reaction speed is so slow that the incoming heat flux is larger than the thermal energy absorbed by the reaction. However a constant temperature plateau develops at temperatures above 440 °C for all experiments. In general, a temperature plateau region during dehydration is characterized by an equilibrium state between the thermal energy absorbed by the endothermic reaction and the heat flux delivered by the heat transfer fluid. It is remarkable that during the experiments A, B and C the plateau develops at the same temperature of 445 °C independently of the heat flux into the reaction bed. Only in experiment D the plateau temperature is slightly lower at 440 °C - but at the same time the charging power seems not anymore of technical relevance due to its long dehydration time.

The results lead to the hypothesis that a very significant change in the rate of reaction occurs at temperatures around 440 °C. At higher temperatures the rate of the reaction is then fast enough and the heat transfer becomes the limiting factor in the conducted experiments. However at low pressures (in this case ~10 kPa) and temperatures below 440 °C the slow effective reaction rate of the material lead to a serious limitation of the operating range of this thermochemical storage: The experiments reveal that if a certain thermal charging power density is required at the respective pressure conditions, the charging temperature has to be around 45 K higher than the value predicted by the equilibrium line.

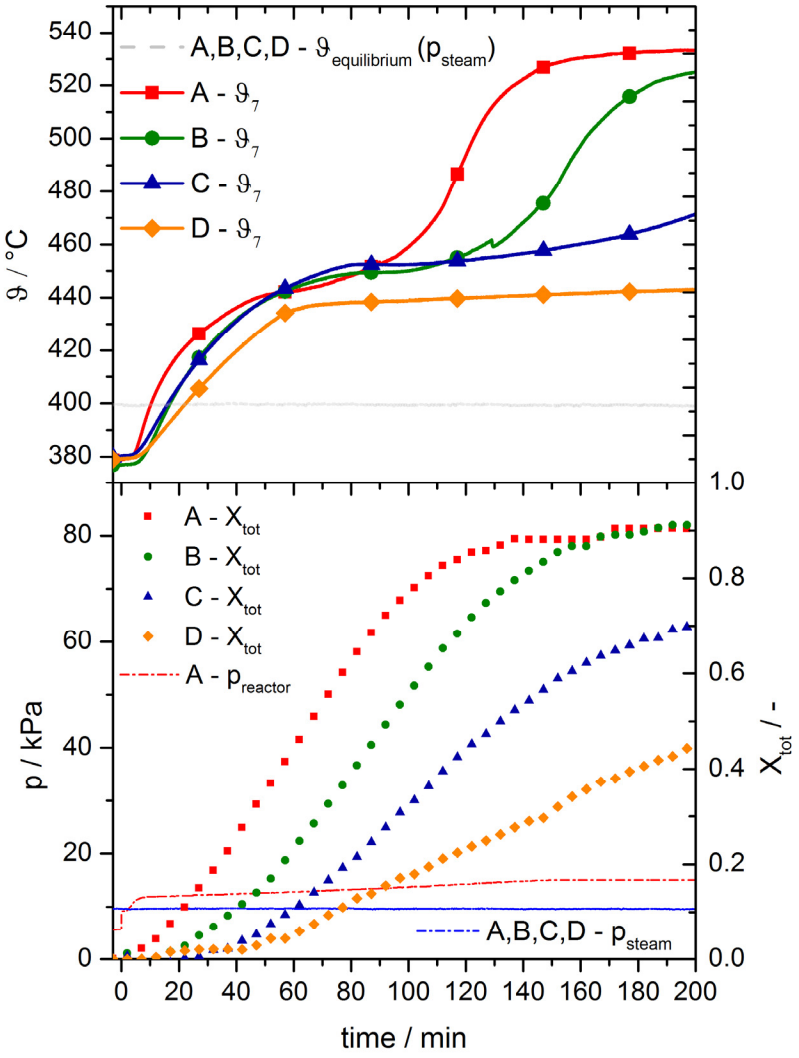

Figure 21 Dehydration experiments at 10 kPa at different heat loads of the heat transfer fluid

Variation of operation mode at 10 kPa

From the experiments where the dehydration is initiated through a temperature increase of the heat transfer fluid the hypothesis arises that the reaction rate seem to slow for a technical application at a temperature of 400 °C and a vapour pressure of 10 kPa. To examine this important phenomenon further we perform additional experiments at the same vapour pressure but with a different operation mode: the dehydration procedures are performed at a constant temperature and the endothermal reaction is initiated through a pressure decrease. Three experiments G, H and J are performed with air volume flows of 20, 24 and 28 Nm³/h in order to vary the heat flux into the reaction bed.

Figure 22 shows the temperature ϑ_1, ϑ_3, ϑ_7, the conversion as well as the pressure trends for all experiments. The air inlet temperature and the casing pipe temperature are constant at 500 °C during the entire procedure. At min 0 the valve to the condenser is opened where a pressure of 10 kPa predominates. In that moment the pressure (dashed dotted lines) in the reaction chamber drops suddenly and simultaneously the temperatures of the reaction bed (solid lines) decline quickly. It can be observed that in the front region of the reaction bed (ϑ_1) where the heat load is initially maximal (due to the incoming air at 500 °C) the temperature stabilize between 442 °C – 445 °C. This short temperature plateau again indicates an equilibrium state between the heat absorbed by the endothermal reaction and the heat flux into the reaction bed and is hold for approximately 10 min before the temperature increases again. The temperature increase indicates that a considerable part of the material is already converted in this part of the reactor. In consequence the heat flux into the bed is larger than the thermal energy which is still absorbed by the reaction. The temperature plateaus which can be observed in the middle region (ϑ_3) of the reactor are longer but arise at the same level of 442 °C– 445 °C. Only in the rear region of the reactor (ϑ_7) where the heat load is initially minimal the plateau arises at 440 °C for the cases H and J. For experiment G, which represents the smallest heat load of all experiments, a minimal plateau temperature of 438 °C is observed. The results of the dehydration induced through pressure decrease accord very good to the results of the experiments where the dehydration was initiated through temperature increase. In all experiments at 10 kPa condensation pressure it is observed that when the heat flux is high plateaus arise at temperatures higher than 442 °C, which corresponds to a distance to the theoretical equilibrium temperature of 45 K. It could also be observed that when the heat load is smaller plateaus between 338 °C and 440 °C are possible but at the same time the charging time prolongs to more than 120 min and is therefore of minor technical relevance. In order to proof that the observed phenomena's are related to kinetic limitations of the material and not to our reactor set up, additional measurements are performed by means of thermogravimetric analysis.

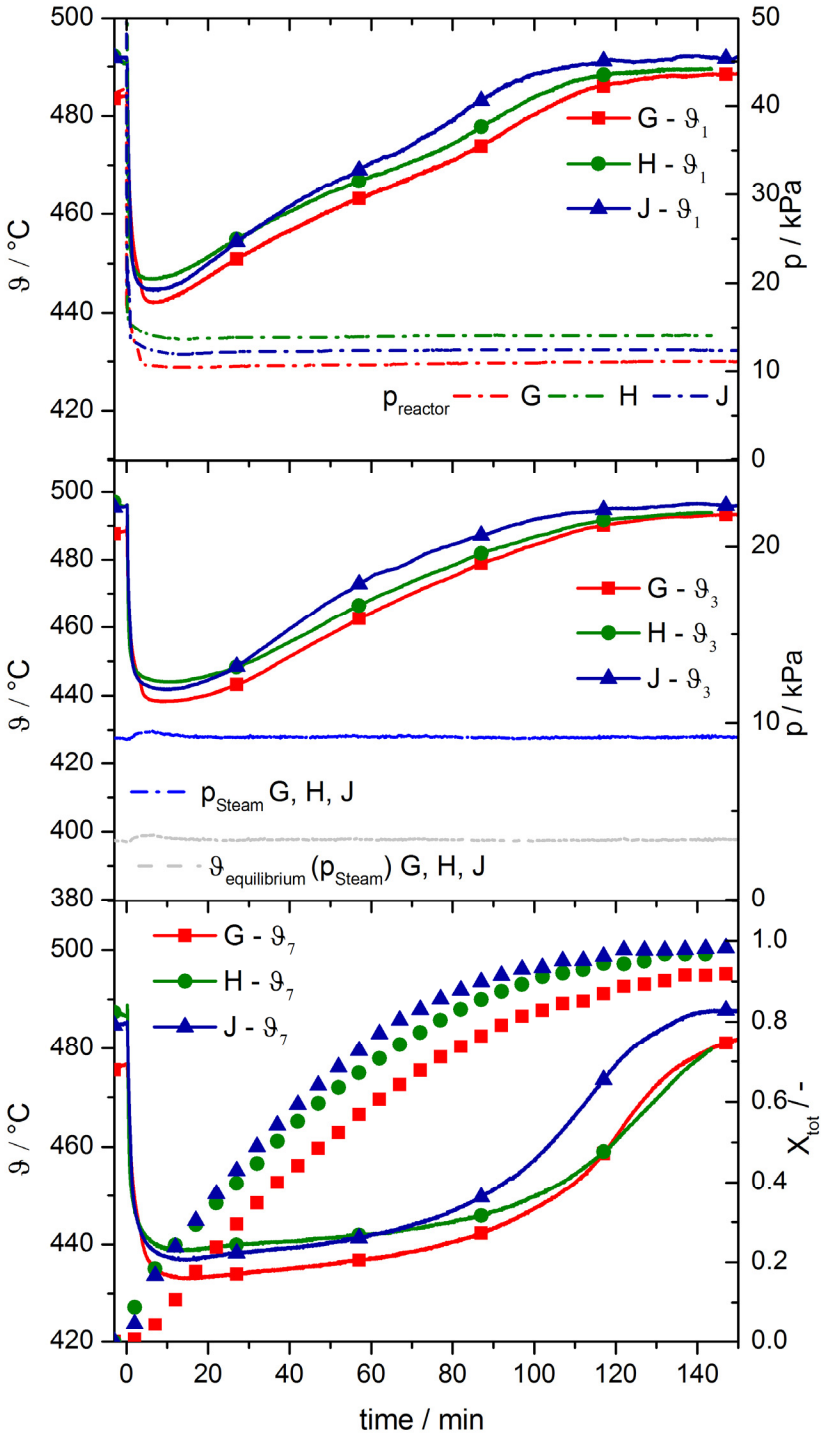

Figure 22 Dehydration at 500 °C induced through sudden pressure drop under different heat loads of the heat transfer fluid

Dehydration at 10 kPa in the TGA

The experiments in the TGA were performed according to the procedure described in section 4.4 and conditions comparable to the reactor experiments. The main differences to generally reported TGA data for $Ca(OH)_2$ are isothermal measurement conditions at very low gas pressures. The used material is from the same batch like the material in the reactor. Six different dehydration experiments at a humid atmosphere inside the furnace of 10 kPa and isothermal temperatures between 410 °C and 450 °C were conducted. Each temperature was remained constant for 1 hour while the mass change was measured.

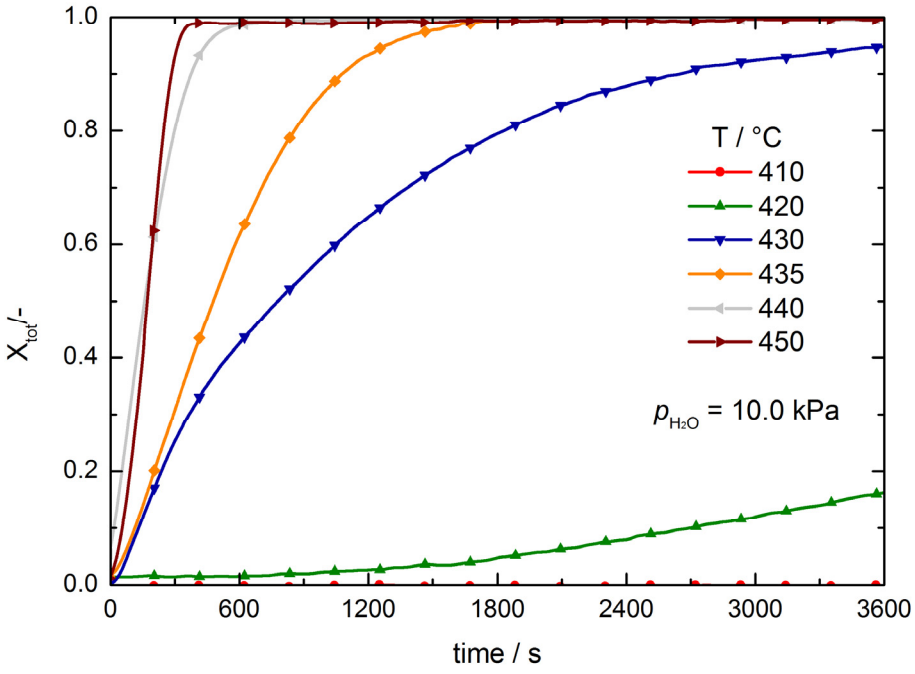

Figure 23 Effect of the temperature on the dehydration reaction of Ca(OH) at a vapor pressure of 10 kPa

Figure 23 shows the conversion trend of $Ca(OH)_2$ to CaO at different isothermal measurements. It can be observed that at 410 °C no mass change occurs within 1 hour. At 420 °C a small mass change was measured, while at 430 °C the rate of conversion changes significantly but conversion is still incomplete after 1 hour. At 435 °C full conversion is reached after 30 min - but with only a slight increase of 5 K to 440 °C the dehydration time is reduced to less than 10 min. A further increase to 450 °C does not result in a significantly faster conversion.

The results from the thermogravimetric analysis accord to what was observed in the reactor. Below a temperature of 440 °C the reaction rate is rather slow thus the heat flux into the reaction bed is higher than the thermal energy absorbed by the reaction. As a consequence the reaction bed heats up sensible. When 440 °C is exceeded the reaction becomes so fast that the heat flux into the reaction bed is completely absorbed by the endothermic reaction. Consequently a constant temperature plateau forms.

4.2.2 Dehydration at pressures 1.4 – 100 kPa

The presented discharge experiments at 10 kPa are highly relevant for many process applications since the pressure corresponds to a condensation temperature of 45 °C. However in different applications or locations, higher or lower condensation temperatures might be available. In order to complete the possible operating range the dehydration performance at various condensation pressures is analysed in this chapter.

Dehydration at 4.3 kPa

Figure 24 shows the thermal charging procedure at a vapour pressure of 4.3 kPa corresponding to a condensation temperature of 30 °C (experiment I in Table 2). The air temperature was initially set to 370 °C which corresponds to the theoretical equilibrium temperature at this pressure. To drive the reaction the air inlet temperature is increased to 480 °C at min 0. A qualitatively similar temperature trend like in the dehydration experiments at 10 kPa (compare Figure 20) can be observed. The material temperatures increase even though the equilibrium temperature is already exceeded all over the reaction bed. Only when the bed temperatures exceed approximately 425 °C the slope of the temperature trends changes significantly. A plateau arises in the middle (ϑ_5) and rear (ϑ_7) region of the reaction bed and accordingly a constant slope in the conversion trend sets in (after min 50). Again, like in the 10 kPa experiments, a distance to the equilibrium temperature is required until the heat flux into the reaction bed and the thermal energy absorbed by the reaction come in an equilibrium state. The required temperature difference for this experiment accounts 55 K. The experiment was stopped after 5 hours with a conversion of 70 %.

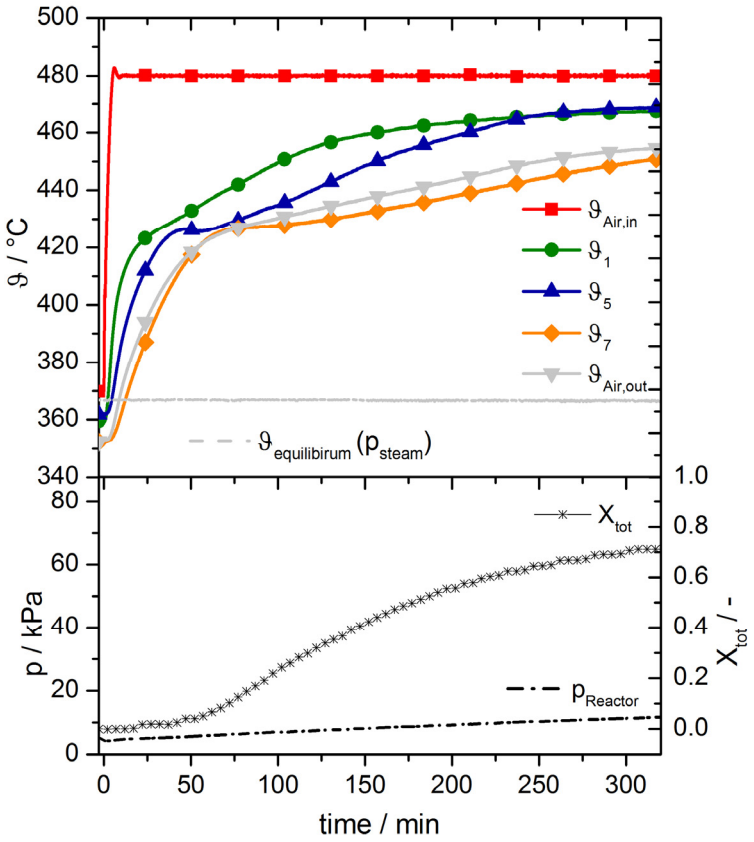

Figure 24 Dehydration at 4.3 kPa and a dehydration temperature of 480 °C

Variation of condensation pressure

To examine the influence of the condensation pressure on the dehydration time and the charging temperature three experiments at different condensation pressures but the same heat load induced by the heat transfer fluid are compared. Figure 25 shows experiment B (green line), the reference dehydration at 10 kPa while experiment E (red line) is performed at 20 kPa and experiment F (blue line) is performed at 1.4 kPa. Each experiment was run with the nominal volume flow and the air inlet temperature was increased to 560 °C. From the conversion curves we can clearly see, that the lower the condensation pressure the faster we reach full conversion. For example for experiment F 80 % is converted after 80 min while for experiment B 80 % conversion is achieved 100 min after the equilibrium temperature is exceeded, respectively after 150 min for experiment E.

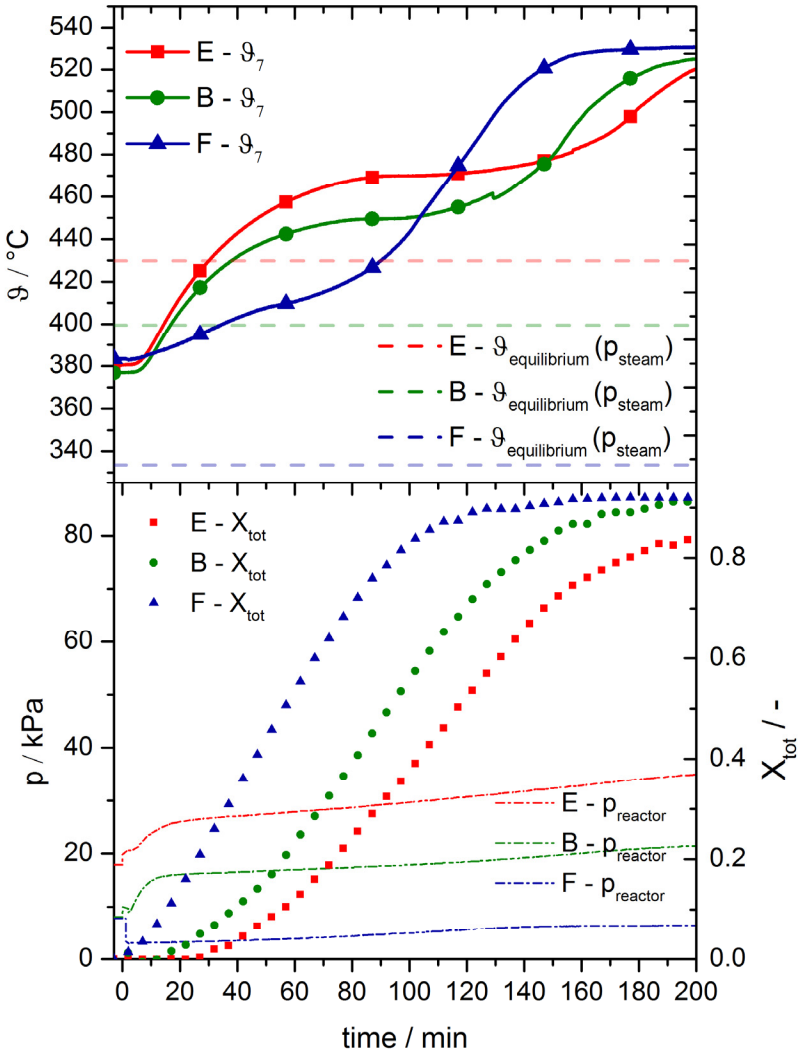

Figure 25 Dehydration experiments at 1.4, 10 and 20 kPa and an air inlet temperature of 560 °C

Even more interesting are the plotted temperature trends for the rear region of the bed. We can see that for the experiments at 10 kPa and 20 kPa the temperature trends are qualitatively similar. The material heats up sensible in the beginning until the reaction becomes as fast that we reach an equilibrium state between heat influx into the reaction bed and the thermal energy absorbed by the reaction (indicated by the constant temperature plateaus). For experiment F no plateau arises indicating that the heat flux into the reaction bed is always higher than the heat flux absorbed by the reaction. In all cases we observe that the above discussed temperature difference to the theoretical equilibrium temperature (red, green and blue dashed line) is required. However the difference

tends to be smaller for higher dehydration pressures: the difference is 35 K at 20 kPa, 45 K at 10 kPa and more than 50 K for 1.4 kPa. But even though a smaller temperature difference to the equilibrium is required, at 20 kPa the dehydration temperature at which reasonable reaction rates can be realized is already 465 °C.

Dehydration at 100 kPa

To complete the charging operating range a dehydration procedure at 100 kPa has been performed. Such an operation would for example allow to incorporate the heat of condensation at 100 °C into a district heating network. The dehydration was initiated through pressure decrease while the air temperature and volume flow was kept constant 560 °C and 24 Nm³/h. Figure 26 shows the temperature trends for the air (inlet and outlet), the reaction bed (ϑ_1, ϑ_3, ϑ_5, ϑ_7) and the conversion trend. At t = 0 min the reactor is connected to the condenser with a pressure of 100 kPa. It can clearly be observed that the material temperatures drop directly and plateaus arise according to the induced heat load. In the front region of the reaction bed (ϑ_1) the plateau arises at approximately 538 °C while in the rear region (ϑ_7) the plateau temperature is around 522 °C (grey solid line). It can be concluded that even at such a high reaction pressure and temperature the charging of the storage requires a significant distance to the theoretical equilibrium temperature.

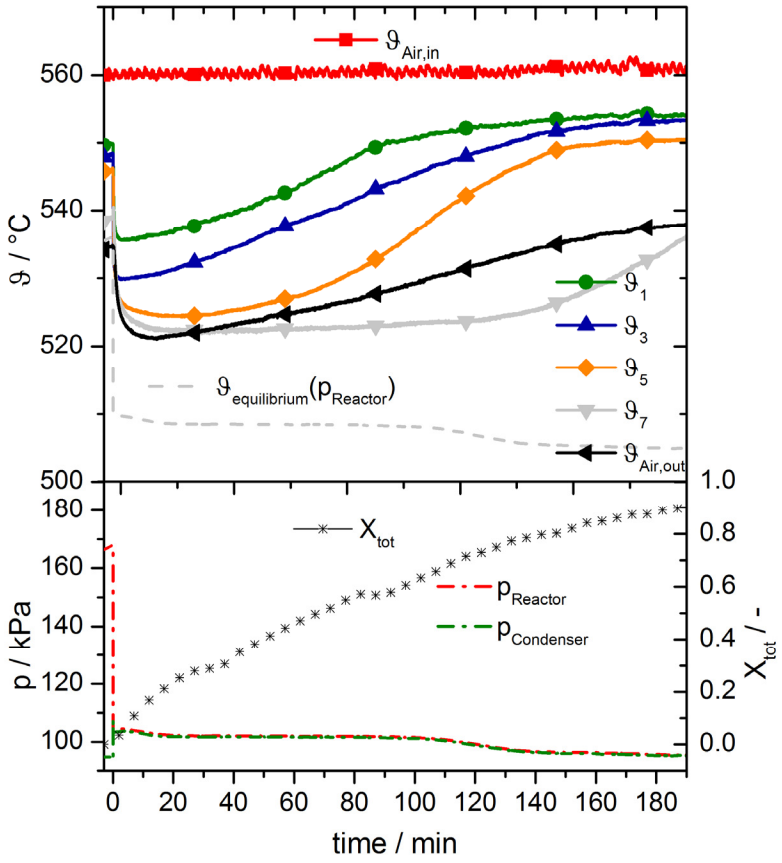

Figure 26 Dehydration at 100 kPa and an air inlet temperature of 560 °C

4.3 Thermal discharging

The operation at discharge conditions regarding temperature and pressure which are relevant for process applications are analysed in this chapter. Table 3 summarizes the parameters for all presented experiments.

Table 3 Conditions for all discharge experiments presented in chapter 5.3

Experiment	$T_{air,\ initial}$ / °C	$\dot{V}_{Air}$ / $\frac{\mathbf{Nm^3}}{\boldsymbol{h}}$	$p_{evaporator}$ / kPa	$T_{evaporation}$ / °C
A	500	16	470	150
B	500	20	470	150
C	500	28	470	150
D	500	20	200	120
E	500	20	270	130
F	280	12	4	30
G	280	12	8.7	43
H	280	16	8.7	43
I	280	12	10	45
J	310	12	20	60
K	350	12	50	81

4.3.1 Hydration at 200 - 470 kPa

Reference experiment

Figure 27 shows the reference discharge experiment. The reaction bed is preheated to a temperature of 500 °C while in the evaporator an evaporation temperature of 150 °C is adjusted. At minute 0 the valve between evaporator and reactor is opened thus the pressure in the reactor increases up to 470 kPa (red dash dotted line). Triggered by the pressure increase the exothermal reaction set in and the material temperatures in the front (ϑ_1), middle (ϑ_3) and rear (ϑ_7) of the reaction bed jump to a maximum of 600 °C. The reached temperature corresponds to the equilibrium temperature (grey dashed line) which was calculated with the measured pressure in the reactor and the correlation given by equation (7) [54]. Furthermore, we observe a clear reaction front in the horizontal

direction of the air flow. At all three measurement points the reaction proceeds at the equilibrium temperature which is indicated by the constant temperature plateaus and the simultaneously measured constant increase in conversion. The temperature (ϑ_1) drops again after 8 minutes which indicates that a major part of the material in the front region is already completely converted. The reactive area moves along the reaction bed until also the material in the rear region has completely reacted and ϑ_7 starts to decreases after 35 minutes. Accordingly 80 % of the total mass is converted after 35 minutes (black cross dots) while a total conversion of 92 % is measured after 60 minutes.

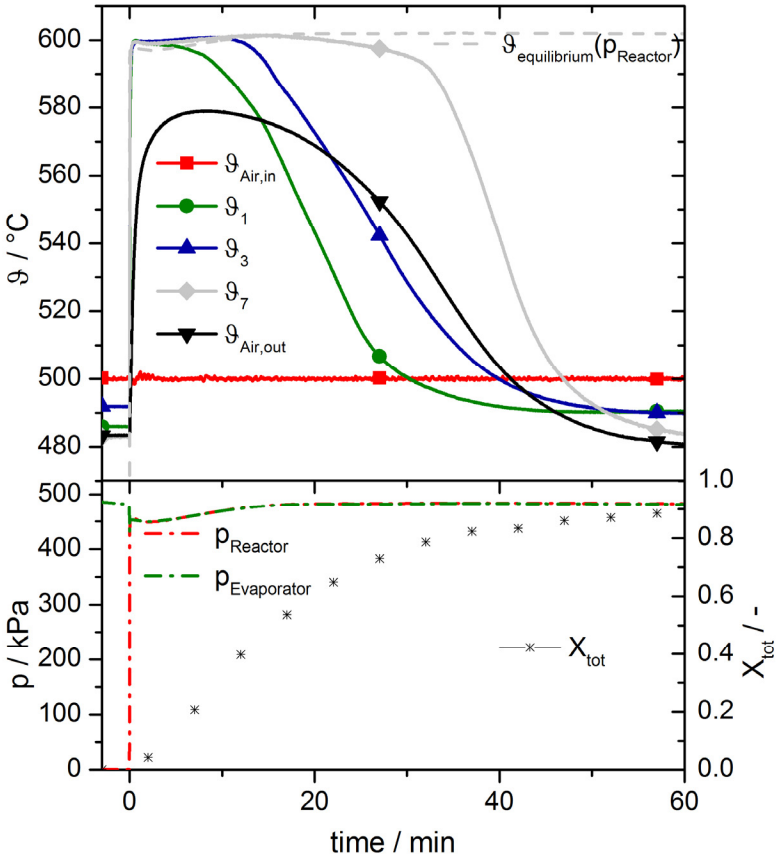

Figure 27 Hydration experiment at 470 kPa and a starting temperature of 500 °C

Variation of cooling load at 470 kPa

In order to analyse the thermal capability of the reaction system at 470 kPa, experiments with three different cooling loads have been performed. Experiment A was conducted with an air volume flow of 16 Nm³/h while the volume

flow was increased to 20 and 28 Nm³/h for the experiments B and C respectively. For all cases a constant air inlet temperature of 500 °C and an evaporation temperature of 150 °C was adjusted (refer to Table 3 for details of the experimental conditions). Figure 28 shows the temperature trends in the front (ϑ_2) and rear (ϑ_6) region of the reaction bed as well as the air outlet temperatures. We can observe that the reaction proceeds at a constant temperature which corresponds to the theoretical equilibrium temperature (dashed lines). The lengths of the plateaus directly correlate to the applied cooling loads. With an increasing cooling load (experiment A to B to C) the plateaus become shorter which can be attributed to a faster conversion. It is remarkable that even at a more than 40 % higher cooling load (compare A to C) no deviation of the plateau temperature from the equilibrium temperature can be observed. This indicates that the heat released by the exothermal reaction keeps up with the heat removed out of the reaction bed for all applied cooling loads. In other words the reaction rate is controlled by the heat transport out of the reaction bed. It can be concluded that at a pressure of 470 kPa the reaction is very fast even very close to the equilibrium temperature.

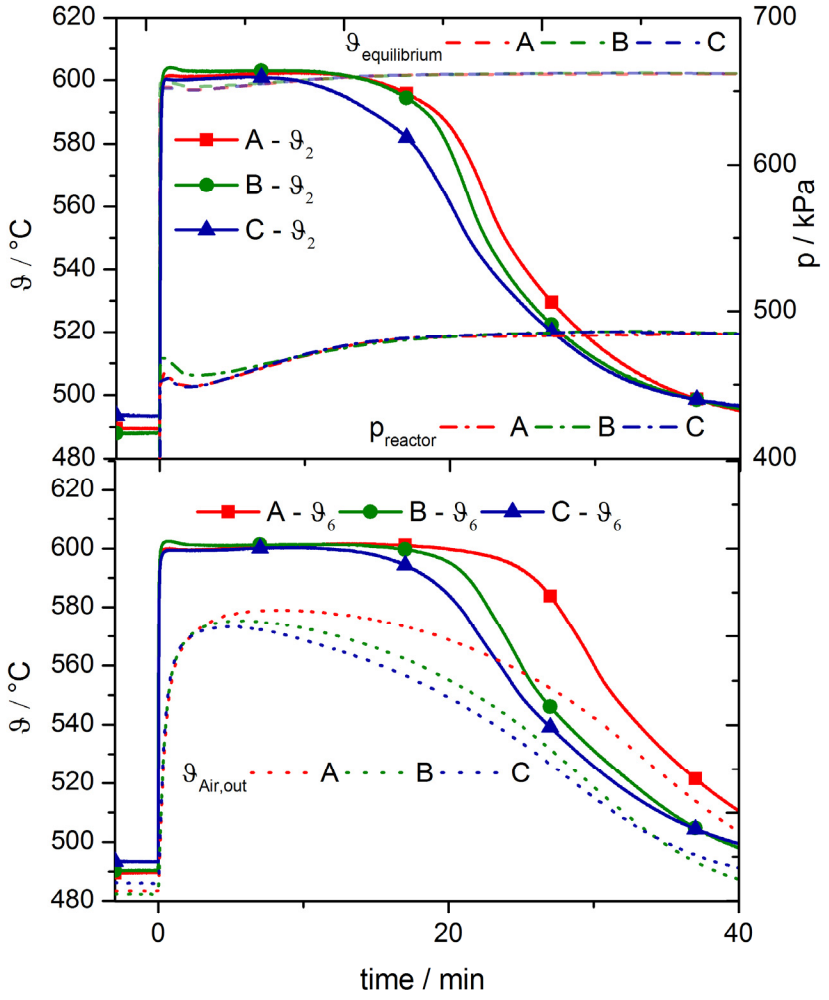

Figure 28 Hydration at 470 kPa and a starting temperature of 500 °C under different cooling loads

Variation of discharge pressure

Even though the discharge of the storage system at 470 kPa showed good performance, it might be reasonable to operate the system at slightly lower vapour pressures depending on the boundary conditions of the process. For example if the available heat source for evaporation has a lower temperature level than 150 °C. Therefore and to complete the operating range between 500 and 600 °C additional discharge procedures at 200 and 270 kPa (experiment D and E).were conducted. The reactor again was operated at a constant air flow rate of 20 Nm³/h and an air inlet temperature of 500 °C.

Figure 29 shows the temperature trends of ϑ_1 (beginning of the reaction bed), ϑ_3 (middle of the reaction bed) and ϑ_7 (end of the reaction bed) for the experiments D and E as well as for comparison the experiment B with a pressure of 470 kPa. We can see that in all cases the reached maximum temperature corresponds to the predicted temperature by the equilibrium line. The small differences within the first minutes can be contributed to pressure differences between the global measured pressure in the casing pipe and the pressure in the reaction bed (compare position of pressure sensor in Figure 16) which occur during the initial dynamic changes. Consistently in all experiments a reaction front moves along the direction of the air flow. Close to the air inlet with initially highest cooling load, the material temperatures (ϑ_1) drop at first due to a decreasing amount of reacting material. The plateaus in the middle region (ϑ_3) are longer while the temperatures in the rear region drop at last.

The cooling loads of the experiments also vary due to the different temperature differences between the air inlet temperature and the plateau temperatures. Accordingly the experiment with the highest plateau temperature (case B) is the first where the heat released by the reaction is completely removed and all reaction bed temperatures reach their initial values again (after 60 minutes at ϑ_7). With lower cooling loads (induced due to lower vapour pressures), in the cases D and E, the duration of the discharge procedure prolongs (timeline is not plotted until the end of the experiments D and E).

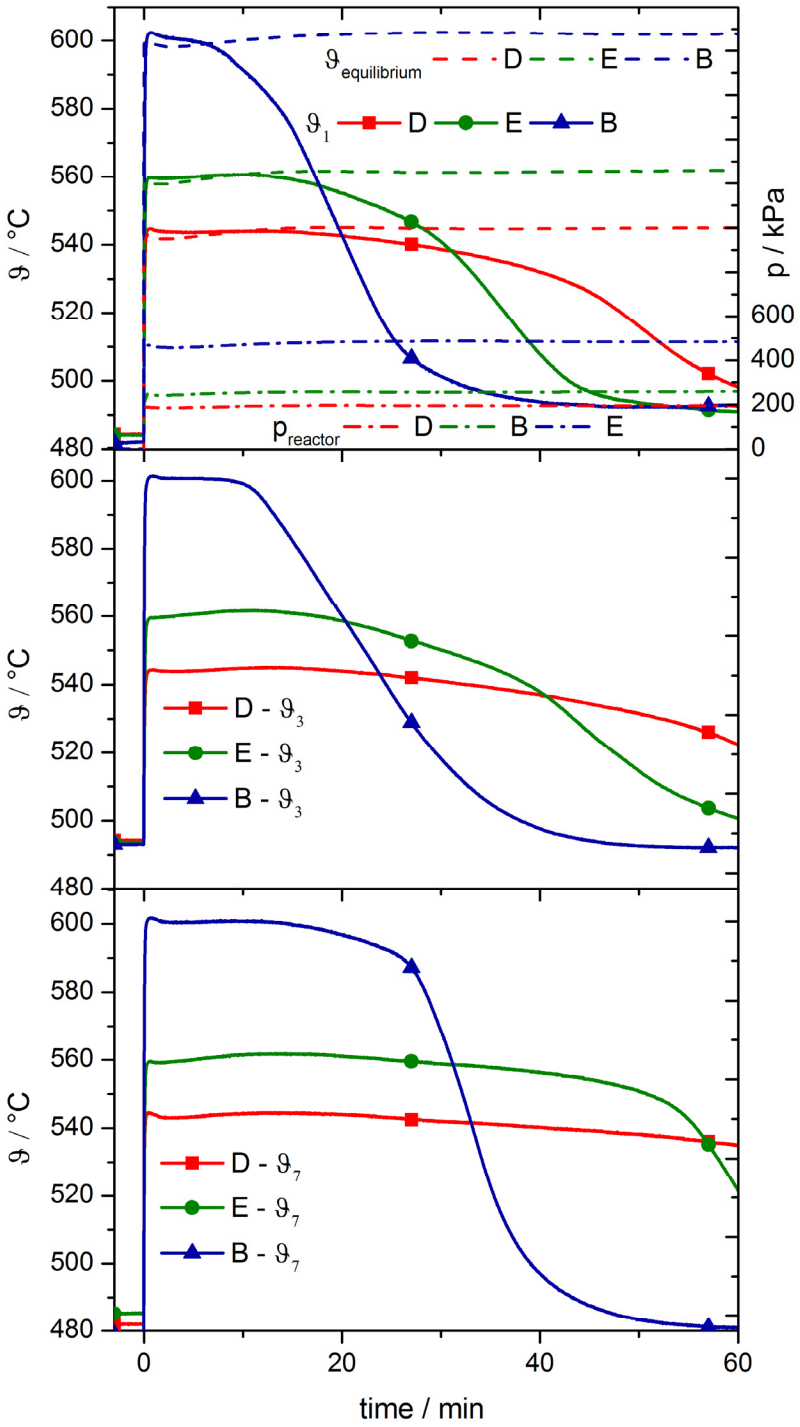

Figure 29 Hydration experiment at 200, 270 and 470 kPa and a starting temperature of 500 °C

4.3.2 Hydration at 8.7 kPa

As explained in section 2.2.3 a thermal discharge at a vapour pressure of 8.7 kPa corresponding to an evaporation temperature of 43 °C is of special interest for efficient process integration. The operation at this pressure would allow incorporating, p. e. the heat of condensation of a steam cycle, to produce the required steam during the discharge procedure and is therefore extensively investigated in this section.

Reference experiment

Figure 30 shows the experiment for the thermal discharging at 8.7 kPa. The initial temperature was set to 280 °C and the evaporator was tempered at 43 °C. At min 0 the valve between evaporator and reactor is opened and the pressure in the reactor increases to ~8.7 kPa (compare black dash dotted line in Figure 29). In the moment when the vapor enters the reactor the bed temperatures escalate due to the heat released by the exothermic reaction. It seems that in the front (ϑ_1) and middle region (ϑ_3) of the bed the temperatures reach slightly lower maxima than in the rear region (ϑ_7). This can be ascribed to the higher cooling load of the reaction bed closer to the air inlet where the temperature difference between bed and the incoming air is maximal.

In the rear region the temperature in the bed reaches a maximum of ~383 °C and stays constant for approximately 20 min. In contradiction to the discharging experiment at pressures between 200 and 470 kPa (compare Figure 29), in this case, at lower vapor pressures, a deviation of the plateau temperature from the equilibrium line of 15 K is observed. Since it is lower than the theoretical equilibrium temperature of the reaction (grey dashed line) one could dedicate this observation to the reaction rate at given conditions: Initially, at the beginning of the experiment, the rate of reaction is high since the temperature difference between the start temperature of 280 °C and the theoretical equilibrium temperature of 398 °C is large. As a consequence more heat is released by the exothermic reaction than removed by the heat transfer fluid which leads in turn to increasing temperatures. The increasing temperature directly leads to a deceleration of the reaction rate, since the driving force (distance to the thermodynamic equilibrium) is reduced. The deceleration of the heat release at the respective low vapor pressures seems to be so pronounced that the temperature

predicted by the theoretical equilibrium line cannot be reached for the given experimental boundary conditions.

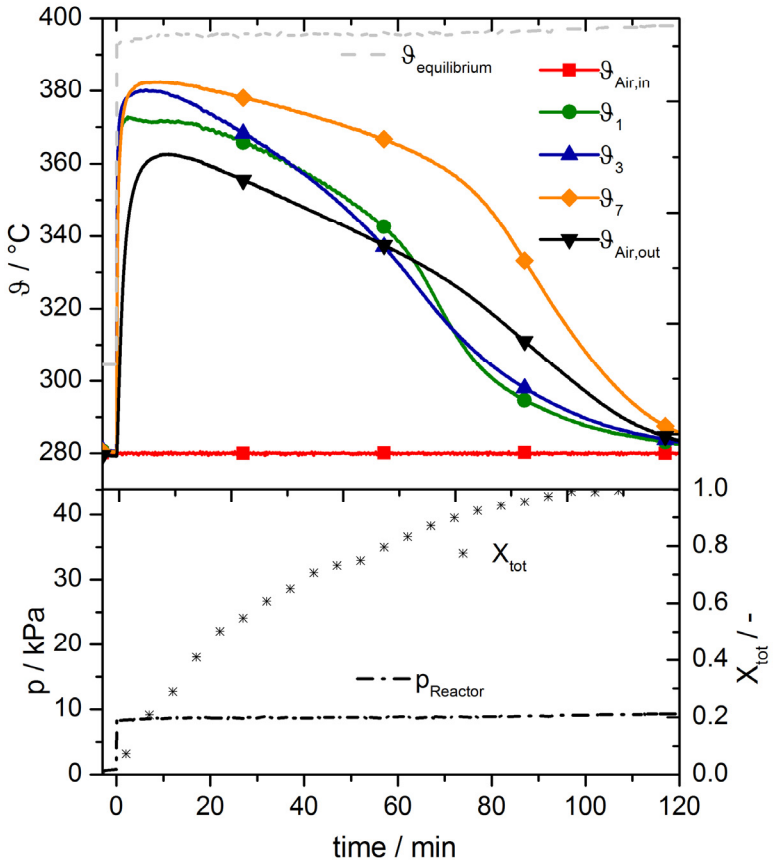

Figure 30 Hydration experiment at 8.7 kPa and a starting temperature of 280 °C

Variation of cooling load of the heat transfer fluid

To analyze the influence of different cooling loads on the discharge temperature, experiments at three different volume flows of the heat transfer fluid have been conducted. The results are shown in Figure 31. Experiment G (red solid lines) was run with a nominal volume flow of 12 Nm³/h while in the experiments H (green solid line) and J (blue solid line) the volume flow was increased to 16 Nm³/h and 20 Nm³/h. In all cases the air inlet temperature was set to 280 °C and the exothermic reaction was induced by a gas pressure of 8.7 kPa. The temperature trends in the front (ϑ_1), middle (ϑ_3) and rear region (ϑ_7) of the bed are plotted.

In particular in the front region of the reaction bed (compare ϑ_1, first diagram of Figure 31) the reached temperatures directly correlate with the volume flow of the heat transfer fluid, respectively the cooling load of the reaction bed. The experiment with the highest cooling load shows the lowest maximum temperature of ~350 °C (blue curve). Whereas the experiment with the medium cooling load (green curve) shows a kind of plateau at ~355 °C and a clear temperature plateau lies at 370 °C for the experiment with the lowest cooling load (red curve). Again, temperature plateaus indicate an equilibrium state between the heat released due to the exothermic reaction and the heat taken up by the heat transfer fluid. Closer to the equilibrium temperature the reaction decelerates thus less heat is released. Accordingly the plateau for lower cooling loads is at higher temperatures. If the cooling load increases, the temperature plateau arises at lower temperatures, since at temperatures further away from the equilibrium temperature, the reaction rate accelerates. This trend can be observed in the first diagram of Figure 31 even though the experiment with the highest cooling load (blue) reaches rather a peak than a plateau.

In the middle region of the reactor (ϑ_3, second diagram Figure 31) we observe that the material temperature for the experiment with the highest cooling load still remains below 350 °C while for the other two experiments the same maximum temperature of 380 °C is reached. In the rear region of the reactor (ϑ_7) the same maximum temperature of around 380 – 383 °C is reached for all experiments. At this position the temperature difference between the reaction and the heat transfer fluid is rather small since the heat exchange first takes place in the front and later in the middle region of the reactor. However, still the maximum temperature is approximately 15 K below the theoretical equilibrium.

Since for these experiments, the inlet temperature was kept constant, the temperature difference between the reaction and heat transfer fluid was generated by the exothermic reaction itself. In contrast to physical storage principles, in this case a high local heat flux is characterized by a reaction at a lower temperature level (compare values for highest heat flux at the front region).

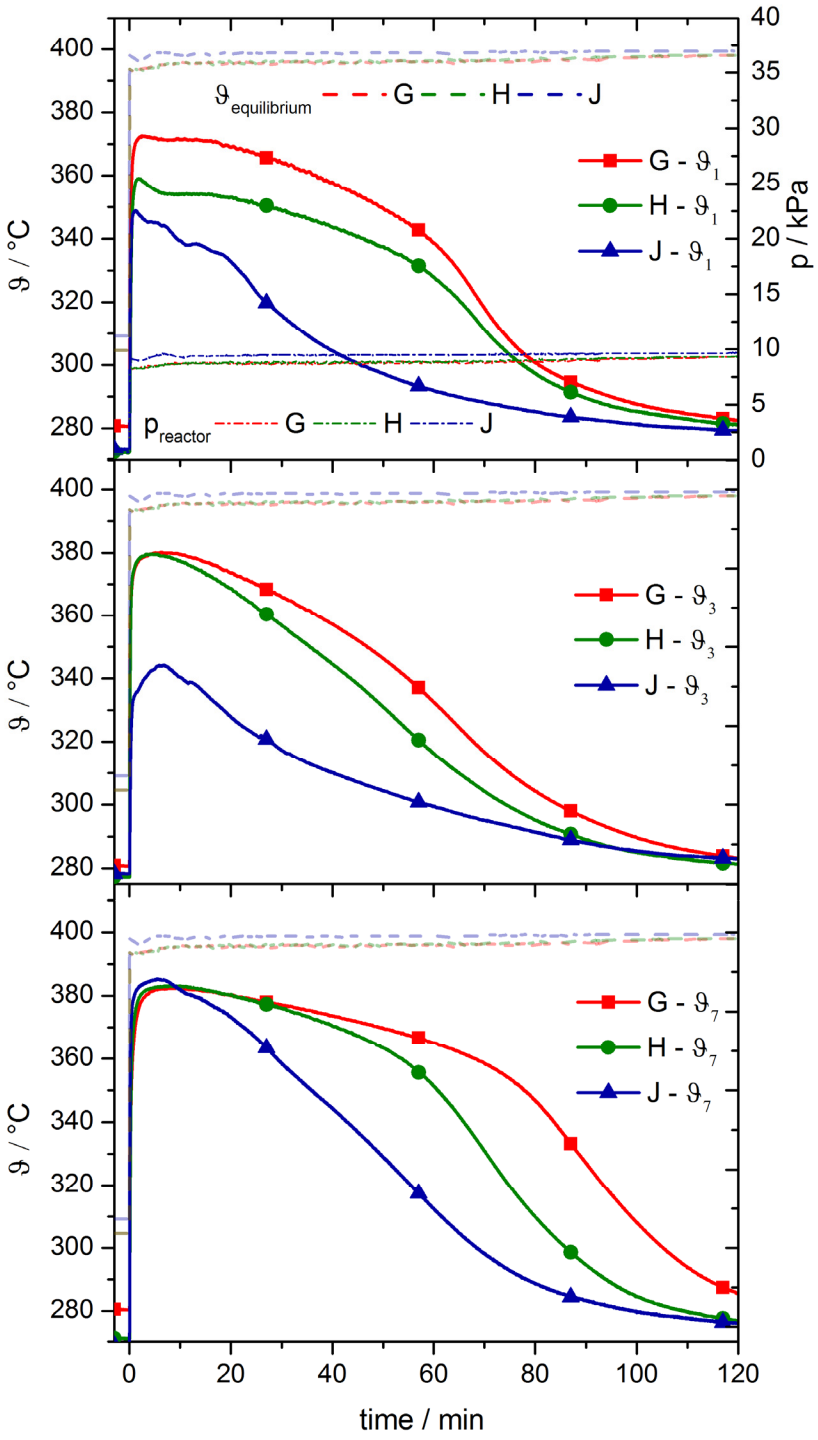

Figure 31 Hydration experiments at 8.7 kPa under different cooling loads of the heat transfer fluid

Hydration at 8.7 kPa in the TGA

To support the findings observed in the reactor the rate of reaction under comparable operating conditions in the thermogravimetric analysis was examined. Before every hydration cycle, $Ca(OH)_2$ was dehydrated under nitrogen atmosphere. The hydration experiments were performed at a water vapor pressure of 8.7 kPa and at different isothermal temperatures between 390 °C and 110 °C. The hydration temperature was reduced by 10 K in each following cycle.

Figure 32 shows the conversion trends for the experiments. It can be seen that for temperatures between 391 °C (theoretical equilibrium is 398 °C) and 367 °C almost no material has reacted after one hour. At 357 °C approximately 30 % of the material is hydrated after 1 hour while at 347 °C almost 80 % is hydrated within the first 20 min. At a temperature of 337 °C 80 % of conversion was achieved within 10 min while at temperatures below 300 °C the conversion accelerates only slightly.

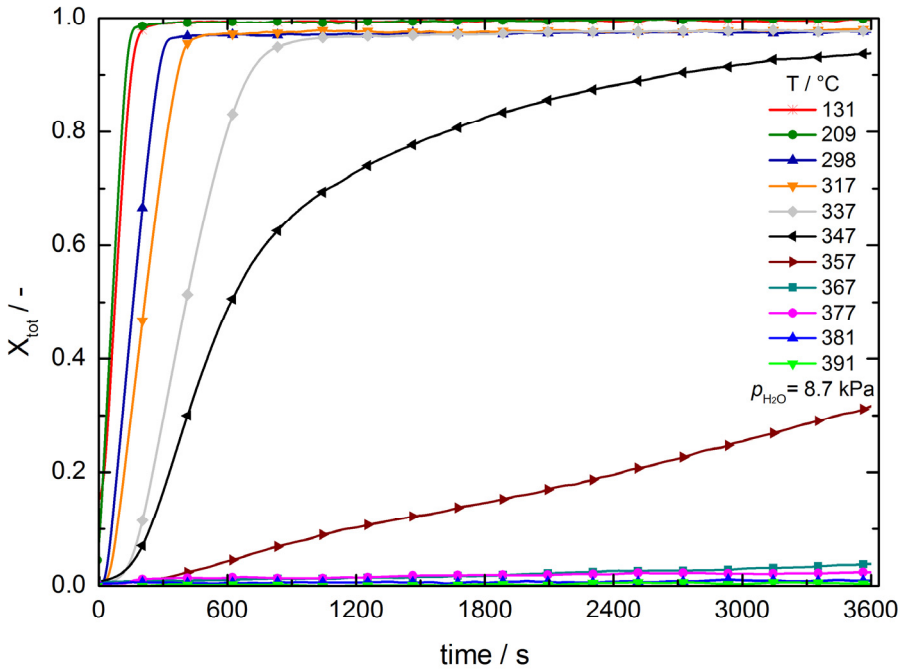

Figure 32 Effect of the temperature on the hydration reaction of CaO at a gas pressure of 8.7 kPa measured by means of TGA

One can conclude that at temperatures above 360 °C the rate of reaction is rather slow while at temperatures below 350 °C the rate of reaction quickly accelerates. Consequently, one can state that the tipping point for a technically relevant discharge reaction of the Ca(OH)2 with a vapor pressure of 8.7 kPa (corresponding to an evaporation temperature of 43 °C) is at around 350 °C. This value is around 48 K below the theoretical discharge temperature according to the equilibrium line.

4.3.3 Hydration at 4-50 kPa

Discharge at 4 kPa

Figure 33 shows the temperature and conversion trend within the first 30 minutes of the discharge experiment at a vapour pressure of 4 kPa. The reaction bed is preheated with an air flow rate of 12 Nm³/h at an inlet temperature of 280 °C (red solid line). The reaction chamber is evacuated while the evaporator is adjusted to a temperature of 30 °C. At t=0 min the valve between reactor and evaporator is opened indicated by the pressure increase in the reactor (red dash dotted line). Correspondingly the material temperatures rise quickly due to the heat released by the exothermal reaction. A particular important observation is that temperature plateaus arise at different levels according to the positions in the reactor. The temperature plateaus indicate an equilibrium state between the heat released by the reaction and the heat absorbed by the heat transfer fluid. Coherently we observe the lowest plateau temperature of 340 °C in the front region (ϑ_1) of the reactor, where the cooling load is maximal due to the proximity to the air inlet. Smaller cooling loads in the middle (ϑ_5) and rear (ϑ_7) region of the reactor lead to higher plateau temperatures of approximately 350 °C (ϑ_5) and 360 °C (ϑ_7). The temperature plateaus of the experiment reveal that a certain gap to the equilibrium needs to be maintained in order to operate at high cooling loads. However it can be stated that the even at this low pressure the discharge reaction is possible and reasonable outlet temperatures can be reached. The operation at 4 kPa is of particular interest because the thermal energy required for evaporation could in this case for example be taken from the ambient at 30 °C. This in turn would greatly increase the efficiency of the storage system.

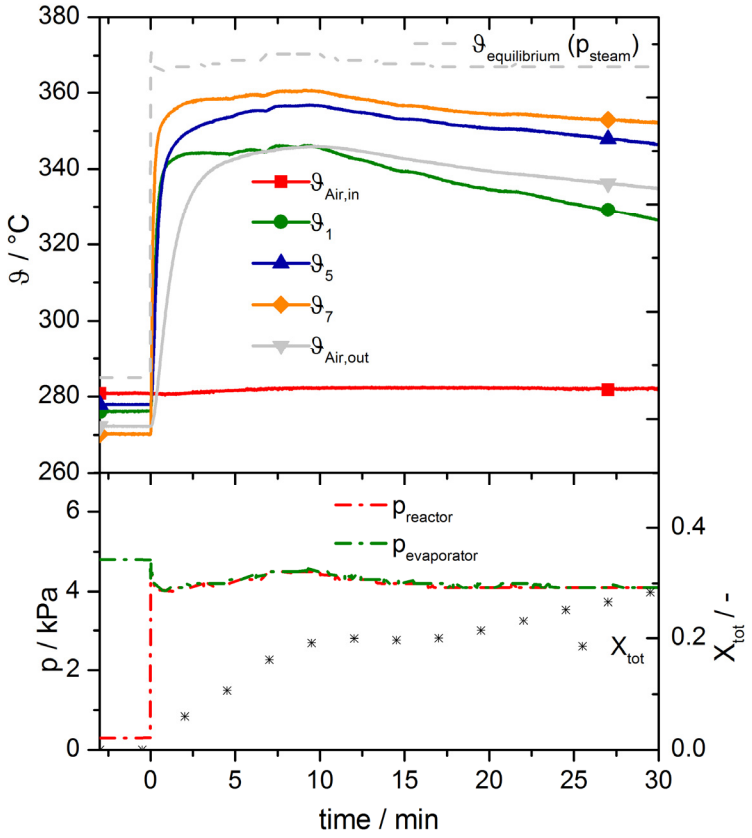

Figure 33 Hydration at 4 kPa and a starting temperature of 280 °C

Variation of discharge pressure

Since in some processes a heat source at a higher temperature might be available the discharge operation at 20 and 50 kPa was analysed. For comparison additional experiments at 4 and 10 kPa are performed under similar thermal load conditions. The air volume flow was 12 Nm³/h for all experiments while the air inlet temperature was constant but different for each case in order to achieve comparable cooling loads. The air inlet temperature and starting temperature in each experiment is set 120 K lower than the theoretical equilibrium temperature at the applied vapour pressure. For example, experiment K was operated at a water vapour pressure of 50 kPa which correspond to an equilibrium temperature of 470°C. Therefore the air inlet temperature was set to 350 °C. For comparison of the experimental parameters please refer to Table 3.

With this parameter study the temperature gap which occurs at technically relevant discharge conditions was investigated. Figure 34 therefore only represents

the temperature ϑ_1 in the front region of the reactor, where initially the cooling load is maximal, as well as the equilibrium temperature based on the measured pressure for each experiment. It can clearly be observed that in all cases plateaus arises while a certain gap to the equilibrium temperature is maintained. The gap is about 15 K for case K and J (50, 20 kPa) while it is approximately 30 K for the cases F and I (4, 10 kPa).

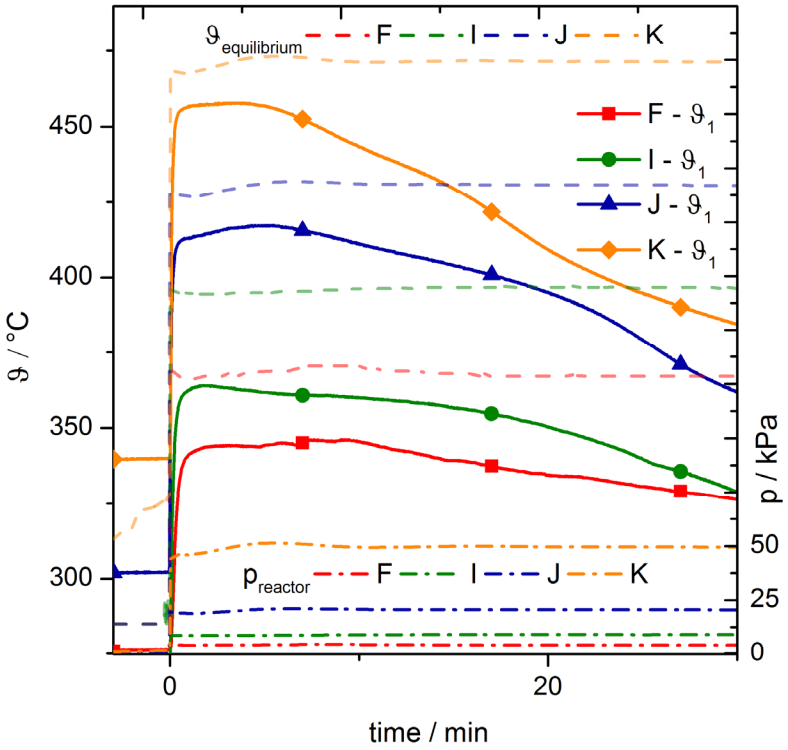

Figure 34 Hydration at 4, 10, 20 and 50 kPa and comparable cooling loads

4.4 Changes of the reaction bed

Cycle stability of the reaction was already demonstrated by means of TGA measurements and was also observed in our reactor. Nevertheless changes in the properties of the bulk do occur. The right picture in Figure 35 shows the reaction bed of $Ca(OH)_2$ when it was removed from the casing pipe after 35 cycles. It can be observed that the reaction bed is slightly compressed and the bulk density increased compared to the initially loose filling (compare Figure 14)

of the storage material. Roughly 20 % of the heat exchange surface is not covered with material anymore due to the compression of the bed. The compression might enhance the thermal conductivity of the bulk on one hand but could also worsen the gas permeability on the other hand. It is assumed that these changes occur within the first cycles and subsequently do not significantly change anymore. Also no effect dedicated to the changes could be observed in our experiments. However the reaction bed design (very thin layer) also was explicitly dedicated to minimize these transport resistances. Nevertheless the observed changes indicate that in larger reactors the changes which occur in large reactive bulks might have a significant influence on the performance. The heat and mass transport phenomena's in a changing reactive bulk should therefore be investigated in an experimental set up especially designed to address these questions. A more detailed description of these transactions in the models will improve simulation results. The picture in Figure 35 left shows the agglomerates after loosening of the bulk but even though the agglomerates look very hard, they fall apart into smaller particles with only slight mechanical strains. This formation of agglomerates has consistently been reported in lab scale reactors, even in the directly heated fixed bed. However, whereas in this indirect concept no negative impact on the reactor performance has been observed, in directly operated reactors the formation of agglomerates (and associated channels) has influenced the performance.

Figure 35 right: reaction bed after 35 cycles; left: larger agglomerates after loosening of the bed

4.5 Summary and discussion of experimental results

Thermal charging

For the process integration the lowest possible reaction temperature is favourable, especially if the thermochemical system is charged by a sensible heat transfer fluid (explained in 2.2.3). The charging performance was therefore examined at all conceivable condensation pressures for different applications. The investigated operating range was between 1.4 kPa and 100 kPa which correspond to condensation temperatures between 12 °C and 100 °C respectively. A special focus was given to the investigation of the charging performance at 10 kPa which was identified as the minimal achievable condensation pressure for a Rankine cycle in hot regions.

First of all the thermal charging at technically relevant powers could be firstly demonstrated within this pressure range. However, the experiments revealed that in all cases a significant gap to the theoretical equilibrium temperature, which could be dedicated to the slow reaction rate of the raw material under these conditions, partially limits the operating range of the storage system.

For a vapour pressure of 10 kPa the charging procedure was intensively examined through a variation of the charging power, of the operation mode (pressure decrease / temperature increase) and additional measurements by means of the TGA. The reactor experiments with high thermal loads (A, B and C) revealed that below a temperature of 445 °C the heat flux into the reaction bed is always higher than the heat absorbed by the endothermic reaction. Above 445 °C the rate of reaction seems fast enough and the process is limited by the heat flux into the reaction bed. Even with drastically increased thermal loads we did not observe plateaus at higher temperatures. In contrast for some cases with very low thermal loads (D, G) or in the rear region of the reactor (where the thermal load is in general smaller) slightly lower plateau temperatures between 438 °C and 440 °C did occur. But at the same time the charging times of these experiments were longer than 120 minutes and are therefore of minor technical relevance. With regard to a later application of $Ca(OH)_2$ as thermochemical storage, it can be concluded that the unmodified material possesses a kind of tipping point: at a condensation pressure of 10 kPa (corresponding to a con-

densation temperature of 45 °C) a charging temperature of at least 445 °C is required to achieve high charging power densities.

Additional TGA measurements, comparable to the reactor experiments, supported these findings. Below a temperature of 430 °C and a pressure of 10 kPa the reaction rate of the material is very slow. At 430 °C the reaction rate accelerates and a power density of 0.375/ (kW/kg) can be calculated by the measured TGA values. Then the transition is very sharp and at temperatures of more than 440 °C the calculated power density increases to 4.5/ (kW/kg) thus it is 10 times higher compared to the rate at 430 °C.

The experiments at 1.4, 4.3, 20 and 100 kPa revealed that at lower reaction temperatures and pressures the required distance to the equilibrium is larger while at higher pressures the required distance becomes smaller. Nevertheless at 20 kPa the required charging temperature for reasonable reaction rates is still around 465 °C. So the smaller required temperature gap does not compensate the anyways higher reaction temperature due to the higher pressure. Lower pressures can lower the reaction temperature: but even at 4.3 kPa the required charging temperature was 425 °C. It can be concluded that if the condensation pressure is lower than 10 kPa the dehydration can be performed at lower temperatures which would in principal be favorable for the integration of the storage system. However it must be taken into account that a lower condensation pressure might require an additional cooling of the condenser. Additionally the large required equilibrium gap observed in the complete pressure range significantly limits the charging performance and needs to be taken into account for any process application.

Thermal discharging

The discharge at pressures between 200 and 470 kPa achieved very good performances. For the first time a discharge temperature of 600 °C and 565 °C at significant cooling loads of the heat transfer fluid was demonstrated. In all experiments even with drastically increased cooling loads the reaction proceeded close to the theoretical equilibrium temperature. It can be summarized that in this operating range reactors with high power densities can be designed to operate with discharge temperatures very close to the theoretical equilibrium temperature.

The thermal discharge at a pressure of 8.7 kPa was intensively investigated due to its high relevance for the efficient operation if electricity is produced via a Rankine steam cycle, during discharge of the thermochemical storage. The experiments revealed that at this low pressure even under small cooling loads the equilibrium temperature was not reached in technically relevant times. Beyond that, the variation of thermal power showed that if higher cooling loads are applied a large distance to the equilibrium temperature has to be maintained. In the reactor a discharge temperature of 350 °C was determined for high cooling loads at 8.7 kPa. Thess findings are supported by additional TGA measurements under comparable conditions, which showed a significant acceleration of the reaction rate at temperatures below 350 °C.

Comparable limitations could be observed for all other investigated discharge pressures below 50 kPa. For 4 kPa the required equilibrium gap accounted 30 K while it was only 15 K for 20 and 50 kPa. But even though the required temperature gap downgrades the theoretical applicability of the storage system and needs to be taken into account, the demonstrated operation characteristic is still promising for a wide range of applications. For example the hydration at 4 kPa allowed for a discharge temperature of 340 °C at a reasonable power density. This in turn means that on one side low grade heat at 30 °C, which has in general a low exergetic value can be incorporated to discharge the storage system and on the other side the storage releases thermal energy with a high exergetic value at 340 °C.

Overall it was firstly demonstrated that the reaction system can supply technically relevant thermal power at vapour pressures between 4 and 50 kPa. However, in this operating range it is particular important that an additional gap to the equilibrium temperature needs to be taken into account which reduces the achievable discharge temperature. This in turn leads to an optimization question for the later application of the thermochemical storage: for low vapor pressures, high power densities directly reduce the quality (temperature level) of the discharged thermal energy.

Figure 36 illustrates and summarizes all investigated operating (temperature and pressure) conditions of this work (additional experiments with different volume flows of the air are not marked). As it can be seen the temperature range

between 290-600 °C relevant for the reference process has been covered. It can be summarized that technically relevant thermal charging and discharging powers were firstly demonstrated in the complete pressure range. However, the experiments revealed that especially at low vapour pressures (the area is marked in grey) the operating range of the storage system is partially limited due to slow reaction rates of the commercial available calcium hydroxide.

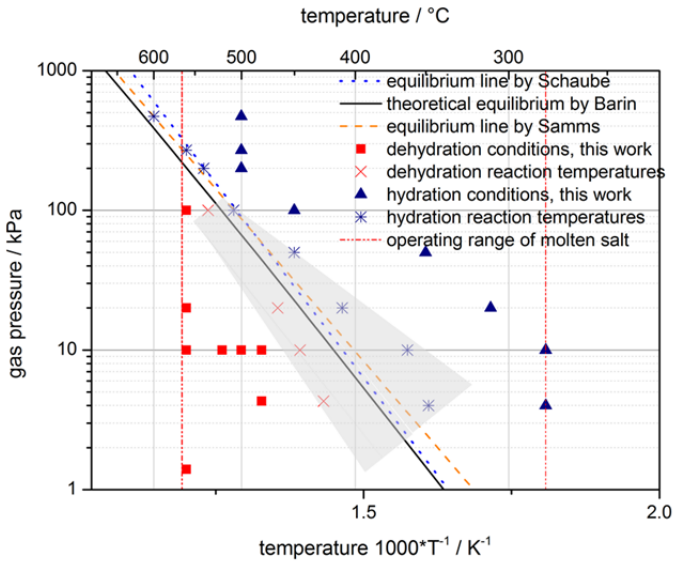

Figure 36 Summary of the operating conditions; grey area marks the temperature and pressure range where operation is partially limited due to slow reaction rate of the raw material

The experimental results provide an understanding of the operation characteristic at realistic conditions as well as the determination of achievable charge and discharge temperatures. Therefore a first integration of the storage system in a reference concentrated solar power plant is conceptually analysed in the following chapter.

5. Process integration based on molten salt CSP

For this integration study the boundary conditions of a current molten salt tower plant [90] are considered. The heat transfer fluid is a molten salt mixture (60 % NaNO3 + 40 % KNO3) operating in a temperature range from 290 °C to 565 °C. For the charging procedure available simulation data for a central receiver power plant provided by DLR institute of solar research is used. For the discharge procedure a state of the art power block configuration is considered.

Special focus in this chapter lies on the analysis of the discharge period of the storage where the power block should run only with thermal energy supplied by the storage system. During this discharging process it is particular important to consider the source of thermal energy required for evaporation since it represents a large share of the energy released by the reaction. Therefore different configurations, including the extraction of low grade heat from the steam cycle, and their effect on the overall storage efficiency are analysed.

During the charging period the temperature of the available heat sink for condensation of the reaction gas has huge influence on the amount of potentially stored thermal energy. Therefore the charging performance is evaluated against a commercial CSP.

5.1 Integration concept for CSP plant

For an application in CSP plants large storage capacities of e. g. up to 15 hours of nominal thermal power are desirable in order to ensure a continuous operation of the plant during most of the year. For a typical configuration with a nominal thermal power of 300 $MW_{thermal}$ this leads to a required storage capacity of 4500 MWh which corresponds to 11250 tons of calcium hydroxide. Taking these numbers into account it becomes obvious that for such large storage capacities the only economically viable way to realize indirectly heated reactors is the separation of power and capacity. In such a concept the heat exchanger is detached from the mass of the storage material. This allows to design the heat

exchanger in respect to the required power level (the major cost) while the storage material can be stored in inexpensive tanks. Recently such an indirectly heated moving bed concept has been experimentally demonstrated in pilot scale [88]. The operation revealed that the gravity assisted flow of the storage material under energy efficient reaction conditions in the reactor is challenging and therefore currently under further investigation. Figure 37 shows the process scheme of a possible integration of a moving bed reactor concept into a CSP plant configuration.

During solar operation the heat transfer fluid delivers at first the nominal thermal load to the power block. As soon as the thermal power at the central receiver exceeds the demand of the power block the excess mass flow is directed into the thermochemical reactor. At this point a corresponding mass flow of $Ca(OH)_2$ is directed into the reactor. Heat is transferred from the hot molten salt to drive the endothermal reaction. CaO particles leave the reactor and are transported to a second storage container. Simultaneously water vapour is freed in the reaction chamber. To keep the reaction running, the water vapour must continuously be removed from the reactor which in turn demands a heat sink (e. g. ambient) to release the heat of condensation.

During non-solar hours the power block should ideally be continuously driven by the storage system. Therefore CaO is introduced into the reactor and additional water vapour needs to be supplied to drive the exothermal reaction. The discharge reaction temperature should ideally be high enough to reach the maximum possible temperature of the heat transfer fluid of 565 °C in order to allow continuous operation of the power block at its nominal conditions. Obviously, an additional heat source is required to supply the enthalpy of evaporation for the discharge steam.

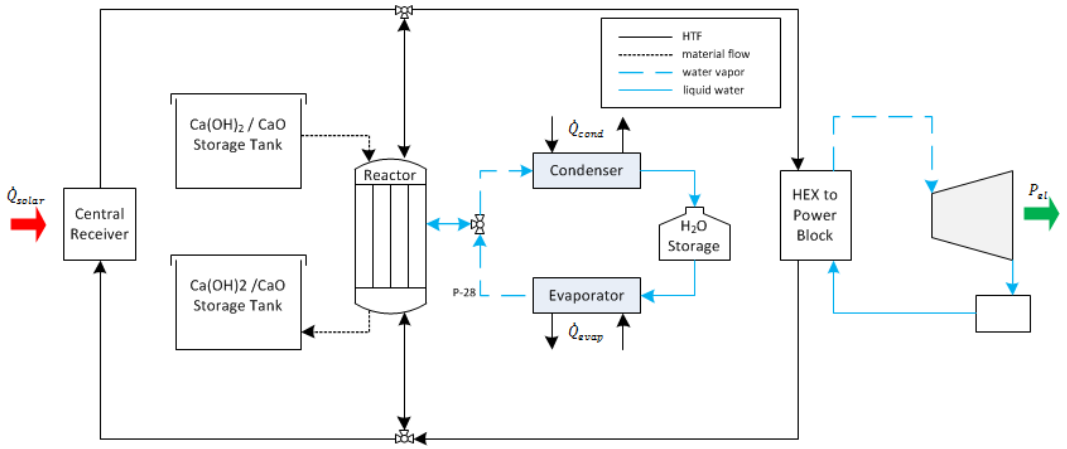

Figure 37 Conceptual process design of an indirectly heated thermochemical reactor in a CSP plant configuration

5.2 Power generation driven by the storage system

The steam cycle for power generation considered in this work is based on a standard Rankine cycle configuration for molten salt solar tower plants. The configuration consists of two high pressure turbine stages, one reheater, and five low pressure turbine stages. Live steam is generated at 136000 kPa and 552 °C according to the maximum upper temperature of 565 °C of the heat transfer fluid. Steam is extracted at 6 turbine stages to preheat the feed water. The cycle is designed for a nominal output of 125 MW_{el} and reaches a gross efficiency of 0.419 at a condensation pressure of 10 kPa. Table 4 summarizes the main nominal parameters of the power block.

Table 4 Nominal values for power block cycle

HTF Parameters	
Nominal Thermal Input / MWth	298.35
Flowrate of HTF / (kg/s)	713.373
HTF Inlet Temperature / °C	565
HTF Return Temperature/ °C	290
Steam Parameters	
Live Steam Flowrate / (kg/s)	384.451
Live/Reheat Steam Pressure / kPa	13600/3200
Live/Reheat Steam Temperature / °C	334/552

Turbine parameters	
Gross Turbine Power / MWelectric	125
Turbine Isentropic Efficiency / %	86
Generator Efficiency/ %	96
Power Block Gross Efficiency / %	41.9
Condenser	
Condensation Pressure / kPa	10
Steam Extraction	
(EXP1) – Pressure/kPa / Flowrate/(kg/s)	5000 / 2.8
(EXP2) – Pressure/kPa / Flowrate/(kg/s)	3400 / 10.9
(EXP3) – Pressure/kPa / Flowrate/(kg/s)	1000 / 5
(EXP4) – Pressure/kPa / Flowrate/(kg/s)	450 / 5.3
(EXP5) – Pressure/kPa / Flowrate/(kg/s)	150 / 4.9
(EXP6) – Pressure/kPa / Flowrate/(kg/s)	40 / 3.7
Thermal Power	
Superheater / MW	89.796
Reheater / MW	41.202
Steam Generator / MW	114.47
Preheater / MW	52.89

Four different operation strategies where the steam cycle is only powered by the thermochemical storage system are analysed. The operation modes differ in the quality and flow rate of steam which is extracted at different turbine stages to supply vapour for the discharge reaction. For each operation mode the required flow rate at the extraction point is calculated by general mass and energy balances. The power block is simulated with the commercial software tool Ebsilon©. By means of the simulation the electrical output in part load mode for the different steam extraction flow rates is determined.

Figure 38 shows the process flow diagram of the steam cycle and the operation of the thermochemical reactor(s) during the discharge procedure. At first the different configurations are described while in the subsequent section the overall storage efficiencies are compared.

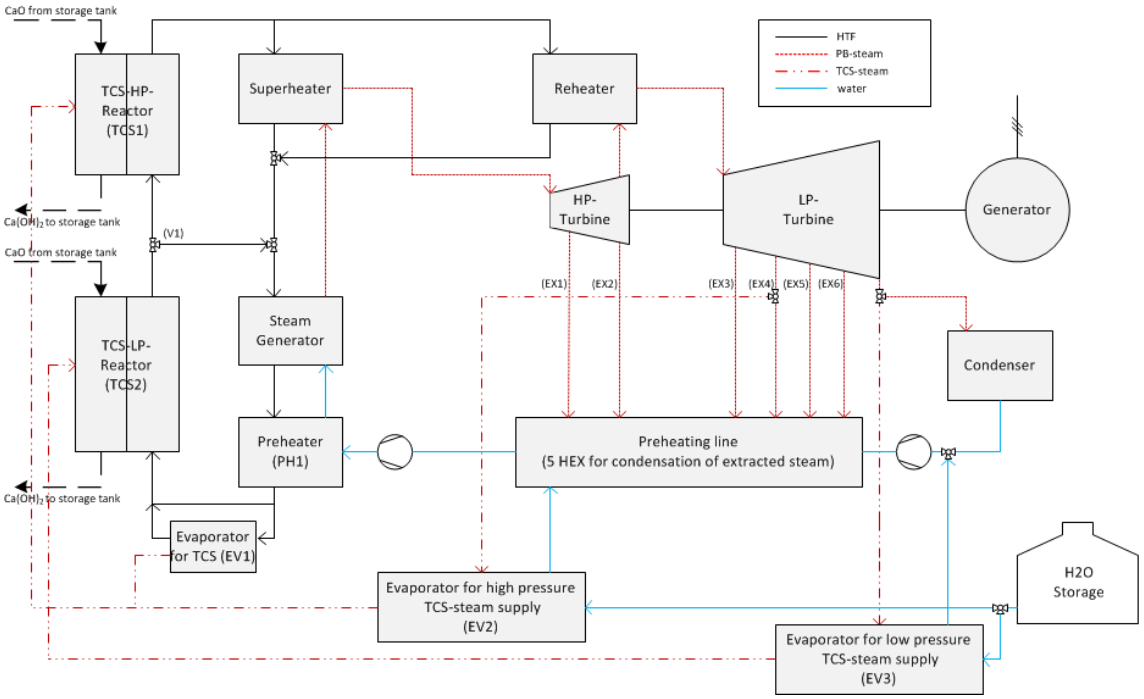

Figure 38 Flow sheet of power block operation with the thermochemical storage system

A – reference case

In the reference case only the high pressure TCS-Reactor (TCS1) and the evaporator (EV1) are in operation. Discharge steam is generated in evaporator (EV1) which is driven by thermal energy supplied by the heat transfer fluid. The molten salt is directed to evaporator (EV1) after it leaves the preheater with an outlet temperature of 290 °C. The steam is generated at a pressure of 470 kPa and directed into the reactor (TCS1). As yet demonstrated in the experimental section, with the operation at 470 kPa a reaction temperature of 600 °C can be reached. Therefore the molten salt can be heated up in the reactor to the nominal upper temperature of 565 °C and the power block can continue to operate at nominal conditions.

In this operation mode the reactor not only has to supply the nominal thermal power of the steam cycle but also the thermal power for the evaporation of the required discharge steam (compare Fig. 11). The required discharge power can thus be calculated by the equations:

$$\dot{Q}_{TCS-discharging-A} = \dot{Q}_{PB_{nominal}} + \dot{Q}_{evaporation} \tag{8}$$

$$\dot{n} * \Delta H_{reaction} = \dot{Q}_{PB_{nominal}} + \dot{n} * \Delta H_{evaporation(147.9°C,450\,kPa)} \tag{9}$$

With the enthalpy values given in Table 5, the required thermal power that has to be delivered by the thermochemical reactor $\dot{Q}_{TCS-discharging-A}$ accounts 470.16 MW in this operation mode.

Table 5 General values for the calculations

General values	
$\dot{Q}_{PB_{nominal}}$ / MW	298.35
$\eta_{PBnominal}$	0.419
$\Delta H_{reaction}$ / (kJ/mol)	104
$\Delta H_{evaporation(147{,}9°C,450\ kPa)}$ / (kJ/mol)	38
M_{H2O} / (kg/mol)	0.018

B – Steam extraction at LP-Turbine

In operation mode B steam is extracted at the second stage of the low pressure turbine at extraction point 4 (EX4). The extracted steam is directed into evaporator (EV2) where steam at 450 kPa is generated for the thermochemical discharge reaction. For this simplified examination, losses related to the heat exchanger (EV2) are neglected. In contrast to operation mode A the thermal power required in this configuration is only the nominal thermal power of the power block (298.35 MW). Thus the molar rate of reaction can be calculated by the equation:

$$\dot{Q}_{TCS-discharging-B} = \dot{Q}_{PB_{nominal}} = \dot{n} * \Delta H_{reaction} \tag{10}$$

With the molar rate of reaction the flow rate of required water vapour for the discharge reaction can be calculated by equation 11:

$$\dot{m}_{vapor} = \dot{n} * M_{H2O} \tag{11}$$

and accounts 51.68 kg/s. Consequently, this amount of steam is not available for power generation. Therefore, the operation of the power block is simulated with a steam extraction of 51.68 kg/s at (EX4) which results in a reduced electrical output of 92.1 MW compared to the nominal output of 125 MW (no steam is extracted for the operation of the thermochemical reactor).

C – Steam extraction at LP-Turbine and use of exhaust steam

In order to further increase the efficiency it seems reasonable to make use of the condensation enthalpy of the exhaust steam at the outlet of the low pressure turbine. Nevertheless this operation mode results in a more complex integration. To incorporate the steam at the condensation pressure of 10 kPa the outlet flow of the low pressure turbine is partially directed to evaporator (EV3). There steam is generated at a pressure of 10 kPa and directed into a second reactor (TCS2) for low pressure operation. Losses of the heat exchanger (EV3) are again neglected. In this operation mode two reactors are necessary because the temperature level which is reached in TCS2 is limited. Taking the experimental results for the discharge at 10 kPa into account (compare Figure 31) a temperature of around 350 °C can be reached. Since the steam generator of the plant operates at 334 °C, the low pressure reactor TCS2 is in principle able to supply the thermal energy for the steam generator and the preheater. Consequently, only the superheater and the reheater need to be driven by TCS1. Therefore the mass flow of the heat transfer fluid is separated after TCS2 at valve (V1). One part is directed to supply the steam generator and the preheater whereas a smaller mass flow is directed into TCS1. The reactor TCS1 again operates at 450 kPa while, like in operation mode B, the required steam comes from evaporator EV2 which in turn is driven by condensation of steam from extraction point 4 (EX4). Since TCS1 now only provides the thermal power required by the superheater and the reheater consequently the necessary thermal power is clearly reduced:

$$\dot{Q}_{TCS1-discharging-C} = \dot{Q}_{superheater} + \dot{Q}_{reheater} = \dot{n}_{TCS1-C} * \Delta H_{reaction} \qquad (12)$$

Accordingly the necessary steam flow rate at (EX4) is calculated to 22.69 kg/s. The molar reaction rate required at TCS2 is calculated by:

$$\dot{Q}_{TCS2-discharging-C} = \dot{Q}_{evaporator} + \dot{Q}_{reheater} = \dot{n}_{TCS2-C} * \Delta H_{reaction} \qquad (13)$$

According to equation 11 the flow rate of steam which needs to be generated by the enthalpy of condensation at 10 kPa is calculated to 28.99 kg/s. Since in this case, a huge fraction of the reaction gas could be derived from the condensation of the power block, the calculated electrical output for this configuration is 109.91 MW.

D - Steam extraction at LP-Turbine and lowering of condensation temperature

According to the experimental results given in Figure 33, it would be in principle even possible to reduce the condensation temperature of the power block. However, it is obvious that operating the system at such low pressure requires huge efforts in gas handling and heat exchange. In this operation mode D, it is assumed that the TCS2 reactor operates at a vapour pressure of 4 kPa. According to the experimental results a reaction temperature of 340 °C can be expected (compare Figure 33), which could be in principle high enough to supply the steam generator and the preheater (comparable to configuration C but with reduced power density of the reaction). Since in this case the evaporator (EV3) operates at an evaporation pressure of 4 kPa (instead of 10 kPa), the higher efficiency of the power block could partially compensate the higher efforts related to the increased volume flow of steam. However, this configuration would require an additional turbine stage (not illustrated in Figure 38) in which 28.99 kg/s of steam can be condensed below the nominal condensation at 4 kPa while 24.7 kg/s are condensed at 10 kPa after the nominal fifth turbine stage. Comparable to case C an additional mass flow 22.69 kg/s of steam are extracted at 450 kPa at (EX4) to supply the TCS1 reactor. This configuration reaches a power output of 112.48 MW which is only slightly higher than case C that could be realized with clearly minor changes of the power block.

Storage efficiency

Table 6 summarizes the results for the different operation modes. It becomes obvious that in the reference case A the power block operates at its nominal electric output but on the other hand the thermal power required at the thermochemical reactor is much higher compared to the configurations where steam is extracted from the power block.

Table 6 Calculated thermal Power, flow rates of extracted steam and electrical output of the power block for the different operation modes

Mode	$\dot{Q}_{TCS1}$/ MW_{th}	$\dot{Q}_{TCS2}$/ MW_{th}	$\dot{m}_{vapor}$(EX4) / (kg/s)	$\dot{m}_{vapor}$(EV3) / (kg/s)	P_{el} /MW_{el}
A	470.16	0	0	0	125
B	298.35	0	51.68	0	92.1
C	130.99	167.376	22.69	28.99	109.91
D	130.99	167.376	22.69	28.99	112.484

Therefore, in order to be able to compare the operation modes an efficiency term has been defined which relates the electric energy output during discharge of the storage to the potential electricity which has not been produced during the period of charging of the storage system. The efficiency is represented by equation 14:

$$\eta_{storage} = \frac{P_{el\ discharging-case\ A-D}}{\dot{Q}_{TCS-charging-case\ A-D} * \eta_{PBnominal}} \quad (14)$$

Further it is assumed that for all cases the thermal power required during discharge is equal to the thermal power supplied during the charging procedure:

$$\dot{Q}_{TCS-charging-case\ A-D} = \dot{Q}_{TCS1-\ discharging-\ case\ A-D} + \dot{Q}_{TCS2-\ discharging\ -\ case\ A-D} \quad (15)$$

Consequently, since losses are neglected the storage can be discharged exactly for the time span as it was charged.

Figure 39 shows the storage efficiency calculated by equation 14 and 15 for the different configurations. The reference case A only reaches an efficiency of 63.4 %. The low efficiency can be mainly attributed to the fact that the energy content of the steam released during the charging process is not used and the steam required for the discharge needs to be generated by thermal energy from the storage itself. Therefore roughly 36 % of the energy content is lost which is related to the ratio of enthalpy of condensation to the enthalpy of reaction (38/104 (kJ/mol)).

In operation mode B a large steam mass flow is extracted at 450 kPa from the low pressure turbine. This clearly reduces the electrical output of the power

block. But on the other hand the thermal power required from the storage during the discharging process is also reduced compared to the reference case A. Overall we reach a clearly increased storage efficiency of 73 %. Advantageous of this concept is that only one TCS reactor is required and it is operated at a relatively high pressure. The higher pressure in principal allows smaller pipe diameters and compact reactor designs. Additionally, as experimentally demonstrated (compare chapter 3.1), a reaction at pressures of >100 kPa allows for outlet temperatures that are very close to the equilibrium even for high required reaction rates.

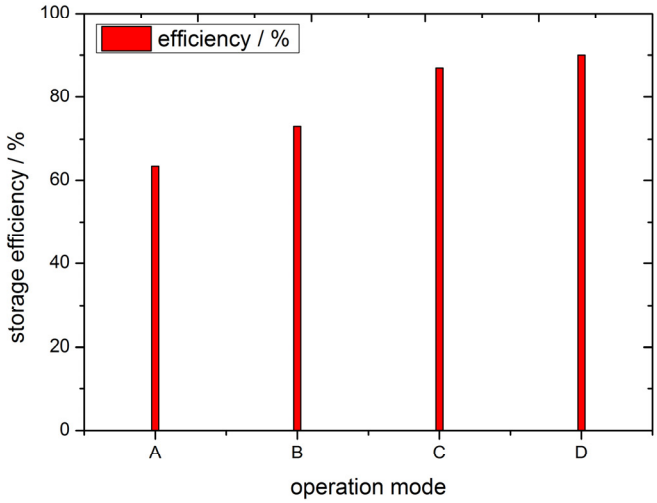

Figure 39 Storage efficiency according to equation 14 and 15 for the different operation modes

Operation mode C greatly improves the overall efficiency to 87 %. In this operation mode only the amount of thermal power required at the higher temperature level of 565 °C is generated in TCS2. The remaining required thermal power is generated in TCS1 where steam which has only low exergetic value in the steam cycle is used for the discharging reaction. Consequently a much smaller mass flow of steam has to be extracted at point 4 (EX4) which in turn increases the electricity output. The obvious disadvantage of this operation mode is that in total four devices are necessary: two TCS-reactors and two evaporators. Additionally the operation of the thermochemical reactor at such a low vapour pressure of 10 kPa might be challenging due to large pipe diameters that are required for the transport of the steam. Besides that, the reactor design becomes

more complex since the reaction gas distribution within the reaction bed is easier for higher pressures. And finally, the reaction temperature which can be reached at this vapour pressures deviates clearly from the theoretical value if technical relevant reaction rates are required (compare Figure 31).

Operation mode D reaches an efficiency of 90 %. But since this increase of the electrical output of the power block would lead to even more challenging operating conditions of the power block and the storage, it is doubtful that this increase of 3 percentage points in storage efficiency will be economically reasonable.

To summarize: the experimental investigation of commercially available $Ca(OH)_2$ shows that in principle the required heat sink of the power block (cooling tower) could be combined with the required low grade heat source of the thermochemical system (evaporator). This concept clearly improves the overall efficiency of the thermochemical storage but requires at the same time to a certain extent modifications of the power block. The simplest configuration reaches a storage efficiency of 73 % (in comparison 63,4 % for the baseline case) while with a more complex and technically challenging integration values of 87 % and more could be reached. It has to be stated that for all operation modes with increased efficiency (mode B, C and D) a large fraction of the nominal steam mass flow has to be extracted at the low pressure turbine. Such a large steam extraction is thermodynamically possible but to the knowledge of the author no turbine, which allows such an operation, is currently available on the market. The design of such a turbine is technically challenging and thus would demand extensive development work. One possibility to overcome this challenge might be to use two separated turbines especially designed for the required boundary conditions instead of extracting a large steam fraction from one low pressure turbine stage.

To which extend the released steam during the charging of the storage can be used to increase the efficiency of the power block and compensates for the reduced power output during the discharging process needs to be evaluated based on a more detailed simulation of the plant including economic aspects.

5.3 Solar charging

To charge the storage system an integration into the molten salt cycle parallel to the central receiver is proposed (compare Figure 37). However in this configuration the amount of thermal energy which can be incorporated into the storage system is limited due to the opposed characteristic of the thermochemical system and the sensible heat transfer fluid. While for the fluid the amount of transferred thermal energy is proportional to the change in temperature, the thermochemical system absorbs the enthalpy of reaction at a constant temperature level. As a consequence only the temperature difference above the reaction temperature can be used to charge the storage system. The temperature level of the reaction in turn depends on the condensation pressure thus on the specific boundary conditions of the plant. In order to reach the lowest possible reaction temperature, in this study it is assumed that the heat of condensation is released to the ambient. For an air cooling system in solar plants located in hot desert this corresponds to a minimal condensation temperature of 45 °C.

By means of simple energy balances the mass flow of molten salt which is directed to the thermochemical reactor is calculated and the thermal power provided to the storage is calculated by the equation:

$$\dot{Q}_{TCS-charging} = \dot{m}_{salt} * cp_{salt} * (T_{inlet} - T_{reaction}) = \dot{n} \quad * \Delta H_{Reaction} \qquad (16)$$

Figure 40 shows the percentage amount of stored thermal energy for two different conditions: an outlet temperature at the TCS reactor of 445 °C and of 400 °C. The reference value (100 %) corresponds to the direct storage of the molten salt in a two tank system. The value of 400 °C corresponds to the thermodynamic minimum temperature that can be calculated according to equation 7 for a given pressure of 10 kPa. It becomes obvious that already at this theoretical minimal outlet temperature of 400 °C, only 59 % of the amount of stored energy in the molten salt tanks can be reached with the thermochemical system. According to our experimental investigation of the commercial $Ca(OH)_2$ (refer to Figure 20), the reaction rate at such low pressures limits additionally the practical operation window of the reaction. If a more realistic outlet temperature of 445 °C is considered only 42 % of the possible amount of thermal energy can be stored. Or, expressed in alternative values: whereas in a direct molten salt

system 10 h of nominal thermal load are stored the investigated thermochemical storage system can theoretically only be charged with 5.9 hours of nominal thermal load and 4.2 hours for the more realistic case of an outlet temperature of 445 °C.

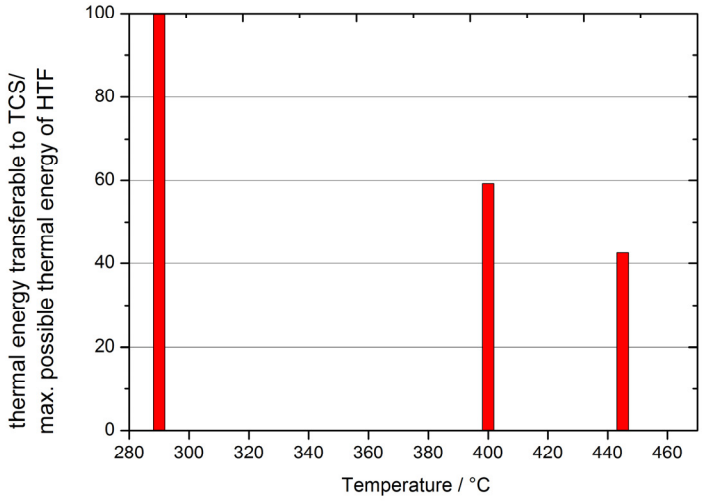

Figure 40 Amount of stored thermal energy for different outlet temperatures at the thermochemical reactor for one given reference day

5.4 Results and discussion

It can be summarized that taking the realistic boundary conditions of CSP plants into account a major part of the thermal energy of the heat transfer fluid cannot be incorporated into the thermochemical storage system during charging. This can be contributed to two reasons: one is that the minimal condensation temperature of the plants location limits the temperature difference between the maximum temperature of the heat transfer fluid and the temperature level of the reaction. The second is that kinetic limitations at low vapour pressure enforce an additional temperature difference of approximately 45 K to the theoretical reaction temperature. Even though it is clear that a proper analysis of this concept requires a more detailed analysis (especially since the inlet temperature into the receiver is higher and consequently less power is required from the solar field), this drastic difference makes it already obvious that a thermochemical storage cannot simply substitute a conventional storage method without changing at least some parts of the overall concept. Consequently, a parallel integra-

tion into the tower plants with molten salt as the heat transfer fluid therefore seems rather inefficient since the boundary conditions of the receiver fit to the power block and not the requirements of the storage.

However, if the complete configuration of the plant will be adapted to the storage system the pointed out problems can be overcome. One proposal with minimal adaptation of the CSP technology would be to have two different central receivers. One receiver would still operate in the nominal temperature range of the power block from 290 - 565 °C to supply the power block during on sun operation. The second receiver cycle would be especially designed to charge the storage system during daytime and operate at temperatures between 565 °C and 455 °C. Of course the higher return temperature of the heat transfer fluid provokes higher losses in the central receiver. Nevertheless a detailed simulation of such a configuration could be worth investigating.

One currently investigated possibility for CSP development is for example to use liquid metal as the heat transfer fluid. Liquid metals can operate at higher maximum temperatures which will improve the possibility to charge the storage system. Additionally since the liquid metal itself might be too costly to serve as storage medium alternative storage solutions are required that can take advantage of the higher temperatures. Besides innovative heat transfer fluids which work at higher temperatures another research line is to use solid particles as heat carrier and storage medium. The charging procedure is then carried out in a particle receiver where the storage material is directly (or indirectly) irradiated. For the calcium hydroxide this would on one hand eliminate the limitation of the charging performance related to the coupling with a sensible heat transfer fluid. And on the other hand the high reachable discharge temperatures of 600 °C or more allow to operate the power block with high efficiency.

6. Summary and outlook

Thermochemical storage systems offer in theory promising advantages for a wide range of applications. In particular the reversible reaction of calcium hydroxide to calcium oxide and water vapour is intensively discussed as an alternative storage solution for concentrated solar power plants and many other applications. The material is cheap, environmentally friendly and discharge temperatures of the reaction of up to 600 °C or more suites well to the operating range of today´s plants. However, experimental data on the operation of the system in lab scale reactors are rarely reported and the few reported experiments do not sufficiently represent the operating conditions which occur in the real application. The scope of this work was therefore to experimentally investigate the reaction system in kg-scale at process relevant boundary conditions.

The relevant operation modes of the storage system were analysed, taking boundary conditions of a real reference process into account. The analysis identified that for the considered generic operation modes, when the storage is charged with a sensible heat transfer fluid and powers a Rankine steam cycle during discharge, an operating range between 1.4 kPa and 470 kPa and 280 °C and 600 °C is required.

In order to investigate the reaction system in this wide operating range a novel reaction bed was designed for a representative mass of storage material and a generic geometry. With this reaction bed 90 experiments (45 cycles) were performed in total. A special focus was given to the analysis of the thermal capability of the storage material in the relevant pressure and temperature range and under different heating and cooling loads induced by the heat transfer fluid. By means of a systematic variation of the parameters the operational limits of the reaction system as well as expectable temperature levels were examined.

One significant result of the experiments is that the thermal charging and discharging at technically relevant thermal powers at low vapor pressures between 1.4 kPa and 50 kPa were demonstrated for the first time. However, the experiments revealed that the operating range of the calcium hydroxide system is partially limited due to the effective reaction rate of the storage material at these

low vapor pressures. For example, for the thermal charging at 10 kPa (condensation at 45 °C) a technically relevant minimum reaction temperature of 445 °C was identified which is around 45 K higher compared to the value predicted by the theoretical thermodynamic equilibrium. For the discharge at 8.7 kPa (evaporation at 43 °C) a reaction temperature below 350 °C, 48 K lower than the theoretical equilibrium temperature, should be maintained in order to reach high discharge powers. Comparable limitations were observed for all technically relevant charging or discharging powers at pressures below 50 kPa and the achievable reaction temperatures were determined.

In addition, the thermal discharge at pressures from 200 kPa to 470 kPa showed promising performance and discharge temperatures of up to 600 °C and 565 °C were demonstrated for the first time. At these high temperatures the reaction proceeded very close to the theoretical equilibrium temperature even with drastically increased cooling loads. This leads to the conclusion that for these high pressures reactors with high power densities and outlet temperatures close to the theoretical equilibrium can be designed.

With the presented work the complete relevant operating range for the thermochemical storage system has been experimentally characterized in lab scale. The obtained data provides an understanding of the operation performance in realistic application oriented conditions as well as the quantification of possible reaction temperatures. Moreover, due to the generic geometry of the reaction bed the presented data will support the validation of simulation models leading to future reactor developments and required enhancements of the material.

Besides the experimental investigation, a first integration of the thermochemical system in a concentrated solar power plant has been conceptually analysed in this work. It could be shown that by integrating the steam production required during discharge into the Rankine steam cycle a high storage efficiency of 87 % can be reached. However, the charging procedure with molten salt as the heat transfer fluid is challenging: kinetic limitations at low condensation pressures restrict the temperature difference between the reaction and the maximum temperature of the molten salt. It became obvious that thermochemical storage cannot simply substitute a conventional storage method without changing at least some parts of the overall concept. On the other hand the posed charging

challenge can be overcome by using heat transfer fluids which allow a higher maximum temperature, for example liquid metal or by charging the storage system in a solar particle receiver. Overall the experimentally demonstrated characteristic of the storage system indicate promising potential for a wide range of applications which should be further investigated.

References

[1] United Nations. Adoption of the Paris agreement. Conference Report Paris: 2015.

[2] Thess A. Die Rolle der Wärme im Energiesystem: Wärmespeicher als Schlüsselkomponente isentroper Energiespeicher. FVEE Themen 2015:19–22.

[3] IRENA. Renewable Energy Technologies: Cost Analysis Series Concentrating Solar Power. IRENA Work Pap 2012.

[4] Flueckiger SM, Iverson BD, Garimella S V. Economic Optimization of a Concentrating Solar Power Plant With Molten-Salt Thermocline Storage. J Sol Energy Eng 2013;136:1–8. doi:10.1115/1.4025516.

[5] Laing D, Steinmann W-D, Tamme R, Richter C. Solid media thermal storage for parabolic trough power plants. Sol Energy 2006;80:1283–9. doi:10.1016/j.solener.2006.06.003.

[6] Zunft S, Hänel M, Krüger M, Dreißigacker V. A Design Study for Regenerator-type Heat Storage in Solar Tower Plants–Results and Conclusions of the HOTSPOT Project. Energy Procedia 2014;49:1088–96. doi:10.1016/j.egypro.2014.03.118.

[7] Odenthal C, Steinmann W-D, Laing ME und D. The CellFlux Storage Concept for Cost Reduction in Parabolic Trough Solar Thermal Power Plants. Energy Procedia 2014;46:142–51. doi:10.1016/j.egypro.2014.01.167.

[8] Steinmann W-D, Laing D, Odenthal C. Development of the CellFlux Storage Concept for Sensible Heat. J Sol Energy Eng 2013;136:1–8. doi:10.1115/1.4024921.

[9] Kuznik F, David D, Johannes K, Roux J-J. A review on phase change materials integrated in building walls. Renew Sustain Energy Rev 2011;15:379–91. doi:10.1016/j.rser.2010.08.019.

[10] Steinmann W-D, Laing D, Tamme R. Latent Heat Storage Systems for Solar Thermal Power Plants and Process Heat Applications. J Sol Energy Eng 2010;132:1–5. doi:10.1115/1.4001405.

[11] Zipf V, Willert D, Neuhäuser A. Active latent heat storage with a screw heat exchanger – experimental results for heat transfer and concept for high pressure steam. vol. 1734, AIP Publishing; 2016. doi:10.1063/1.4949142.

[12] Pointner H, Steinmann W-D, Eck M. Introduction of the PCM Flux Concept for Latent Heat Storage. Energy Procedia 2014;57:643–52. doi:10.1016/j.egypro.2014.10.219.

[13] Jamekhorshid A, Sadrameli SM, Farid M. A review of microencapsulation methods of phase change materials (PCMs) as a thermal energy storage (TES) medium. Renew Sustain Energy Rev 2014;31:531–42. doi:10.1016/j.rser.2013.12.033.

[14] Kenisarin MM. High-temperature phase change materials for thermal

energy storage. Renew Sustain Energy Rev 2010;14:955–70. doi:10.1016/j.rser.2009.11.011.

[15] Abedin AH, Rosen MA. A Critical Review of Thermochemical Energy Storage Systems. Open Renew Energy J 2011;4:42–6.

[16] Atkins P-W, Paula J-D. Physikalische Chemie. 4. Auflage. WILEY-VCH; 2006.

[17] Wongsuwan W, Kumar S, Neveu P, Meunier F. A review of chemical heat pump technology and applications. Appl Therm Eng 2001;21:1489–519. doi:10.1016/S1359-4311(01)00022-9.

[18] Prieto C, Cooper P, Fernández AI, Cabeza LF. Review of technology: Thermochemical energy storage for concentrated solar power plants. Renew Sustain Energy Rev 2016;60:909–29. doi:10.1016/j.rser.2015.12.364.

[19] Pardo P, Deydier A, Anxionnaz-Minvielle Z, Rougé S, Cabassud M, Cognet P. A review on high temperature thermochemical heat energy storage. Renew Sustain Energy Rev 2014;32:591–610. doi:10.1016/j.rser.2013.12.014.

[20] Cot-Gores J, Castell A, Cabeza LF. Thermochemical energy storage and conversion: A-state-of-the-art review of the experimental research under practical conditions. Renew Sustain Energy Rev 2012;16:5207–24. doi:10.1016/j.rser.2012.04.007.

[21] Medrano M, Gil A, Martorell I, Potau X, Cabeza LF. State of the art on high-temperature thermal energy storage for power generation. Part 2—Case studies. Renew Sustain Energy Rev 2010;14:56–72.

[22] Kuravi S, Trahan J, Goswami DY, Rahman MM, Stefanakos EK. Thermal energy storage technologies and systems for concentrating solar power plants. Prog Energy Combust Sci 2013;39:285–319. doi:10.1016/j.pecs.2013.02.001.

[23] Molenda M, Stengler J, Linder M, Wörner A. Reversible hydration behavior of CaCl2 at high H2O partial pressures for thermochemical energy storage. Thermochim Acta 2013;560:76–81. doi:10.1016/j.tca.2013.03.020.

[24] van Essen VM, Zondag HA, Gores JC, Bleijendaal LPJ, Bakker M, Schuitema R, et al. Characterization of MgSO4 Hydrate for Thermochemical Seasonal Heat Storage. J Sol Energy Eng 2009;131:1–7. doi:10.1115/1.4000275.

[25] Kato Y, Takahashi R, Sekiguchi T, Ryu J. Study on medium-temperature chemical heat storage using mixed hydroxides. Int J Refrig 2009;32:661–6. doi:10.1016/j.ijrefrig.2009.01.032.

[26] Pan Z, Zhao CY. Dehydration/hydration of MgO/H2O chemical thermal storage system. Energy 2015;82:611–8. doi:10.1016/j.energy.2015.01.070.

[27] Shkatulov A, Ryu J, Kato Y, Aristov Y. Composite material “Mg(OH)2/vermiculite”: A promising new candidate for storage of middle temperature heat. Energy 2012;44:1028–34. doi:10.1016/j.energy.2012.04.045.

[28] Schaube F, Wörner A, Tamme R. High Temperature Thermochemical Heat Storage for Concentrated Solar Power Using Gas–Solid Reactions. J Sol Energy Eng 2011;133. doi:10.1115/1.4004245.

[29] Agrafiotis C, Roeb M, Schmücker M, Sattler C. Exploitation of thermochemical cycles based on solid oxide redox systems for thermochemical storage of solar heat. Part 1: Testing of cobalt oxide-based powders. Sol Energy 2014;102:189–211. doi:10.1016/j.solener.2013.12.032.

[30] Block T, Schmücker M. Metal oxides for thermochemical energy storage: A comparison of several metal oxide systems. Sol Energy 2016;126:195–207. doi:10.1016/j.solener.2015.12.032.

[31] Richter M, Bouché M, Linder M. Heat transformation based on CaCl2/H2O – Part A: Closed operation principle. Appl Therm Eng 2016;102:615–21. doi:10.1016/j.applthermaleng.2016.03.076.

[32] Bouché M, Richter M, Linder M. Heat transformation based on CaCl2/H2O – Part B: Open operation principle. Appl Therm Eng 2016;102:641–7. doi:10.1016/j.applthermaleng.2016.03.102.

[33] Zamengo M, Ryu J, Kato Y. Magnesium hydroxide – expanded graphite composite pellets for a packed bed reactor chemical heat pump. Appl Therm Eng 2013;61:853–8. doi:10.1016/j.applthermaleng.2013.04.045.

[34] Mastronardo E, Bonaccorsi L, Kato Y, Piperopoulos E, Milone C. Efficiency improvement of heat storage materials for MgO/H2O/Mg(OH)2 chemical heat pumps. Appl Energy 2016;162:31–9. doi:10.1016/j.apenergy.2015.10.066.

[35] Miguel SÁ de, Gonzalez-Aguilar J, Romero M. 100-Wh Multi-purpose Particle Reactor for Thermochemical Heat Storage in Concentrating Solar Power Plants. Energy Procedia 2014;49:676–83. doi:10.1016/j.egypro.2014.03.073.

[36] Circle of Blue. China's Karst Region: Infographics - Circle of Blue n.d. http://www.circleofblue.org/2010/world/chinas-karst-region-infographics/ (accessed November 25, 2016).

[37] Stanmore BR, Gilot P. Review—calcination and carbonation of limestone during thermal cycling for CO2 sequestration. Fuel Process Technol 2005;86:1707–43. doi:10.1016/j.fuproc.2005.01.023.

[38] USGS. LIME - USGS minerals 2011. https://minerals.usgs.gov/minerals/pubs/commodity/lime/mcs-2012-lime.pdf (accessed January 12, 2017).

[39] Hewlett PC. Lea's chemistry of cement and concrete. 4th ed. Elsevier Butterworth-Heinmann; 2004.

[40] Stark J, Wicht B. Zement und Kalk. Basel: Birkhäuser Basel; 2000. doi:10.1007/978-3-0348-8382-5.

[41] Lhoist S. A. Eisen und Stahl | Lhoist - Mineralien und Kalk Produzent n.d. http://www.lhoist.com/de_de/market-segment/eisen-und-stahl (accessed January 29, 2017).

[42] Rheinkalk KDI. Die Bedeutung von Kalk und Kalkdüngung in der pflanzlichen Produktion 2013. http://www.rheinkalk-

kdi.de/File/Kalkbroschuere_neu.pdf (accessed November 25, 2016).

[43] Halstead PE, Moore AE. 769. The thermal dissociation of calcium hydroxide. J Chem Soc 1957:3873–5. doi:10.1039/jr9570003873.

[44] Darkwa K. Thermochemical energy storage in inorganic oxides: An experimental evaluation. Appl Therm Eng 1998;18:387–400. doi:10.1016/S1359-4311(97)00052-5.

[45] Azpiazu MN, Morquillas JM, Vazquez A. Heat recovery from a thermal energy storage based on the Ca(OH)2/CaO cycle. Appl Therm Eng 2003;23:733–41. doi:10.1016/S1359-4311(03)00015-2.

[46] Perez-Davis ME, Mckissock BI, Difilippo F. Thermochemical energy storage for a lunar base. Int Sol Energy Conf 1992. https://ntrs.nasa.gov/archive/nasa/casi.ntrs.nasa.gov/19920005267.pdf (accessed November 25, 2016).

[47] Rosemary JK, Bauerle GL, Springer TH. Solar Energy Storage Using Reversible Hydration-Dehydration of CaO-Ca(OH)2. J Energy 1979;3:321–2. doi:10.2514/3.62440.

[48] Ervin G. Solar heat storage using chemical reactions. J Solid State Chem 1977;22:51–61. doi:10.1016/0022-4596(77)90188-8.

[49] Brown DR, La Marche JL, Spanner GE. Chemical Energy Storage System for Solar Electric Generating System (SEGS) Solar Thermal Power Plant. J Sol Energy Eng 1992;114. doi:10.1115/1.2930008.

[50] Fujimoto S, Bilgen E, Ogura H. CaO/Ca(OH)2 chemical heat pump system. Energy Convers Manag 2002;43:947–60. doi:10.1016/S0196-8904(01)00081-4.

[51] Kanzawa A, Arai Y. Thermal energy storage by the chemical reaction augmentation of heat transfer and thermal decomposition in the powder. Sol Energy 1981;27:289–94. doi:10.1016/0038-092X(81)90061-X.

[52] Schaube F, Koch L, Wörner A, Müller-Steinhagen H. A thermodynamic and kinetic study of the de- and rehydration of Ca(OH)2 at high H2O partial pressures for thermo-chemical heat storage. Thermochim Acta 2012;538:9–20. doi:10.1016/j.tca.2012.03.003.

[53] Matsuda H, Ishizu T, Lee SK, Hasatani M. Kinetic study of Ca(OH)2/CaO reversible thermochemical reaction for thermal energy storage by means of chemical reaction. KAGAKU KOGAKU RONBUNSHU 1985;11:542–8. doi:10.1252/kakoronbunshu.11.542.

[54] Samms JAC, Evans BE. Thermal dissociation of Ca(OH)2 at elevated pressures. J Appl Chem 2007;18:5–8. doi:10.1002/jctb.5010180102.

[55] Barin I. Thermochemical Data of Pure Substances. Weinheim, Germany: Wiley-VCH Verlag GmbH; 1995. doi:10.1002/9783527619825.

[56] Mikhail RS, Brunauer S, Copeland LE. Kinetics of the thermal decomposition of calcium hydroxide. J Colloid Interface Sci 1966;21:394–404. doi:10.1016/0095-8522(66)90005-5.

[57] Dutta S, Shirai T. Kinetics of drying and decomposition of calcium hydroxide. Chem Eng Sci 1974;29:2000–3. doi:10.1016/0009-2509(74)85021-9.

[58] Murthy MS, Raghavendrachar P, Sriram SV. Thermal decomposition of doped calcium hydroxide for chemical energy storage. Sol Energy 1986;36:53–62. doi:10.1016/0038-092X(86)90060-5.

[59] Chen D, Gao X, Dollimore D. The application of non-isothermal methods of kinetic analysis to the decomposition of calcium hydroxide. Thermochim Acta 1993;215:65–82. doi:10.1016/0040-6031(93)80082-L.

[60] Irabien A, Viguri JR, Ortiz I. Thermal dehydration of calcium hydroxide. 1. Kinetic model and parameters. Ind Eng Chem Res 1990;29:1599–606. doi:10.1021/ie00104a004.

[61] Galwey AK, Brown ME. Thermal Decomposition of Ionic Solids: Chemical Properties and Reactivities of Ionic Crystalline Phases. 1st ed. Elsevier Science; 1999.

[62] Criado YA, Alonso M, Abanades JC. Kinetics of the CaO/Ca(OH) 2 Hydration/Dehydration Reaction for Thermochemical Energy Storage Applications. Ind Eng Chem Res 2014;53:12594–601. doi:10.1021/ie404246p.

[63] Lin S, Harada M, Suzuki Y, Hatano H. CaO Hydration Rate at High Temperature (∼1023 K). Energy & Fuels 2006;20:903–8. doi:10.1021/ef050257o.

[64] Wang Y, Lin S, Suzuki Y. Effect of CaO content on hydration rates of Ca-based sorbents at high temperature. Fuel Process Technol 2008;89:220–6. doi:10.1016/j.fuproc.2007.09.009.

[65] Schaube F. Untersuchungen zur Nutzung des CaO / Ca (OH) 2 - Reaktionssystems für die thermochemische Wärmespeicherung. Dissertation Universität Stuttgart, Dr. Hut, 2012.

[66] Chase MW, Curnutt JL, McDonald RA, Syverud AN. JANAF thermochemical tables, 1978 supplement. J Phys Chem Ref Data 1978;7:793–940. doi:10.1063/1.555580.

[67] Lander JJ. Experimental Heat Contents of SrO, BaO, CaO, BaCO 3 and SrCO 3 at High Temperatures. Dissociation Pressures of BaCO 3 and SrCO 3. J Am Chem Soc 1951;73:5794–7. doi:10.1021/ja01156a094.

[68] Ryu J, Hirao N, Takahashi R, Kato Y. Dehydration Behavior of Metal-salt-added Magnesium Hydroxide as Chemical Heat Storage Media. Chem Lett 2008;37:1140–1. doi:10.1246/cl.2008.1140.

[69] Shkatulov A, Aristov Y. Modification of magnesium and calcium hydroxides with salts: An efficient way to advanced materials for storage of middle-temperature heat. Energy 2015;85:667–76. doi:10.1016/j.energy.2015.04.004.

[70] Kariya J, Ryu J, Kato Y. Development of thermal storage material using vermiculite and calcium hydroxide. Appl Therm Eng 2016;94:186–92. doi:10.1016/j.applthermaleng.2015.10.090.

[71] Yan J, Zhao CY. First-principle study of CaO/Ca(OH)2 thermochemical energy storage system by Li or Mg cation doping. Chem Eng Sci 2014;117:293–300. doi:10.1016/j.ces.2014.07.007.

[72] Fujii I, Tsuchiya K, Higano M, Yamada J. Studies of an energy storage system by use of the reversible chemical reaction: CaO + H2O ⇌

Ca(OH)2. Sol Energy 1985;34:367–77. doi:10.1016/0038-092X(85)90049-0.

[73] Schaube F, Utz I, Wörner A, Müller-Steinhagen H. De- and rehydration of Ca(OH)2 in a reactor with direct heat transfer for thermo-chemical heat storage. Part A: Experimental results F. Chem Eng Res Des 2013;91:865–73. doi:10.1016/j.cherd.2013.02.019.

[74] Roßkopf C, Haas M, Faik A, Linder M, Wörner A. Improving powder bed properties for thermochemical storage by adding nanoparticles. Energy Convers Manag 2014;86:93–8. doi:10.1016/j.enconman.2014.05.017.

[75] Pardo P, Anxionnaz-Minvielle Z, Rougé S, Cognet P, Cabassud M. Ca(OH)2/CaO reversible reaction in a fluidized bed reactor for thermochemical heat storage. Sol Energy 2014;107:605–16. doi:10.1016/j.solener.2014.06.010.

[76] Rougé S, A. Criado Y, Soriano O, Abanades JC. Continuous CaO/Ca(OH) 2 Fluidized Bed Reactor for Energy Storage: First Experimental Results and Reactor Model Validation. Ind Eng Chem Res 2017;56:844–52. doi:10.1021/acs.iecr.6b04105.

[77] Ogura H, Yamamoto T, Kage H, Matsuno Y, Mujumdar AS. Effects of heat exchange condition on hot air production by a chemical heat pump dryer using CaO/H2O/Ca(OH)2 reaction. Chem Eng J 2002;86:3–10. doi:10.1016/S1385-8947(01)00265-0.

[78] Yan J, Zhao CY. Experimental study of CaO/Ca(OH)2 in a fixed-bed reactor for thermochemical heat storage. Appl Energy 2016;175:277–84. doi:10.1016/j.apenergy.2016.05.038.

[79] Schmidt P, Bouché M, Linder M, Wörner A. Pilot Plant Development of High Temperature Thermochemical Heat Storage. Proc. Innostock, 2012, p. 1–9.

[80] Schmidt M, Szczukowski C, Roßkopf C, Linder M, Wörner A. Experimental results of a 10 kW high temperature thermochemical storage reactor based on calcium hydroxide. Appl Therm Eng 2014;62:553–9. doi:10.1016/j.applthermaleng.2013.09.020.

[81] Schmidt M, Roßkopf C, Linder M, Wörner A. Operation modes and process integration of a thermochemical heat storage system based on CaO/Ca(OH)2. Proc. Eurotherm Semin. No 99, Lleida, Spain: 2014.

[82] Linder M, Roßkopf C, Schmidt M, Wörner A. Thermochemical Energy Storage in kW-scale based on CaO/Ca(OH)2. Energy Procedia 2014;49:888–97. doi:10.1016/j.egypro.2014.03.096.

[83] Criado YA, Alonso M, Abanades JC, Anxionnaz-Minvielle Z. Conceptual process design of a CaO/Ca(OH)2 thermochemical energy storage system using fluidized bed reactors. Appl Therm Eng 2014;73:1085–92. doi:10.1016/j.applthermaleng.2014.08.065.

[84] Rougé S, Huille A, Criado YA, Abanades JC. Proof of concept of the CaO/Ca(OH)2 reaction in a continuous heat- exchanger BFB reactor for thermochemical heat storage in CSP plants. SOLARPACES 2016 Int. Conf. Conc. Sol. Power Chem. Energy Syst., AIP Publishing; 2017.

[85] Roßkopf C. Entwicklung eines Reaktorkonzepts mit bewegtem Reaktionsbett für thermochemische Energiespeicher. Dissertation

Universität Stuttgart, Dr. Hut; 2015.

[86] TCS Power - European research project n.d. http://www.tcs-power.eu/home.html (accessed November 27, 2016).

[87] Roßkopf C, Afflerbach S, Schmidt M, Görtz B, Kowald T, Linder M, et al. Investigations of nano coated calcium hydroxide cycled in a thermochemical heat storage. Energy Convers Manag 2015;97:94–102. doi:10.1016/j.enconman.2015.03.034.

[88] Schmidt M, Gollsch M, Giger F, Grün M, Linder M. Development of a moving bed pilot plant for thermochemical energy storage with CaO/Ca(OH)2. SOLARPACES 2015 Int. Conf. Conc. Sol. Power Chem. Energy Syst., vol. 1734, AIP Publishing; 2016, p. 50041. doi:10.1063/1.4949139.

[89] Dunn RI, Hearps PJ, Wright MN. Molten-Salt Power Towers: Newly Commercial Concentrating Solar Storage. Proc IEEE 2012;100:504–15. doi:10.1109/JPROC.2011.2163739.

[90] Liu M, Steven Tay NH, Bell S, Belusko M, Jacob R, Will G, et al. Review on concentrating solar power plants and new developments in high temperature thermal energy storage technologies. Renew Sustain Energy Rev 2016;53:1411–32. doi:10.1016/j.rser.2015.09.026.

Appendix

A Technical drawings

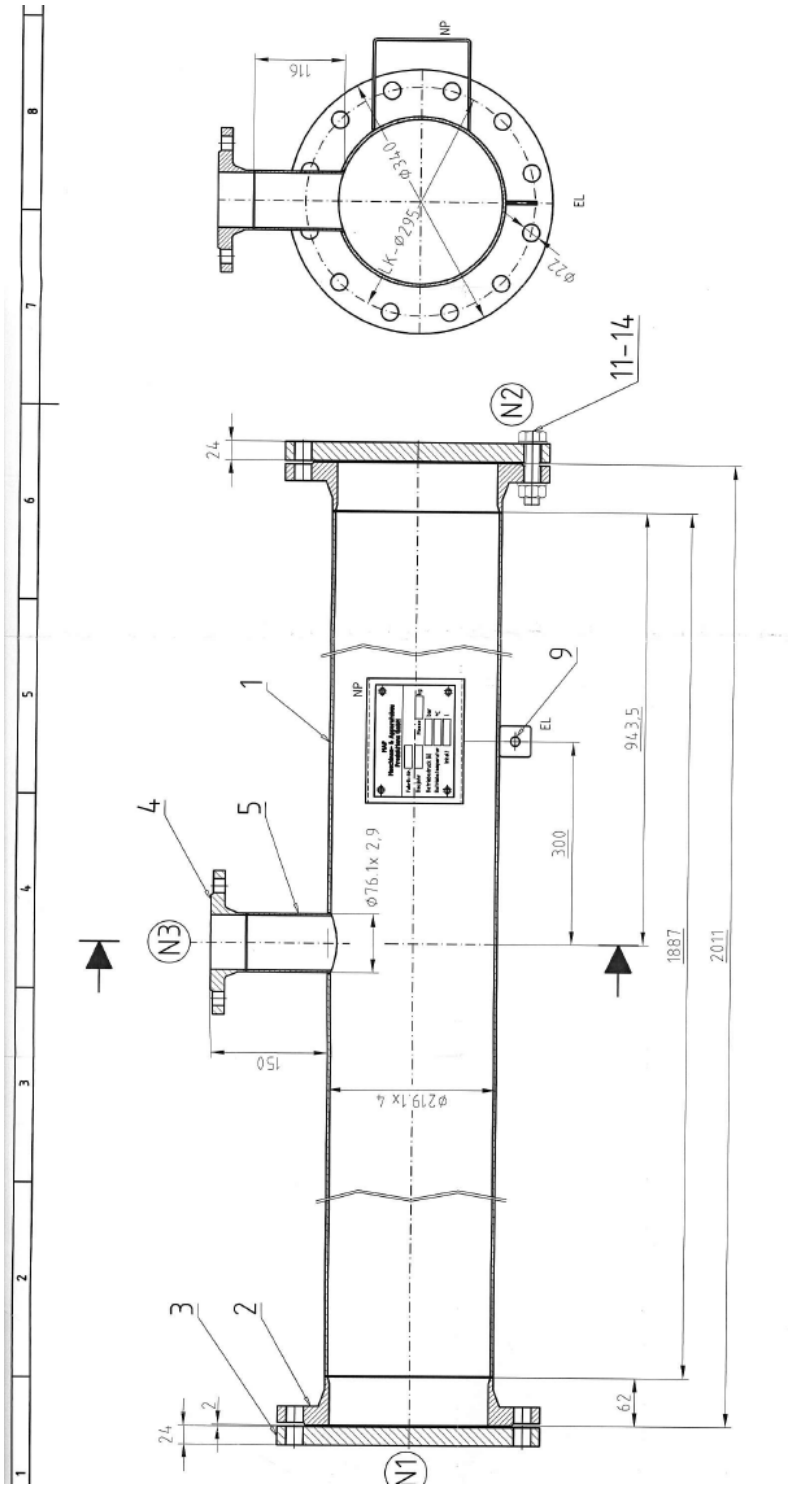

Figure 41 Technical drawing of pressure resistant casing pipe

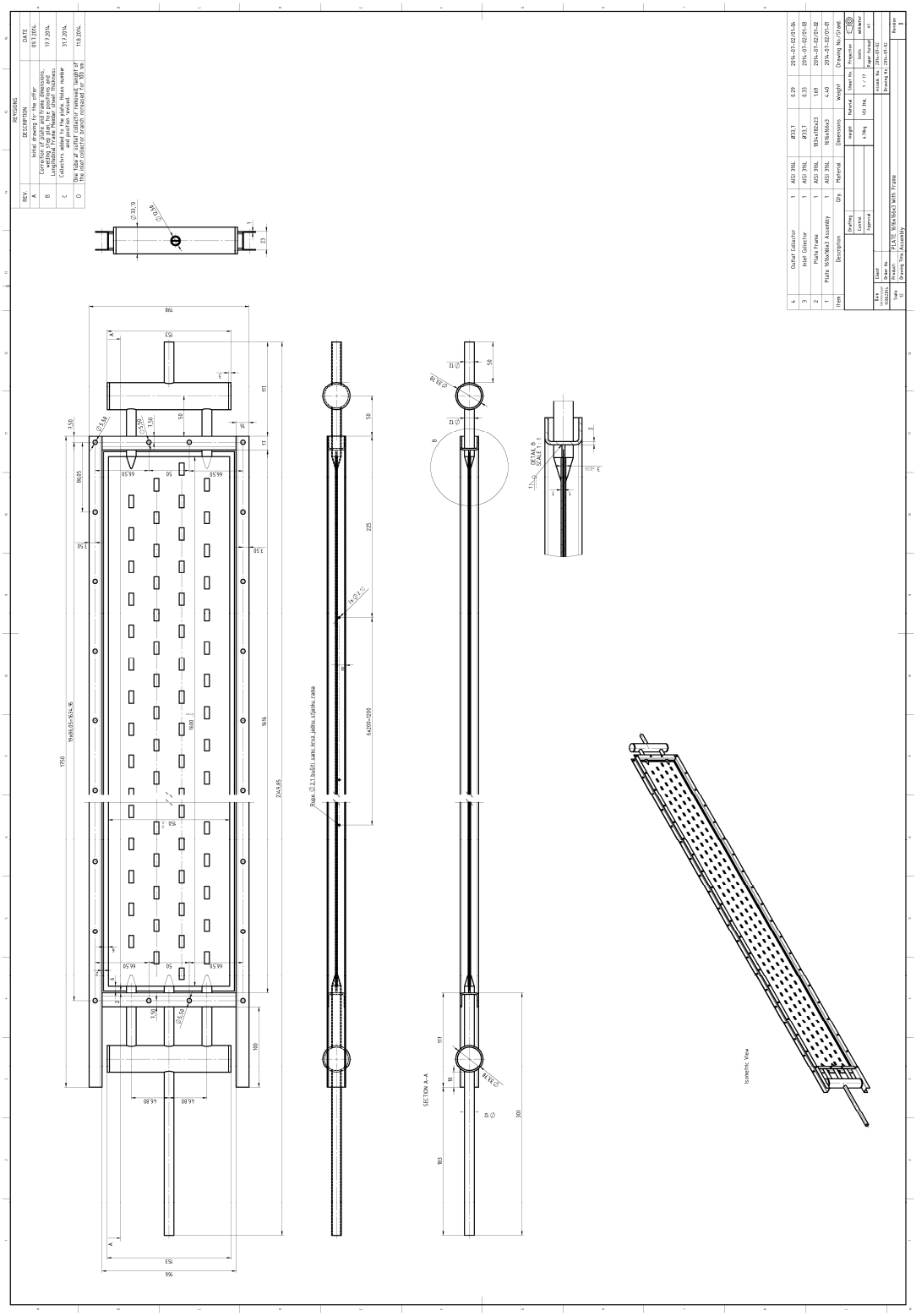

Figure 42 Technical drawing of heat exchanger plate

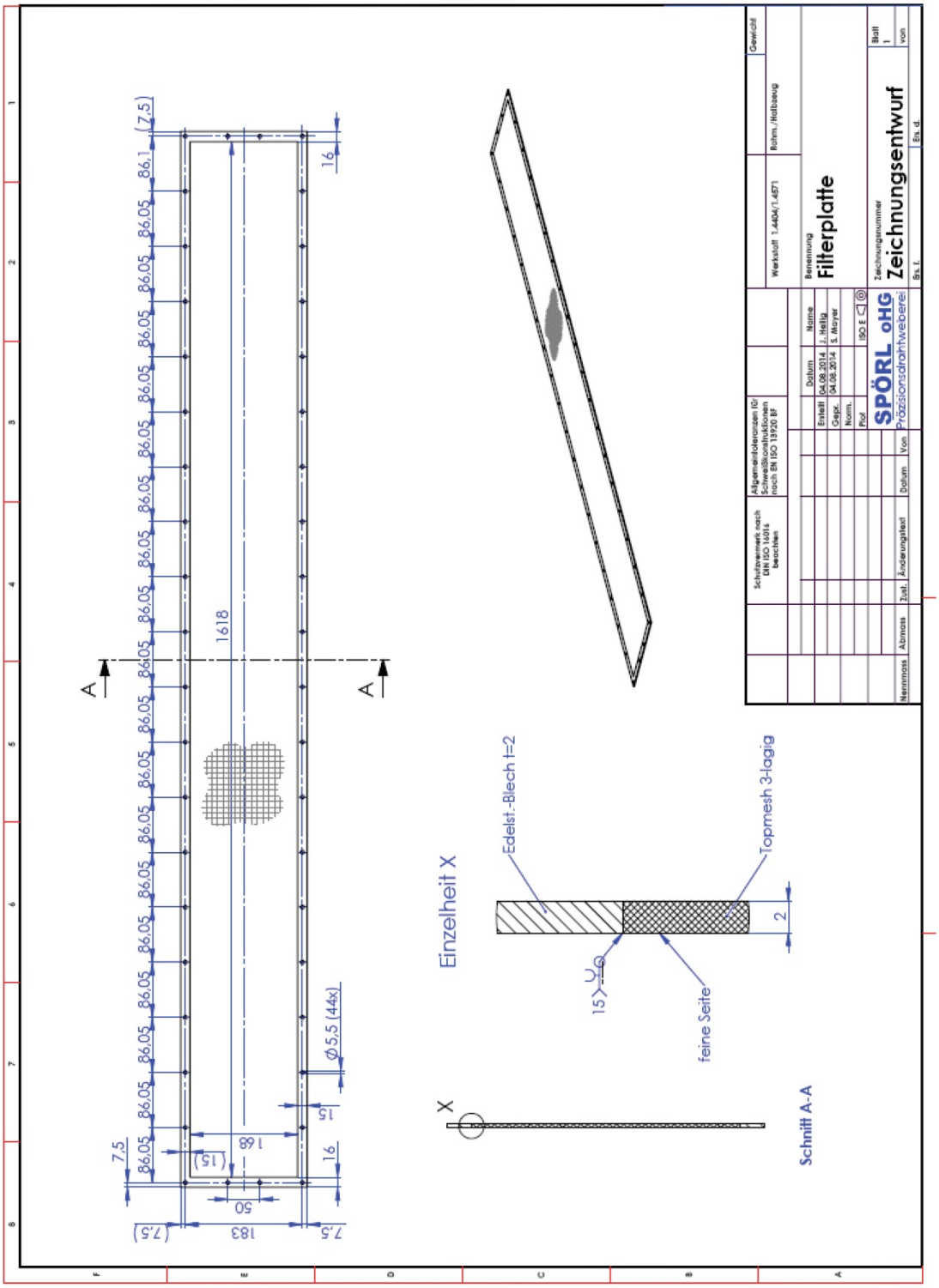

Figure 43 Technical drawing of filter plate

B Calibration of filling level meter

The water level height in the condenser/ evaporator is continuously measured by a filling level meter. The relation between the filling height in the condenser and the corresponding volume of water was initially determined. Step by step a volume of 0.25 L water was added into the condenser and the filling height was measured. Figure 44 shows the measurement points and the corresponding linear trend. The slope of the line was determined to 76.64 (mm / L). By means of this value the amount of water taken up or released by the reaction, respectively the conversion of the reaction was calculated.

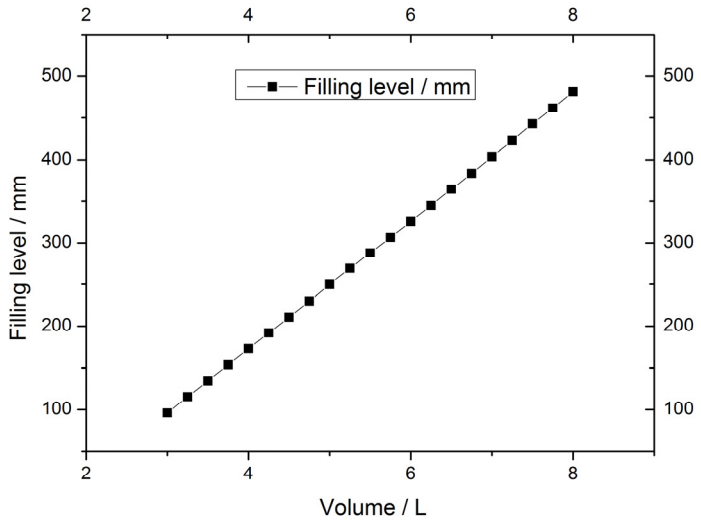

Figure 44 Determination of correlation between filling level height in the condenser and volume of water

C Insulation of the reactor

In order to reduce the influence of radiative heat transfer between the reaction bed and the casing pipe two sheets of insulation material wrapped in aluminium foil were placed into the reaction chamber. Figure 15 shows the placement of the insulation sheets. The insulation material was Pyrogel® XT supplied by Stadur Sued. Table 7 summarizes values for the thermal conductivity of the material in the applied temperature range. The sheets were 1850 mm long 20 mm wide and 10 mm thick.

Table 7 Temperature dependent heat conductivity of insulation material (Pyrogel® XT)

Temperature / °C	200	300	400	500	600
λ / (mW/(mK))	28	35	46	64	89

The casing pipe was insulated with the material Contherm BTM 1100. At first a layer of 50 mm thickness was placed onto the outer surface of the pipe. On this first insulation layer an aluminium foil was placed and 4 electrical heating cables (each had a power of 1 kW) were attached to the aluminium foil. A second 50 mm thick insulation layer was placed on top of the aluminium foil. Figure 45 shows the installation of the heating cables on the left and the fully insulated pipe on the right side. The total insulation thickness of the casing pipe was 100 mm. The thermal conductivity of the insulation material is given in Table 8. The flange of the casing pipe at the air inlet was covered with an electrically heated insulation sleeve which was 40 mm thick and had a power of 0.5 kW. The flanges at the air outlet and the reaction gas outlet were also covered with an insulation sleeve of 40 mm thickness but the sleeves were not electrically heated.

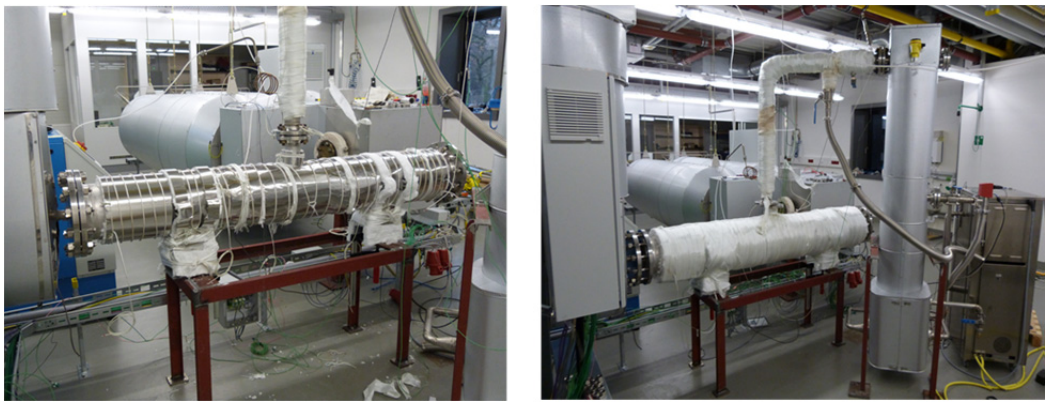

Figure 45 left: heating cables attached to the firs insulation layer; right: complete insulation of the casing pipe

Table 8 Temperature dependent heat conductivity of insulation material (Contherm BTM 1100)

Temperature / °C	200	300	400	500	600
λ / (W/(mK))	0.06	0.08	0.1	0.13	0.16

D Measurement uncertainty

Temperature measurement

The uncertainty of the temperature measurement can be mainly attributed to the deviation of the thermocouples. The deviation is given by the manufacturer and accounts +-0.4 %*T. The deviation of the temperature measurement thereby accounts 1.2 to 2.4 K in the temperature range between 300 and 400 °C.

Pressure measurement

The uncertainty of the pressure sensor is specified by the manufacturer to +-0.8 kPa. Since the reactor was operated in a pure water vapour atmosphere the vapour pressure in the system could additionally be determined by the measured temperature of the water reservoir in the condenser/ evaporator. With this method the pressure measured in the reactor was checked against the pressure calculated with the known correlation for saturated steam and the measured temperature of the water reservoir. The results showed always very good accordance.

Filling level meter

The measurement of the filling level is specified to have a deviation of +-2 mm. The relation between filling height and volume of water accounts 76.64 (mm/L) according to the calibration shown in appendix B. Thus the measurement deviation accounts +- 0.026 L .Related to the 0.6 L of water which is released or taken up by the reactive material the deviation of the calculated total conversion therefore accounts approximately +- 4 %.

Mass flow controller

The deviation of the mass flow controller is specified with +-0.4 %. Additional losses due to leakage after the mass flow controller might occur but cannot be determined.